Developing a unifying phenomenology of the
high-temperature superconducting cuprates from NMR
shift and relaxation data

Der Fakultät für Physik und Geowissenschaften
der Universität Leipzig
eingereichte
D I S S E R T A T I O N
zur Erlangung des akademischen Grades

doctor rerum naturalium

Dr. rer. nat.

vorgelegt

von M.Sc. Marija Avramovska

geboren am 02.10.1995 in Kumanovo, Mazedonien

Gutachter:
Prof. Dr. Dirk Morr
Prof. Dr. Jürgen Haase

Tag der Verleihung: 10.07.2023

Bibliographische Beschreibung

Avramovska, Marija

Developing a unifying phenomenology of the high-temperature superconducting cuprates from NMR shift and relaxation data

Universität Leipzig, Dissertation
109 S. [*] 55 Lit. [†] 3 (+28[‡]) Abb., 1 Anlage

Abstract

Nuclear magnetic resonance—a bulk, local probe of materials' electronic properties—has been significant for theories of high-temperature superconducting cuprates. However, more recent NMR experiments revealed several contradictions in the early interpretation of the NMR data. This cumulative thesis, comprised of six publications, aims to develop a new phenomenology based on the entirety of Cu and O NMR shift and relaxation data.

The data revealed that a suppression of the Cu shifts is behind the failure of the Korringa relation, while the Cu relaxation measured with one direction of the field $(c \perp B_0)$ is similar for all cuprates and is Fermi-liquid like. The Cu shift and relaxation anisotropies could be explained by assuming two-spin components with different doping and temperature dependencies. A later analysis of all planar O shift and relaxation showed that a metallic-like density of states is ubiquitous to all the cuprates, irrespective of doping and material, and carries a temperature-independent but doping-dependent pseudogap, as similarly seen in the electronic entropy. This temperature-independent pseudogap is behind the suppression of the Cu shifts, but it has no influence on the Cu relaxation. Additionally, the Cu shifts measured with $c \parallel B_0$ direction of the field reveal a family dependence. We propose a two-spin component model, explaining the family dependence in the Cu shifts, the complex Cu shift anisotropy and relaxation, and the disparity in the temperature dependence between the Cu and O shifts. This model also accounts for the missing negative shift and the long-standing Cu orbital shift discrepancy.

While these conclusions are phenomenological, they must be explained by a detailed theory of the cuprates

---

[*]S.: Seitenzahl insgesamt
[†]Lit.: Anzahl der im Literaturverzeichnis ausgewiesenen Literaturangaben
[‡]in den veröffentlichten wissenschaftlichen Arbeiten und den Anlagen

Acknowledgments

A great many people helped me with this project and supported me along the way. I would like to use this opportunity to thank them.

I thank Prof. Jürgen Haase for giving me the opportunity to work on this very interesting project, for all the helpful advice and countless discussions from which I learned a lot. Prof. Dieter Freude, I thank for teaching me all the details of experimental NMR work and for all the support throughout these years.

I also want to thank my colleagues who contributed greatly to the work presented in this thesis. I thank Danica Pavićević for the help with data analysis and discussions, as well as the great friendship. I thank Jakob Nachtigal for the great work handling the oxygen data. I am very grateful to Michael Jurkutat for all the discussions on cuprates which greatly expanded my knowledge. I also thank Stefan Tsankov and Robin Gühne for all the insightful comments, as well as the whole MQF group for the nice working atmosphere.

I would also like to thank all the people who helped with my experimental work and the ceramics project. For the technical help, I thank Gert Klotzsche and the masters of glass from the glassblowing workshop. I thank Prof. Jörg Kärger for help with interpreting the data. Additionally, I would like to thank all our collaborators from Tel Aviv, Krakow, and Erlangen for the nice collaboration.

On a more personal level, I want to thank all the people who made these few years most memorable. I especially want to thank Javier for all the care-work and wonderful cooking skills (I owe you big time). I thank Ana for all the support, the endless discussions on art and philosophy which kept me sane during this time, and for the astute reading of all my writings. I'm immensely grateful to Shubhangi—my perfect b2b partner—for the great musical collaboration and the wonderful friendship. To Leon, Jakob, Laetitia, Seunghye, Nora—for being amazing friends. I also want to thank *Azadi* for always being a safe space for us to hang out at.

I thank my parents for their unwavering support and care.

Preface

Nuclear magnetic resonance (NMR) is a bulk, local probe of materials' electronic properties, and given its importance for the Bardeen Cooper Schrieffer theory of superconductivity, it has also been a benchmark probe for early theories of the high-temperature superconducting cuprates dating back to their discovery by Bednorz and Müller in 1986. However, with an accepted microscopic theory lacking, the early interpretation of the NMR data had to be questioned. In particular, since the growing body of NMR data accumulated by many groups over the years revealed more inconsistencies in the old phenomenology that was developed on just a few systems.

In recent years, since discovering that NMR could quantify the charges in the Cu $3d(x^2 - y^2)$ and O $2p_\sigma$ orbitals of all materials—information obtained from electric hyperfine splittings—our group was involved in developing a different view of the cuprates based on the sharing of charge in the CuO_2 plane that is ubiquitous in the cuprates. Interestingly, this sharing of the charges sets the maximum T_c across all families. Motivated by these findings, it seemed necessary to review all NMR shift and relaxation data.

This cumulative thesis has its focus on the magnetic properties of the cuprates. The six enclosed publications document how our thinking about the cuprates developed as we analyzed all data from extensive literature studies of the related NMR parameters. The entirety of the magnetic data (shifts and relaxation) suggests a very different NMR scenario of the cuprates.

When I entered the group, all Cu shifts had been collected and the family dependent discrepancies were striking. Consequently, we focused on all Cu relaxation data

and soon arrived at more notable observations, e.g., the Cu relaxation measured with the field in one direction $c\perp B_0$ is ubiquitous for all doping and materials. This also means that where the famous Korringa relation fails, the shifts are suppressed, different from the proposed enhancement of Cu relaxation from spin fluctuations. Hence, we began looking at simple models that can explain Cu shift and relaxation. In the next step, the focus had to be on planar oxygen shift and relaxation. The entirety of the O data pointed to a temperature-independent pseudogap at the Fermi surface of a simple metal, with states outside the gap being ubiquitous to all the cuprates, irrespective of doping or family. We then realized that the suppression of the Cu shifts had to be due to the temperature-independent pseudogap but while O could be explained within a simpler scenario, the Cu data still warranted a two-component description.

These phenomenological conclusions, based on the entirety of Cu and O NMR shift and relaxation data, present a reliable framework for theory.

Over the last few years, I was also involved in NMR experiments studying rehydroxylation in ceramics, as well as experiments on Zn-modified zeolites, where the aim was to understand the role of Zn species in the activation of particular C-H bonds of alkane and its aromatization on zeolite catalysts. This resulted in two publications and one currently in preparation. This experimental work contributed greatly to my understanding of NMR and its broader applications in solid-state physics. These topics will, however, not be discussed here and the mentioned publications are not part of this cumulative thesis.

Contents

Chapter 1

Introduction

It has been almost half a century since [Bednorz and Müller, 1986] first reported on superconductivity in the Ba-La-Cu-O system. In search of Jahn-Teller polaron formations, they investigated the metal-insulator transition in mixed perovskites. This led them to the discovery of materials with the highest observed transition temperature (T_c) of superconductivity at the time. Hence, the race began for finding ways to maximize T_c and achieve room temperature superconductivity.

Motivated not only by the great intellectual challenge but also by the promise of a wide range of applications, the discovery of the cuprate superconductors sparked an extensive research endeavor both in experimental and theoretical physics continuing to this day.

Over the years, well over a hundred cuprate superconductors were invented. Already within a year after the first discovery of high-T_c in LaBaCuO, with a $T_c = 30$ K, experiments with pressure led to the invention of the $YBa_2Cu_3O_{7-\delta}$ compound—first superconductor with T_c above the boiling point of liquid nitrogen—discovered by replacing the larger La^{3+} by the smaller Y^{3+} cation, [Wu et al., 1987]. Since then, the highest known transition temperature has increased substantially. There are several parameters that influence T_c. It appears to be family specific, it depends on the number of CuO_2 layers, and more recently, it was discovered that T_c depends on the oxygen hole content and the charge transfer gap size, [Rybicki et al., 2016], [Ruan et al., 2016]. The cuprate with the highest known T_c is a triple-layered mercury system with a

T_c =133 K [Schilling et al., 1993]. Later on, its T_c was enhanced to nearly 160 K, by using high pressure, [Gugenberger et al., 1994].

Nowadays, newer systems that show unusually high transition temperatures of superconductivity attract a lot of scientific attention, e.g., iron-pnictides which are structurally and phenomenologically quite similar to the cuprates, carbon-based or organic superconductors, and hydrides which hold the record for highest T_c above 200 K at extremely high pressures of 160 GPa, [Li et al., 2022, Kong et al., 2021]. The cuprates, however, due to the large promise for applications with their high transition temperatures—over the boiling point of nitrogen at ambient pressure for most systems—remain in the spotlight of high-T_c research.

Since the early days of cuprate research, nuclear magnetic resonance (NMR) has been a widely utilized technique and played an important role in studying high-temperature superconductivity. NMR is a local, bulk probe, and with it, various nuclei can be probed. Since NMR is also sensitive to magnetic and electric effects, multiple sites can be distinguished (e.g., Cu sites in the planes or chains of $YBa_2Cu_3O_{7-\delta}$). This makes NMR suitable for studying both the cuprates' normal and superconducting state, as they are Type II superconductors.

The early NMR studies provided important information about these materials' chemical and electronic properties. The focus was largely on shift and relaxation measurements and comparing the cuprates with normal metals and BCS superconductors. It was known for Fermi-liquids that relaxation is related to the shift through the well-known Korringa relation, [Korringa, 1950]. It was found that the highly-overdoped cuprates behaved as Fermi-liquids, while also obeying the Korringa law. However, an important discovery came from ^{89}Y shifts from various doping levels of $YBa_2Cu_3O_{7-\delta}$, when it was shown that as doping was lowered, the shifts gained a temperature-dependence and decreased far above T_c. This was seen as the first indication of a spin gap, [Alloul et al., 1989]. Furthermore, the shifts and relaxation rates also rapidly dissipated below T_c, indicating spin-singlet pairing, [Yosida, 1958].

Since NMR can measure the electric field gradient (EFG) at a certain nuclear site by measuring the quadrupole splitting, it can be used to determine the partial

occupation of anisotropic orbitals. Many attempts were made to determine the local hole densities at Cu and O in the CuO_2 plane. [Haase et al., 2004] introduced an approach for determining the local hole densities by using the electric hyperfine coefficients from atomic spectroscopy and accounting for the doping-independent contribution to the EFG using the NMR data of the parent compound. They gave the local hole distribution in the CuO_2 plane of $La_{2-x}Sr_xCuO_4$ and $YBa_2Cu_3O_{7-\delta}$ and found that in $La_{2-x}Sr_xCuO_4$ upon doping, all the doped holes reside on oxygen, but in $YBa_2Cu_3O_{7-\delta}$, some holes go also on Cu.

Later on, [Jurkutat et al., 2014] determined the hole densities for all cuprate families where data on the quadrupole splitting was available for both hole and electron-doped cuprates. They found that the variation of the hole content upon doping between Cu and O is a family-specific property. Moreover, the materials with higher T_c have a larger n_P. Then followed the discovery by [Rybicki et al., 2016] that the charge transfer of the copper hole to planar oxygen is what sets the maximum critical temperature. Very recently, [Kowalski et al., 2021] predicted these findings using CDMFT cluster calculations in the three-band Hubbard model.

The understanding of the charges showed that one needs to look at the cuprate NMR data in its entirety, across all families and doping. In the early days, the NMR research focused mainly on $YBa_2Cu_3O_{7-\delta}$, the stoichiometric $YBa_2Cu_4O_8$, and $La_{2-x}Sr_xCuO_4$; hence theoretical frameworks were based mainly on those results. Since then, sample quality has improved substantially, and NMR data for more systems and doping levels has become available.

Since the very beginning, the single- versus two-component picture has been a topic of debate. The idea of the single component picture is based on the works of Zhang and Rice, who proposed that the Cu spin would couple with the O electron spin into a singlet state, forming the mobile charge carrier produced with doping. [Zhang and Rice, 1988, Mila and Rice, 1989].

One year afterwards, NMR experiments on $YBa_2Cu_3O_{7-\delta}$ verified the single component picture and established the magnetic hyperfine scenario. Early experiments showed the existence of a hole in the Cu $3d(x^2-y^2)$ orbital [Pennington et al., 1989]. However, while the shift associated with such a hole was expected to be negative,

due to the well-known negative hyperfine coefficient [Pennington et al., 1989], the measured shifts were positive. This required the hyperfine scenario to include a transferred hyperfine term in addition to the onsite. Surprisingly, the Cu shift measured with the field in $c \parallel B_0$ direction was found to be even temperature and doping-independent. This was interpreted within the single-spin component picture as an accidental cancellation of the Cu onsite and transferred hyperfine coefficients, [Takigawa et al., 1989a, Takigawa et al., 1989b]. The Cu $c \perp B_0$ and O shifts also followed the same temperature dependencies, [Takigawa et al., 1991]. This was further proof of the validity of the single-component view.

Later measurements on $La_{2-x}Sr_xCuO_4$ showed that the $La_{2-x}Sr_xCuO_4$ planar Cu and O shifts did not have the same temperature dependence. This suggested that the system may require a two-component description. [Haase et al., 2009]

As more compounds were being investigated, reconciling the single-component view with the experimental data became more difficult. For example, some systems showed a temperature-dependent Cu shift also for $c \parallel B_0$ direction, putting into question the accidental cancellation of the hyperfine coefficients. Also, more recent experiments on $HgBa_2CuO_{4+\delta}$ [Rybicki et al., 2015], showed temperature-dependent Cu $c \parallel B_0$ shifts and a specific shift anisotropy of 2.5. In a single-component view, this would require significant changes in the hyperfine coefficients, which seems implausible.

Additionally, in the early days, a different reference compound was used for the Cu shift measurements. It was later found that this reference compound has a significant Van Vleck contribution, [Renold et al., 2003]. Even after correcting for the reference, there was still a disparity between the calculated and measured orbital shifts for one direction, as well as the question of the mysteriously missing negative shift for $c \parallel B_0$ shifts. These discrepancies with the Cu shift data still needed to be understood

Even though an increasing number of experiments showed the failure of the old shift interpretation, the single-component view remained widely adopted. With the intense focus on a few materials in the beginning and in the light of newer experiments, it became clear that a new and unified shift phenomenology is needed.

Hence in 2017 [Haase et al., 2017] did an extensive literature review and collected all Cu shifts measured by groups from around the world. They corrected the shift data where a different reference was used for the orbital shifts and focused on the Cu shift anisotropy. They found that the calculated and measured orbital shifts for $c \perp B_0$ were in agreement; however, the calculated $c \parallel B_0$ orbital shift was too small and the measured $(T \rightarrow 0)$ values of the $c \parallel B_0$ shifts appeared to be family specific. Furthermore, they realized that most materials show a temperature dependence in the shifts measured with $c \parallel B_0$. The data also showed a doping-dependent and isotropic change in the shifts for both directions, which also behaved in a family-specific way.

We later collected and analyzed all available cuprate shift and relaxation data from planar ^{63}Cu, ^{17}O, and also ^{89}Y. From this endeavor, a new phenomenology emerged. This thesis focuses on the insights gained from it.

In the first step, we focused on all available Cu NMR shifts. The analysis of the Cu shifts revealed a suppression of the shifts for both directions of the magnetic field in dependence on doping, i.e., smaller shifts as doping is lowered, with the shifts for materials with the highest doping showing metallic behavior (for which the Korringa relation also holds). To explain the data, we invoked a two-spin component scenario, where one component is due to the onsite spin from the Cu $3d(x^2 - y^2)$ hole, and another due to planar O. In this scenario, the large discrepancy between the calculated and experimental orbital shift for one direction of the magnetic field $(c \parallel B_0)$, and the complex shift anisotropy, could be explained by a negative shift in the $c \parallel B_0$ direction. [Avramovska et al., 2020]

We further collected and analyzed all Cu relaxation data. This revealed a very simple phenomenology, namely ubiquitous relaxation across all families and all doping levels (for $c \perp B_0$ only). The relaxation anisotropy differs between systems, however, it always remains temperature independent [Jurkutat et al., 2019]. Moreover, the relaxation showed signature Fermi-liquid like behavior for all the systems. This revealed that it is, in fact, the suppression of the shifts and not an enhancement of relaxation that is behind the failure of the Korringa relation.

The planar O data from all the cuprates also showed quite a simple scenario. A temperature-independent pseudogap at the Fermi surface of a simple metal governs O shift and relaxation data. The density of states outside this gap is the same for all the cuprates, irrespective of doping and material, also true for highly overdoped materials with no pseudogap. The O shift and relaxation anisotropies for all the cuprates are in accord with theoretical hyperfine coefficients. The anisotropic O orbital shifts also agree with what was expected from first principles calculations, [Nachtigal et al., 2020] [Avramovska et al., 2022a].

The early ^{89}Y data, which marked the discovery of the pseudogap in the cuprates, are also governed by the same temperature-independent pseudogap and a metallic density of states. [Avramovska et al., 2022a]

Lastly, to reconcile the new insights gained from the analysis of all O data with the complicated Cu hyperfine scenario, we compared O and Cu shifts. It became clear that the suppression of the Cu shifts is due to the same temperature-independent pseudogap as seen in the O data. Nevertheless, the family dependence of the Cu shifts for $c \parallel B_0$ direction could not be explained by assuming only a temperature-independent pseudogap and a metallic density of states, pointing to a two-component scenario. [Avramovska et al., 2022b]

The Cu relaxation, in contrast to O, is not influenced by the pseudogap. However, it is the only parameter that clearly shows the onset of T_c.

In the following chapters, I give an introduction into the topic of high-temperature superconducting cuprates (chapter 2) and introduce some basic concepts of NMR (chapter 3). Then, in chapter 4, follows a presentation of six publications with summaries at the beginning, where the details of the above mentioned findings are laid out.

Chapter 2

High-T_C superconducting cuprates

The successful efforts in liquefying Helium in the laboratory of Kammerlingh Onnes in 1908 opened up a perfect opportunity to test the behavior of resistivity in metals at low temperatures. At that time, several contradicting theories persisted; however, without the necessary technology to reach low temperatures, the theories remained hypothetical. Elemental mercury was chosen to investigate resistivity at low temperatures due to the possibility of purifying mercury with repeated distillations. In 1911 Kammerlingh Onnes made the unexpected observation of the resistivity's rapid drop to zero below 4.5 K. This marked the discovery of conventional superconductivity, [Onnes, 1911]. Shortly after, it was discovered that other metals, like tin or lead, are also perfect conductors below a certain critical temperature T_c, [de Bruyn Ouboter, 1987].

A great effort followed to explain the phenomenon of superconductivity. Still, it wasn't until 1957 that Bardeen, Cooper, and Schrieffer (BCS), [Bardeen et al., 1957] would propose a microscopic quantum theory of superconductivity. It is based on the idea that an interaction of electrons with lattice vibrations, phonons, leads to an electron pairing mechanism and the formation of the so-called Cooper pairs—a pair of electrons with opposite spin and momentum—with a total spin of zero. For their theory, Bardeen, Cooper, and Schrieffer were awarded the Nobel Prize in 1972.

Finally, the explanation of superconductivity had been put forward, and researchers worldwide were already thinking of ways to enhance T_c. The goal was

to invent a superconductor with a T_c above the boiling point of liquid nitrogen and ideally room temperature. Many materials were invented; however, after some point T_c remained stagnant. The record T_c was achieved in 1974—22 K in Nb_3Ge thin films, [Gavaler, 1973]. Moreover, the highest T_c that the BCS theory allowed for was 30 K. It was clear that in order to achieve superconductivity at high temperatures, one needs to think of a different pairing mechanism. So 22 K remained the record T_c until the discovery of the cuprates.

Bednorz and Müller thought of a different approach. They considered a lattice-mediated pairing mechanism, however, not in terms of classic phonons but in terms of the Jahn-Teller polaron mechanism [Bednorz and Müller, 1986]. The idea behind the Jahn-Teller effect is that lattice distortions can lift the degeneracy of electronic states and lower the ground state energy, [Englman and Englman, 1972]. The Jahn-Teller polaron describes the coupled electron-lattice mobile objects.

Since Cu^{2+} is a strong Jahn-Teller ion, Bednorz and Müller focused on cuprates in their search for high-temperature superconductivity. In 1986 they reported their results on superconductivity in the cuprate La-Ba-Cu-O system, [Bednorz and Müller, 1986]. Shortly after, the efforts in pressure experiments led to the discovery of $YBa_2Cu_3O_{7-\delta}$, the first cuprate with a T_c above the boiling point of liquid nitrogen, [Wu et al., 1987].

Nowadays, dozens of cuprate superconductors have been invented; they vary in composition and T_c, but most of the underlying properties are similar across all these materials. The highest known transition temperature has increased up to 135 K and even up to 165 K under a pressure of 31 GPa in triple layered $HgBa_2Ca_{m-1}Cu_mO_{2m+2+\delta}$, [Gao et al., 1994].

Nevertheless, even after the intense efforts of more than half a century, both experimental and theoretical, there is still no comprehensive theory explaining the origin of high-temperature superconductivity in the cuprates.

2.1 Structure of high-T_c cuprates

The superconducting cuprates are perovskite-type ceramic materials. They have a layered structure consisting of CuO_2 planes stacked between charge reservoir layers

which have insulating properties and ensure charge neutrality and crystal stability. The composition of the charge reservoir layers can be varied, giving rise to a large number of cuprate materials.

The CuO_2 planes are conducting and are responsible for superconductivity in these materials. As an example, Fig. 2.1 **(A)** shows the structure of $La_{2-x}Sr_xCuO_4$. More details on the structure and structural phases of the cuprates can be found in [Pickett, 1989] and [Cava, 2000].

The CuO_2 plane consists of Cu^{2+} ions, with $3d^9$ configuration and O^{2-} ions with $2p^6$ configuration. Due to the crystal field, the degeneracy of the d orbital is lifted and we have fully filled four d orbitals (xz, yz, xy and $3z^2 - y^2$), whereas the orbital with the highest energy $x^2 - y^2$ is half filled. The Cu $3d(x^2 - y^2)$ orbital hybridizes with the $2p_\sigma$ orbitals of the four surrounding oxygens forming a square planar arrangement (see Fig. 2.1, **(B)**) [Pickett, 1989].
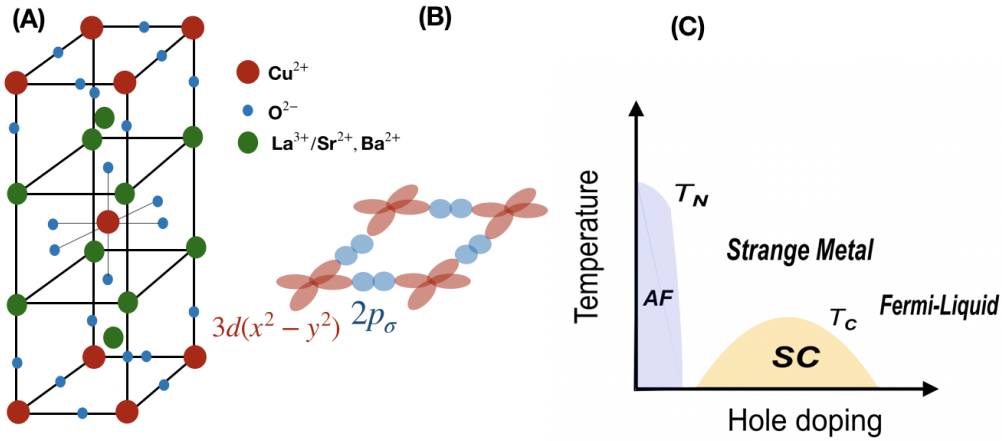

Figure 2.1: **(A)** shows the structure of a single-layered, T-structured cuprate, $La_{2-x}Sr_xCuO_4$. **(B)** shows the CuO_2 plane with the indicated bonding orbitals. The Cu $3d(x^2 - y^2)$ orbital hybridizes with the $2p_\sigma$ orbitals of the four surrounding oxygens forming a square planar arrangement.**(C)** Sketch of the temperature vs hole doping cuprates phase diagram based on $La_{2-x}Sr_xCuO_4$.

Depending on the composition of the charge reservoir layer, the cuprates can be classified into several families, such as Tl-based, La-based, Y-based, or Hg-based.

They can also differ in their layering schemes. In single-layered cuprates, e.g., $\mathrm{La_{2-x}Sr_xCuO_4}$, each single $\mathrm{CuO_2}$ layer is separated by two layers of LaO. The $\mathrm{CuO_2}$ planes can also be stacked on top of each other and embedded between two charge reservoir layers, resulting in double or triple-layered systems. This way of layering the $\mathrm{CuO_2}$ plane was also found to affect T_c, with maximum T_c arising for triple-layered systems.

2.2 Basic phenomenology of the cuprates

The phase diagram of the hole-doped cuprates (in this case based on $\mathrm{La_{2-x}Sr_xCuO_4}$) is shown in Fig. 2.1, **(C)**. The undoped parent compound shows Cu-based antiferromagnetic, insulating properties, although according to band structure, the parent material ought to be a metal. This is due to the strong Coulomb interaction between electrons. As more holes—or electrons in the case of electron-doped cuprates—are introduced, done by altering the charge reservoir layers, i.e., by replacing some of the atoms in the charge reservoir layer with atoms with a different oxidation state (in $\mathrm{La_{2-x}Sr_xCuO_4}$, $\mathrm{La^{3+}}$ is replaced by $\mathrm{Sr^{2+}}$), the antiferromagnetic state is broken and we move along the phase diagram. For example, hole doping suppresses antiferromagnetism and T_N, c.f., Fig. 2.1 **(C)**, rapidly decreases as doping increases. In the underdoped regime, various phases appear, e.g., charge density waves, spin density waves, nematic order, and the pseudogap. In the pseudogap regime, multiple methods, including NMR, report the opening of an energy gap. Adding more holes results in superconductivity, where the superconducting transition temperature has a dome-like dependence, with materials at optimal doping (at $x \approx 0.15$) exhibiting the highest T_c. At temperatures above superconductivity is the so-called strange metal phase since the materials show metallic-like properties. However, here the resistivity is $\propto T$, unlike $\propto T^2$, as it is in normal metals. Upon further doping, the materials show typical metallic-like properties.

The orbital hole content on Cu and O had become available through NMR measurements. The hole content on the Cu $3d(x^2 - y^2)$ and O $2p_\sigma$ orbitals was shown to be directly related to the experimentally measured NMR quadrupole frequencies

$^{63}\nu_Q$ and $^{17}\nu_Q$, with prefactors derived from atomic spectroscopy [Haase et al., 2004]. [Rybicki et al., 2016] showed that a better way of looking at the phase diagram is not in terms of average doping level but in terms of the oxygen hole content on the $2p_\sigma$ bonding orbital, n_p, and the Cu hole content on the $3d(x^2 - y^2)$ orbital, n_d. Moreover, they pointed out that $n_P \propto T_c$, i.e., T_c increases as the oxygen hole content, n_P, increases at the cost of the Cu hole content n_d. The sharing of the hole content between Cu and O appears to be a family-specific property, as shown in [Jurkutat et al., 2014] and at $\zeta = 0$, i.e., in the parent materials, there are already differences between families, while the relation:

$$1 + \zeta = n_d + 2n_p \tag{2.1}$$

holds for all materials, both hole and electron-doped. The parameter ζ was introduced in [Avramovska et al., 2019] and is the doping as measured by NMR. For example, in $\mathrm{La_{2-x}Sr_xCuO_4}$ $\zeta = x$, however, it is not always the case, as shown in [Jurkutat et al., 2021], where the superconducting domes do not always fall on top of each other in a $T - \zeta$ phase diagram.

Adding or removing holes is not the only way to move along the phase diagram. It can also be achieved by varying pressure. It was known long ago that T_c in the cuprates could be increased with pressure, [Schilling, 2007]. Recently, NMR experiments at high pressure showed that pressure changes the local doping and also the redistribution of planar Cu-O orbital hole content, [Jurkutat et al., 2021].

Chapter 3

Basics of nuclear magnetic resonance

Nuclear magnetic resonance is a widely used and versatile technique that provides important information about the properties of materials and it is especially powerful for studying condensed matter.

This chapter is a brief introduction to the basic concepts of NMR, which are needed to follow the results of this thesis.

Some of the strengths of NMR are that it is a bulk probe with which we can investigate the full sample. It is also a non-destructive technique since only radio-frequency pulses are used and power ranges remain low. NMR can probe any system on the condition that it has nuclei with non-zero nuclear spin. Various sample sizes can be investigated, ranging from a few μm to several meters. NMR is also site-specific, so nuclei that are in different surroundings can be studied effectively. We can also count the number of nuclei in a sample, making NMR a quantitative technique. We can also study both magnetic and electric properties (for nuclei with nuclear spin $I > 1/2$) of materials.

These strengths and the plethora of information that can be gained through NMR, makes its applications widespread, ranging from medicine to material science to even some applications in oil logging.

The NMR setup is quite simple. One needs to place the sample in a large and homogeneous magnetic field, in order to polarize the nuclear spins and make them precess around this field. Furthermore, a perpendicularly placed coil of conducting wire is wound around the sample. This is used in order to send RF pulses to excite the nuclear spins and to pick up any signal arising from the induced voltage of the precessing nuclear spins. Then this signal is recorded and analyzed.

The literature on NMR is quite abundant; therefore, in this chapter, I will focus solely on brief explanations of basic concepts that are relevant for following the results described in this dissertation. More detailed discussions can be found in [Slichter, 1990], [Abragam, 1961], [Levitt, 2013], [Walstedt, 2007], and this chapter follows the work therein.

3.1   Nuclear magnetism

If the number of protons and neutrons in a given nucleus is odd, then they have a nuclear spin larger than zero. Nuclei with spin posses a magnetic moment given by $\vec{\mu} = \hbar\gamma\vec{I}$, where γ is the gyromagnetic ratio which is a constant specific to each isotope and $\vec{I}$ is the nuclear spin vector. $\vec{I}$ is a typical angular momentum vector. In a simple classical picture, one can think that once the nuclear spin is placed in a magnetic field, the field would cause it to precess along its direction. The frequency of precession is given by the Larmor frequency:

$$\omega_0 = -\gamma B_0 \tag{3.1}$$

The Larmor frequency is fixed by the IUPAC convention for all the nuclei and gyromagnetic ratios [Harris et al., 2008] in the given external fields.

When placed in an external magnetic field, B_0, a nucleus with non-zero spin, will experience Zeeman splitting into $(2I + 1)$ energy levels (See Fig. 3.1). In a quantum mechanical sense nuclei with spin can be in one of their $(2I + 1)$ spin angular momentum eigenstates, denoted by the wavefunctions $|I, m\rangle$, with I being the nuclear spin quantum number and m the spin substates. The energy eigenvalues

of the Zeeman Hamiltonian are given by:

$$E_m = -\gamma\hbar B_0 m \tag{3.2}$$

The energy levels are equally spaced with:

$$\Delta E = \gamma\hbar B_0 = \hbar\omega_0 \tag{3.3}$$

Typically, in NMR, an alternating magnetic field, perpendicular to the static field, is applied. This field is applied at frequencies which match the transition energies (ω_0) and it excites transitions between energy levels.

By applying an external magnetic field, the degeneracy of the energy levels is lifted and the population of the energy levels follows the Boltzmann distribution, i.e., $p_m \propto \exp(-E_m/k_B T)$. After a certain characteristic time, the spins placed in an external magnetic field will develop the following population difference between energy levels.

$$\frac{p_m}{p_{m-1}} = \exp\left\{\frac{\Delta E}{k_B T}\right\} = \exp\left\{\frac{\hbar\gamma B_0}{k_B T}\right\} \tag{3.4}$$

Correspondingly, a net magnetization $\langle M_z\rangle$ builds up along the axis of the external field B_0, and we have (in the high temperature limit, $\hbar\gamma B_0 << k_B T$) the Curie law:

$$\langle M_z\rangle = \frac{N}{V}\frac{\gamma^2\hbar^2 I(I+1)}{3k_B T}B_0 \tag{3.5}$$

The macroscopic net magnetization is probed with NMR and Eq. 3.5 shows that the NMR signal is dependent on field, temperature, and the spin density. The signal intensity is what gives us the quantitative information.

3.2 Perturbing the Zeeman hamiltonian

Nuclei in solids do not solely interact with the external magnetic field but also with other nuclei and electrons in their environment. These interactions are small com-

pared to the Zeeman Hamiltonian and can be treated with perturbation theory. They can be measured as shifts of the resonance frequency when compared to the Larmour frequency, or they can also influence the relaxation processes.

3.2.1   Hyperfine interaction

The interaction of the nuclear spin with the surrounding electrons is called hyperfine interaction. The hyperfine Hamiltonian is given as:

$$\mathcal{H}_{HF} = 2\gamma\hbar\mu_B\vec{I}\cdot\left[\frac{\vec{l}}{r^3} - \frac{\vec{s}}{r^3} + s\frac{\vec{r}(\vec{s}\cdot\vec{r})}{r^5} + \frac{8}{3}\pi\vec{s}\delta(r)\right] \tag{3.6}$$

where $\vec{l}$ and $\vec{s}$ are the orbital and spin angular momentum vectors, and μ_B is the Bohr magneton.

The first term of the hyperfine Hamiltonian describes an orbital interaction, the second, and third terms describe a dipolar interaction and the final term is the Fermi-contact term. The Fermi-contact term (or s-contact term) describes dipolar interaction for which $\vec{r} \to 0$, as is the case for electrons in s-wave orbitals.

These interactions affect the local field that the nucleus experiences, thus causing a shift of the resonance frequency ω_0. The shift K can be expressed as:

$$K = \frac{\omega_0 - \omega_L}{\omega_L} = A_{hf}\chi \tag{3.7}$$

where A_{hf} is the hyperfine coupling constant and χ is the susceptibility arising from the different terms in (3.6).

3.2.2   Dipolar interaction

Another interaction that causes a magnetic field at the nucleus is the dipole-dipole interaction between same or different nuclei. The interaction Hamiltonian is given by:

$$\mathcal{H}_D = \gamma_1\gamma_2\hbar^2\vec{I}_1\cdot\left[\frac{\vec{I}_2}{r^3} - 3\frac{\vec{r}(\vec{I}_2\cdot\vec{r})}{r^5}\right] \tag{3.8}$$

In the case of liquids, due to the rapid motion of the moments, the dipolar interaction is averaged; however, in solids the dipolar coupling causes a B_0 independent broadening of the linewidth. Since the dipolar interaction depends on the angle between the internuclear axis and the external magnetic field, it can vanish for angles $\theta \approx 54.74°$, called the magic angle.

3.2.3 Quadrupolar interaction

Nuclei with spin $I > 1/2$ additionally possess a quadrupole moment. The electric charge of the nucleus is non-uniformly distributed; this causes an electric field gradient (EFG) with which the nuclear spin's magnetic moment interacts.

The quadrupole Hamiltonian is written as:

$$\mathcal{H}_Q = \frac{e^2 q Q}{4I(2I-1)} \left[3I_z^2 - \vec{I}^2 + \frac{1}{2}\eta(I_+^2 + I_-^2) \right] \tag{3.9}$$

Where Q is the nuclear quadrupole moment, η is the asymmetry parameter, $(0 < \eta < 1)$. The quadrupole frequency can be expressed as $\nu_Q = \frac{3eQV_{ZZ}}{2I(2I-1)}$, where V_{ZZ} is a principal component of the traceless EFG tensor, conventionally assigned as $|V_{xx}| \leq |V_{YY}| \leq |V_{ZZ}|$ and the anisotropy is defined as: $\eta = (V_{XX} - V_{YY}/V_{ZZ})$.

Considering the case where $\mathcal{H}_{\mathcal{Z}} > \mathcal{H}_{\mathcal{Q}}$, and integer spin nuclei, there is a shift of the frequency in 1st order for transitions $m \to m + 1$:

$$\delta\nu_Q = -\nu_Q(m - \frac{1}{2})\frac{3\cos^2\theta - 1}{2} \tag{3.10}$$

The central transition is not affected by the quadrupole interaction in 1st order, however it is affected in 2nd order.
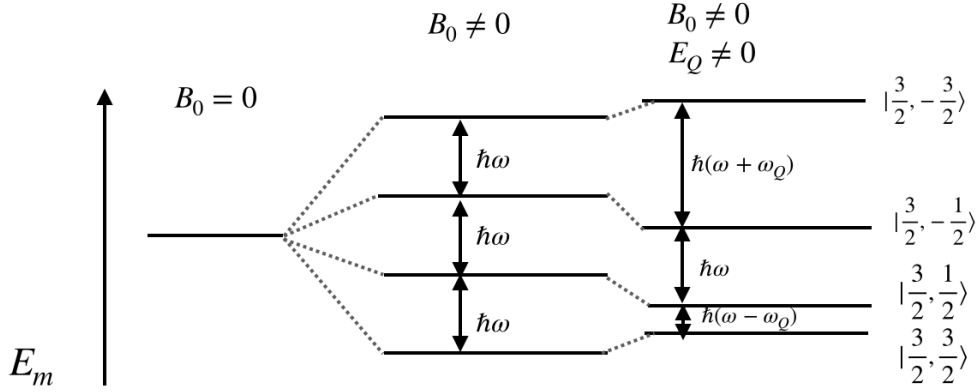
Figure 3.1: Sketch of the Zeeman and the first order quadrupole energy levels for an $I = 3/2$ spin system. The Zeeman interaction lifts the degeneracy of the energy levels at $B_0 \neq 0$, and the energy levels are uniformly separated. An EFG further changes the energy levels producing first-order satellites in the spectrum.

3.2.4 NMR relaxation

In an NMR experiment the equilibrium magnetization in z-direction, $\langle M(0)_z \rangle$, is flipped into the xy-plane by applying an alternating magnetic field:

$$B_{RF} = 2B_1 \cos wt \tag{3.11}$$

depending on the pulse duration, the magnetization can be flipped by an angle $\theta = \gamma B_1 \tau$. If $\gamma B_1 \tau_{\pi/2} = \pi/2$, then the magnetization is flipped in the laboratory xy-plane. After this pulse, the flipped magnetization, which now precesses in the xy-plane and therefore induces a voltage in the RF-coil (which we detect), will dephase and relax to its equilibrium state given in Eq. (3.5). Consequently, the signal decays, and we have what is called a free induction decay (FID).

The characteristic time that describes the relaxation of the magnetization to its equilibrium value is the spin-lattice relaxation time, or T_1.

The longitudinal spin-lattice relaxation arises due to an interaction of the nuclear

spins with the "lattice" which acts as a thermal bath. If we put a spin system in a magnetic field, due to perturbations of the Zeeman term (through a coupling of the spin system to the thermal bath; this can be the influence of phonons, impurities, etc), we have a population difference given by Eq.(3.4), and we have a build-up of magnetization.

The magnetization follows:

$$M(t) = M_0(1 - e^{t/T_1}) \qquad (3.12)$$

with T_1 being the characteristic time it takes for the magnetization to build up.

For quadrupolar nuclei the situation is somewhat more complicated if $\nu_Q \neq 0$, and the magnetization can be described as:

$$M(t) = M_0 \left(1 - b \cdot \sum_{i=1}^{2I} a_i e^{-\lambda_i t} \right) \qquad (3.13)$$

The scenarios that lead to eq. (3.13) are described in [Suter et al., 1998] and the references therein.

Another type of relaxation is the spin-spin or T_2 relaxation. It arises due to a loss of phase coherence of the nuclear spins in the xy plane, leading to a loss of measurable signal. This type of decay is not a result of heat exchange with the lattice and is usually shorter than T_1.

After the spins have been flipped to the xy-plane they lose coherence depending on the distribution of the local fields that the nuclei experience. If the distribution is Lorentzian, then the FID has an exponential decay.

Sometimes, the dephasing of the magnetization after a $\pi/2$ pulse is too quick; hence, due to the NMR spectrometer dead time the FID can not be detected. In this case, a Hahn-echo sequence is used and the magnetization is refocused following a π pulse.

3.3 Shift and relaxation in metals and BCS superconductors

The shift of the resonant frequency is usually measured with respect to a reference frequency of the same nucleus, resonating in a different material, but under identical conditions (and for which the real shift is known). It is usually expressed in percentage.

$$K = \frac{\omega - \omega_{ref}}{\omega_{ref}} \tag{3.14}$$

The measured shift is usually comprised of a spin shift part K_s, i.e., the shift arising from the hyperfine interaction of the nucleus with the spins of the surrounding electrons and orbital shift K_L—the shift arising due to the orbital angular momentum of the electrons coupling to the nucleus.

The shift is expressed in field independent form as:

$$\omega = \gamma B_0 (1 + K) \tag{3.15}$$

where $K = K_s + K_L$ is the total shift.

For shift referencing, it is important to use a reference sample where the shift does not contain a large paramagnetic (Van Vleck) contribution and is largely dominated by core electrons.

From the hyperfine interactions, represented in Eq. (3.6), the Fermi-contact term has the largest effect on the nucleus, in metals. It was measured for the first time by W.D.Knight [Knight, 1949], and is also called Knight shift.

For a metal, usually, Eq. (3.7) is used where χ is the conduction electrons' Pauli susceptibility and $A_{hf} = \frac{8\pi}{3} \langle |\psi_s(0)|^2 \rangle_{FS}$, where $\langle |\psi_s(0)|^2 \rangle_{FS}$ is the square of the wave function at the nucleus averaged over the Fermi surface.

The magnetic interaction of the nucleus with the conduction electrons in metals also gives rise to the spin-lattice relaxation mechanism. Similarly, as for the Knight shift, the Fermi-contact term dominates, resulting in a proportionality between $1/T_1$ and T, known also as the Heitler-Teller relation for relaxation in metals

[Heitler and Teller, 1936], derived already in 1936, before the advent of NMR.

Korringa later proposed a relation between the Knight shift and relaxation, famously known as Korringa relation, [Korringa, 1950]:

$$T_1 T K_s^2 = \frac{\hbar}{4\pi k_B T} \left(\frac{\gamma_e}{\gamma_n} \right)^2 \tag{3.16}$$

Fig. 3.2 shows the dependence of the relaxation, **(A)**, and shift, **(B)**, in dependence of temperature, for metals.
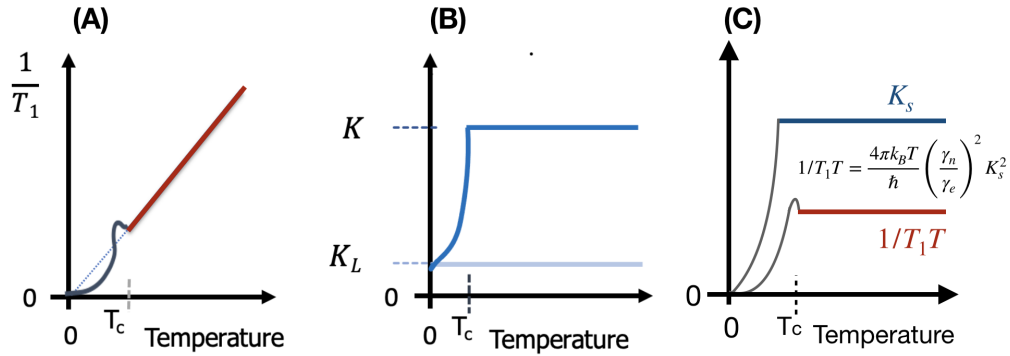

Figure 3.2: **(A)** In normal metals, the relaxation rate is proportional to temperature ($1/T_1 \propto T$). For BCS superconductors, we observe a rapid drop of relaxation at T_c due to spin-singlet pairing and the appearance of a coherence peak. **(B)** The spin shift (K_s) for normal metals is temperature independent. For BCS superconductors, we observe a rapid disappearance of spin shift at T_c due to spin-singlet pairing. **(C)** Shows the spin shift (K_s) and $1/T_1 T$, with the indicated coherence peak at T_c. In metals, the shift and relaxation are related through the Korringa relation: $T_1 T K^2 = (\hbar/4\pi k_B T)(\gamma_e/\gamma_n)^2$.

Before the invention of the BCS theory for classical superconductors, the "two-fluid" model was a popular way of thinking at the time. According to this model, it was expected that the spin-lattice relaxation rate in classical superconductors, given by the interaction with the conduction electrons, should decrease rapidly with temperature due to the decrease of the electronic density of states. Hebel and Slichter measured the temperature dependence of the relaxation rate of Al and found that

quite the opposite was true. The relaxation rate increased right below T_c and then decreased rapidly, [Hebel and Slichter, 1959]. A gap in the density of states at T_c could easily explain this increase. Shortly after, the BCS theory was invented, and it was shown to be in perfect agreement with these NMR results. BCS predicted that the density of states in superconductors has an energy gap and a peak at the edge. Following the BCS theory, it is expected for T_1, [Schrieffer, 2007]:

$$\frac{1}{T_1} \propto e^{\frac{-\Delta_0}{k_B T}} \tag{3.17}$$

Where Δ_0 is the gap at $T = 0$. The NMR results also provided information on the type of pairing below T_c, which was shown to be spin-singlet.
A more complete test of the BCS theory was done by [Masuda and Redfield, 1962] using T_1 measurements of Al.

The NMR shift in classical superconductors is expected to vanish as $T \to 0$, i.e., χ vanishes since there is no magnetic moment at $T = 0$. Yosida derived an expression for the Knight shift, [Yosida, 1958], demonstrating the exponential decay of the susceptibility due to spin-singlet pairing.

Chapter 4

Toward a new phenomenology of the cuprates

4.1 Understanding Cu NMR shift and relaxation data

This chapter focuses on the Cu NMR shift and relaxation data. Here, three published papers will be presented.

The first publication deals with a subset of Cu shift and relaxation data (only measured in $c \perp B_0$ direction). An account of the full set of Cu shifts was published earlier in 2017. It showed stark differences between the cuprates, i.e., most strikingly, the Cu shift anisotropy assumed several characteristic slopes. Since the Cu shift $^n K_d(T)$ can be measured for different directions of the B_0 field, d, and for different nuclei, n, the requirement for a single component picture would be that $\Delta^n K_d(T) \propto \Delta^m K_e(T)$. As this is not the case for most of the shift data, the explanation using the old magnetic hyperfine scenario and a single spin component does not suffice. These findings gave rise to an interest in relaxation and we began a literature survey of all Cu relaxation data. The data revealed that Cu relaxation is independent of material and doping and only influenced by T_c, where we observe a sudden drop. Moreover, the Cu relaxation is Fermi-liquid like, i.e., proportional to

temperature—in a certain range right above T_c —and the Korringa relation holds for some cuprates—those with highest doping. With the relaxation being similar for all systems, it could be concluded that the failure of the Korringa relation is due to a suppression of the shifts and not due to an enhancement of relaxation, as assumed early on [Walstedt et al., 1988].

We proposed a simple model with two electronic spin components to explain the shift data. One of the components couples through an isotropic hyperfine constant with the nuclei, the other, as expected from the partially filled $3d(x^2 - y^2)$ orbital, is responsible for the anisotropic term. We also assume a coupling between the components, already found in [Haase et al., 2009]. Nevertheless, at that point, we could not account for the outliers in the data—$La_{2-x}Sr_xCuO_4$ is an outlier for both shift and relaxation—and our model could not explain the Cu relaxation.

In the next paper, we presented a more complete phenomenology of Cu relaxation. There, all literature Cu NMR relaxation data were collected and analyzed—both directions of the magnetic field were taken into account. It was concluded that the relaxation rates measured with $c \perp B_0$ are indeed similar for all systems, irrespective of doping and family, apart from only a varying and temperature-independent relaxation anisotropy, which seemed to be family and doping-dependent. For the most overdoped systems, the hallmark Fermi-liquid behavior could be observed, i.e., $1/T_1 \propto T$, with rapid drops at T_c. What is striking is that also systems with lower doping exhibit a similar temperature-dependence, and $1/T_1T$ reaches a value of $1/T_1T \approx 21$K/s for all systems. This value also seems to agree with the Korringa relation, using the shifts of the highly overdoped samples, as pointed out in the previous paper.

In the third paper, we revisit the Cu shift and relaxation data, as well as provide a model explaining Cu relaxation, while also accounting for the $La_{2-x}Sr_xCuO_4$ outlier data. Similarly as in the previous paper, we suggest a two-component model, where the two components are due to the Cu $3d(x^2 - y^2)$ spin density, which couples to the nucleus through the anisotropic $A_{\perp,\parallel}$ hyperfine coefficient and another likely due to O $2p_\sigma$, coupling to the nucleus through an isotropic hyperfine, B. The characteristic slopes in the shift anisotropy plots—including the $La_{2-x}Sr_xCuO_4$ data—can

be explained as changes in the individual spin components as a function of temperature and doping. There is a substantial spin shift left for $c \parallel B_0$ at $T \approx 0$, which accounts for the discrepancy with the calculated orbital shifts for $c \parallel B_0$ direction, [Renold et al., 2003].

The relaxation can be explained in the simple fluctuating field model by assuming fast electronic, Fermi liquid-like, and correlated spin fluctuations acting on the Cu nucleus through two different hyperfine coefficients. The onsite $3d(x^2 - y^2)$ spin is much larger (about 10 times) than the spin due to its $2p_\sigma$ neighbor. The variations in the Cu relaxation anisotropy can be explained by a change of the neighboring spin density as a function of doping and material. The $La_{2-x}Sr_xCuO_4$ relaxation data could also be accounted for in this model.

ORIGINAL PAPER

Properties of the Electronic Fluid of Superconducting Cuprates from ^{63}Cu NMR Shift and Relaxation

Marija Avramovska[1] · Danica Pavićević[1] · Jürgen Haase[1] ●

Abstract

Nuclear magnetic resonance (NMR) provides local, bulk information about the electronic properties of materials, and it has been influential for theories of high-temperature superconducting cuprates. NMR reported early that nuclear relaxation is much faster than what one expects from coupling to fermionic excitations above the critical temperature for superconductivity (T_c), i.e., what one estimates from the Knight shift with the Korringa law. As a consequence, special electronic spin fluctuations have been invoked. Here, based on literature relaxation data, it is shown that the electronic excitations, to which the nuclei couple with a material and doping-dependent anisotropy, are rather ubiquitous and Fermi liquid-like, i.e., they are only affected by T_c not the pseudogap. A suppressed NMR spin shift rather than an enhanced relaxation leads to the failure of the Korringa law for most materials. Shift and relaxation below T_c support the view of suppressed shifts, as well. A simple model of two coupled electronic spin components, one with $3d(x^2 - y^2)$ orbital symmetry and the other with an isotropic s-like interaction, can explain the data. The coupling between the two components is found to be negative, and it must be related to the pseudogap behavior of the cuprates. We can also explain the negative shift conundrum and the long-standing orbital shift discrepancy for NMR in the cuprates.

Keywords Cuprates · NMR · Electronic properties

1 Introduction

Nuclear spins are powerful quantum sensors of their local electronic environment, so that the versatile methods of nuclear magnetic resonance (NMR) can be decisive for theories of condensed matter systems. However, deciphering the nuclear response is usually not a straightforward task if microscopic theory is missing, as is the case for high-temperature superconducting cuprates. Nevertheless, NMR contributed vital information for the understanding of these materials, early, e.g., concerning singlet pairing and the pseudogap [1, 2]. Through magnetic shift and

✉ Jürgen Haase
j.haase@physik.uni-leipzig.de

Marija Avramovska
marija.avramovska@hotmail.com

Danica Pavićević
danicas.dp@gmail.com

[1] Felix Bloch Institute for Solid State Physics, University of Leipzig, Linnéstr. 5, 04103, Leipzig, Germany

nuclear relaxation, NMR can sense the field-induced electronic moments and local fluctuating fields, respectively, both related to the electronic susceptibilities. In addition, the electric quadrupole interaction, e.g., of Cu and O nuclei in the ubiquitous CuO_2 plane, allows for the determination of the local charge [3–5].

For useful conclusions, however, the hyperfine interactions have to be known. For the electric interaction, a convincing understanding could be achieved only recently [6], which led to, e.g., the discovery of the correlation between the sharing of charge between planar Cu and O, and the maximum T_c [7], as well as the measurement of charge ordering in the unit cell [8]. The fact that the charges at planar Cu and O are shared quite differently between the families that have different maximum T_c values suggests that one might expect fundamental differences between different cuprate families in terms of magnetic shift and relaxation, as well.

The magnetic hyperfine scenario was established rather early [9, 10], predominantly on the $YBa_2Cu_3O_{6+y}$ family of materials. Here, the consequences of the apparent $3d(x^2 - y^2)$ hole of Cu^{2+} were investigated, and indeed, the quadrupole splitting of Cu was found to be in qualitative

agreement with such a hole [3]. However, and surprisingly, a related negative spin shift that must arise from such a hole is not observed [3, 9]. Rather, the total shift was found to be positive [9]. Moreover, at lower doping, the shift is temperature (T)-dependent, even above the superconducting transition temperature (T_c), which marked the discovery of a spin gap above T_c [11]. However, this shift was not T-dependent for Cu when the magnetic field is perpendicular to the CuO_2 plane.

This mysterious behavior was interpreted as an accidental cancellation of the spin shift from a very anisotropic sum of hyperfine coefficients $A_\alpha + 4B'$, where A_α is anisotropic due to the $3d(x^2 - y^2)$ orbital and B' an isotropic transferred coefficient from the neighboring four Cu atoms in a single band scenario (B' in order to distinguish it from B as introduced later). With this explanation of the shifts, a single electronic spin component could be salvaged and was supported by measurements on two materials [10, 12]. One problem with the understanding of the shifts is the separation of orbital and spin shift contributions, and one adopts the following chain of arguments. Orbital shift is not temperature-dependent, and since a temperature-dependent component is observed, it is taken as the spin shift term. Furthermore, since there is singlet pairing, the spin shift should nearly disappear at low temperatures for all directions of the field. The thus deduced orbital shifts fit the single ion estimates for Cu orbital shift [3] but were not expected to hold for the realistic chemistry of the CuO_2 plane [3].

Nuclear relaxation data, also mostly on the $YBa_2Cu_3O_{6+y}$ family of materials, were hampered by the assignment of Cu sites in the plain and chain. The Y nucleus, situated between the two CuO_2 planes, showed Fermi liquid relaxation, as well as one Cu site. Surprisingly, it turned out later that the chain site, rather than the planar Cu site was more Fermi liquid-like. More importantly, it appeared that the Korringa relation did not hold and that there must be an about 10-fold increase of relaxation [13]. With $A_\parallel + 4B' = 0$ in one direction, antiferromagnetic fluctuations in a single band scenario would turn this term into a large pre-factor $|A_\parallel - 4B'| \gg 0$ (correlations between neighboring spins are negative), and one could explain the data (but not in connection with other methods, e.g., neutron scattering [14]). With most available measurements for $c \parallel B_0$ (aligned powders and NQR) and material and sample-dependent rates, many approaches were developed to understand shift and relaxation.

Over the last 10 years, it was shown with a set of experiments on different materials that the adopted single-spin component view does not hold, rather, two coupled spin components appear to be necessary to explain the NMR shifts [15–18]. Finally, a simple literature survey of all Cu NMR shifts uncovered significant differences between the cuprates, which points directly to a new shift phenomenology, at odds with the hitherto used hyperfine scenario, and that cannot be understood with a single-spin component [19].

These findings raised the interest in nuclear relaxation, e.g., the apparently large isotropic hyperfine coefficient, and we began gathering the Cu relaxation data. Here, we show that the Korringa relation, (c.f Fig. 1) does nevertheless hold for some cuprates, i.e., those with the highest doping levels. And since the nuclear relaxation is rather similar for all cuprates (only its anisotropy changes among the systems), a suppression of the spin shifts for certain cuprates is behind the failure of the Korringa relation for these systems, not an enhancement of nuclear relaxation. In particular, there cannot be substantial spin fluctuations, except for rather low doping levels where there are no NMR data, and for one outlier system, $La_{2-x}Sr_xCuO_4$, that we find has an additional relaxation mechanism. We propose that a negative coupling between two electronic spin components already found in 2009 [20] is behind the suppression of the shifts, while hardly affecting a universal Fermi liquid–like relaxation.

2 Observations from Shifts and Relaxation

We begin with an overview of results from literature shift and relaxation analyses (for a full review of literature shifts, see [19], and after the first submission of this manuscript, a more comprehensive review of the relaxation was prepared, as well [21]).

Throughout the manuscript, quantities measured with the magnetic field (B_0) parallel to the crystal c-axis ($c \parallel B_0$) are labeled like $\hat{K}_\parallel$ (total magnetic shift), $K_\parallel$ (spin shift), or $1/T_{1\parallel}$ (also the relaxation in NQR measurements carries the same label since it is dominated by crystallites for which the nuclear quantization axis is parallel to c due to quadrupole interaction). Measurements with the magnetic field in the CuO_2 plane ($c \perp B_0$) are labelled like $\hat{K}_\perp$, $K_\perp$, or $1/T_{1\perp}$; note that measurements along special in-plane axes are very rare since c-axis-aligned powders are most easily measured and twinning can be a problem even for single crystals.

2.1 Magnetic Shifts

As mentioned in section 1, early experiments showed that $\hat{K}_\parallel$ is T-independent, while $\hat{K}_\perp(T)$ appears to have a Fermi liquid–like spin component near or above optimal doping in the sense that one observes a decrease as T is lowered. This decrease is more abrupt when it occurs at T_c, but it can also start far above T_c (which is the assumed pseudogap behavior). So it was argued that $\hat{K}_\parallel$ contains no spin shift ($K_\parallel = 0$), only orbital shift contributions ($K_{L\parallel} \approx \hat{K}_\parallel$). The spin shift was only extracted from $\hat{K}_\perp$ by defining as
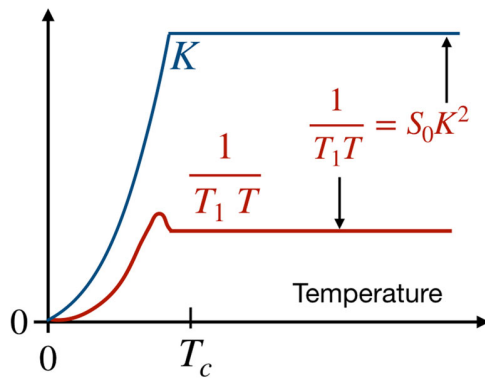
Fig. 1 Fermi liquid shift and relaxation: the spin shift K is temperature-independent above the critical temperature for superconductivity (T_c) and vanishes below it for spin singlet pairing. The nuclear relaxation rate ($1/T_1$) is proportional to the temperature (T) so that $1/T_1 T$ is temperature-independent above T_c, and the Korringa relation holds roughly, where $S_0 = \gamma_n^2 / \gamma_e^2 4\pi k_B/\hbar$ contains only fundamental constants, e.g., the nuclear (n) and electronic (e) gyromagnetic ratios. $1/T_1 T$ vanishes below T_c for singlet pairing. In early analyses of the cuprates, it was found that $1/T_1 T$ is much larger than what was expected from K, and special spin fluctuations were invoked to account for the discrepancy

spin shift $K_\perp = \hat{K}_\perp(T \to 0)$. Since the spin response should be isotropic in the cuprates, this anisotropic behavior was explained with anisotropic hyperfine coefficients, i.e., $A_\parallel + 4B' = 0$, $A_\perp + 4B' \neq 0$ (in the original literature, it was B, not B') [2].

Later, materials were investigated that also showed a significant temperature dependence for $K_\parallel(T)$ (for references, see [19]); however, their shift anisotropy was found to be temperature-dependent [17, 18], which is not expected in a single-spin component scenario. Furthermore, an explanation within the old scenario would require

rather different hyperfine coefficients (up to about 30%), which appears to be unrealistic given the unique CuO_2 plane.

A convenient and useful overview of both shifts can be obtained by plotting $\hat{K}_\perp(T)$ vs. $\hat{K}_\parallel(T)$ [19]. This is illustrated in Fig. 2 that should help understand the real data plotted in the same way in Fig. 3. Note that the total shifts $\hat{K}$ are plotted in order to avoid a biased analysis by subtracting unknown orbital shifts.

Key features of such a plot are the following (cf. [19]). There is a common low temperature shift for $c \perp B_0$, $\hat{K}_\perp(T \to 0) \approx 0.35\%$. It agrees reasonably well with first-principle calculations of the orbital shift that give 0.30% [22]. Interestingly, $\hat{K}_\parallel(T \to 0)$ can be very different for different cuprates.

Different families have slightly different isotropic shift lines (defined by changing doping at high temperatures). New shift reference points are generated where $\hat{K}_\perp(T \to 0) \approx 0.35\%$ intersects isotropic shift lines. These points could define $K_{L\parallel}$, but they are still in strong disagreement with the calculated orbital shift of 0.72% [22] (for the figure origin, we assumed $K_{L\parallel,\perp}$ as found from first-principle calculations).

Different from changes due to doping, as the shifts change as a function of temperature, their anisotropy changes, i.e., the shifts depart from the isotropic shift line in Fig. 3. However, the slopes with respect to temperature, $\delta_T \hat{K}_\perp / \delta_T \hat{K}_\parallel$, appear to be constant in certain ranges of T, which causes the characteristic linear regions in that figure. Characteristic slopes as a function of T are (1) $\delta_T K_\perp / \delta_T K_\parallel \approx 1$ (the same slope as the isotropic shift lines, but here as function of T); (2) a rather steep slope $\delta_T K_\perp / \delta_T K_\parallel \geq 10$; and (3) $\delta_T K_\perp / \delta_T K_\parallel \approx 5/2$. This has been discussed in more detail previously [19].
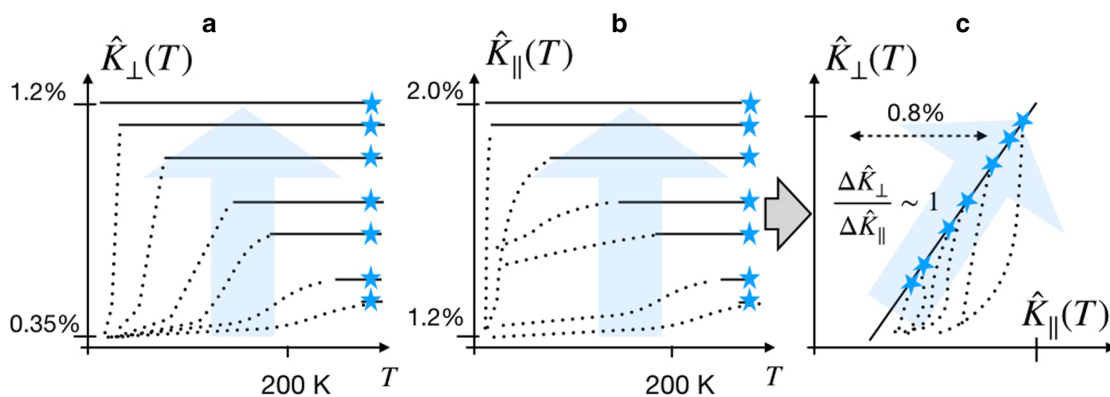

Fig. 2 Sketch of cuprate total magnetic shifts, **a**, $\hat{K}_\perp(T)$, and **b**, $\hat{K}_\parallel(T)$. Increasing the doping (blue arrow) increases the temperature-independent shifts that extend to lower temperatures. Shifts become temperature-dependent at lower T and head for a common value for $\hat{K}_\perp$, but not for $\hat{K}_\parallel$. **c**, a useful overview of the shift is obtained by plotting $\hat{K}_\perp(T)$ vs. $\hat{K}_\parallel(T)$. The high temperature shifts fall on a more or less straight line with slope ~ 1, i.e., an "isotropic shift line" is created by changes in doping, which demands a dominant isotropic hyperfine coefficient. As the shifts become temperature-dependent, they depart from the isotropic shift line with special slopes, but stay in the lower right triangle

Fig. 3 Examples of ^{63}Cu NMR shifts from ref. [19]. $\hat{K}_{\perp}(T_j)$ is plotted against $\hat{K}_{\parallel}(T_j)$ (the *hat* denotes the total magnetic shifts, including orbital shifts). The plot origin reflects first-principle calculations of the orbital shifts of $K_{L\parallel} = 0.72\%$, $K_{L\perp} = 0.3\%$ [22]. Nearly isotropic shift lines are indicated by dashed lines. The maximum high temperature shift increases with doping (x). The arrows indicate T_c (OD, overdoped; OP, optimally doped; UN, underdoped materials, cf. Appendix). Inset: Materials with the highest T_c depart from the isotropic shift line at the NMR pseudogap temperature far above T_c, unlike strongly overdoped systems in the main panel, for which T_c determines the departure point
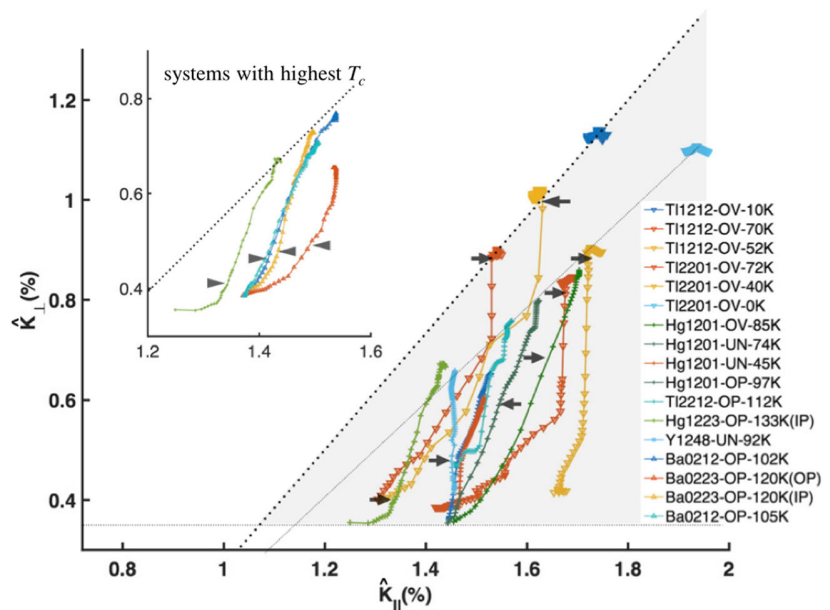
Perhaps the most surprising fact concerns the nearly isotropic change in shift as function of doping, as this points to a large isotropic hyperfine coefficient that has not been discussed so far. In addition, since a variation in temperature can lead to different slopes, one must conclude that different spin components are at play that couple to the nucleus. We do not see a possibility to account for the shift scenario with a single temperature- and/or doping-dependent spin component [19]. These are similar conclusions to those deduced with very different shift experiments [16–18, 20].

2.2 Nuclear Relaxation

Clearly, given the different phenomenology that appears from viewing all the cuprate shifts, one has to take an unbiased look at relaxation data as well. After the first presentation of our short relaxation summary here, we prepared a more comprehensive account that is available now, as well [21].

The few outstanding observations from viewing the relaxation data are the following. First, the relaxation rate $1/T_{1\perp}$ measured for $c \perp B_0$ is rather similar for all cuprates, above T_c. In particular below about 200 K, the most overdoped system that is not superconducting has a similar Fermi liquid–like dependence as an underdoped cuprate (there are not enough data to conclude on strongly underdoped systems). This is seen in Fig. 4 where we plot typical examples (for more data, see [21]). Second, $1/T_{1\parallel}$ behaves differently, but as we show in the inset of Fig. 4, both rates are nearly proportional to each other, above and below T_c. Thus, it is only the relaxation anisotropy that changes among the systems and with doping, from $(1/T_{1\perp})/(1/T_{1\parallel}) \approx 1$ to 3.4. Since there was

a clear emphasis on $1/T_{1\parallel}$ measurements and since some systems were investigated only later, this behavior was not discovered (however, Walstedt et al. noted the anisotropy for YBa$_2$Cu$_3$O$_7$ [13]).

In particular, the relaxation just above T_c is very similar for all (conducting) cuprates in terms of $1/T_{1\perp}T$, i.e., it is material-independent and it does not change very much across the phase diagram. Just above T_c, we have $1/(T_{1\perp}T)(T \gtrsim T_c) \approx 17$ to $25 /Ks$, which gives a shift of about 0.8% from the Korringa relation. Note that this is the maximum shift observed in Fig. 3.

Third, if one includes the differences in anisotropy among different families of materials, the relaxation rates below T_c are very similar, as well (see below).

2.3 Shifts and Relaxation

The fact that the nuclear spins are coupled to an electronic thermal bath with relaxation rates that are nearly independent on material and doping (in particular near T_c) points to a very robust property. This special relaxation rate with $1/T_{1\perp}T \approx 20 /Ks$ is already present at the highest doping levels for systems that must be rather close to a Fermi liquid. It appears to be out of question, then, that these excitations (this liquid) are present in all materials and dominate relaxation above T_c (at higher temperatures, the rate lags somewhat behind, and $1/(T_1T)$ falls off in a characteristic way for more or less all the systems). This conclusion is not weakened by a doping- or material-dependent relaxation for the other direction of the field ($c \parallel B_0$) since both rates are proportional to each other. It rather points to an anisotropic coupling of the nuclear spins to a unique fluid, which can depend on doping and material.
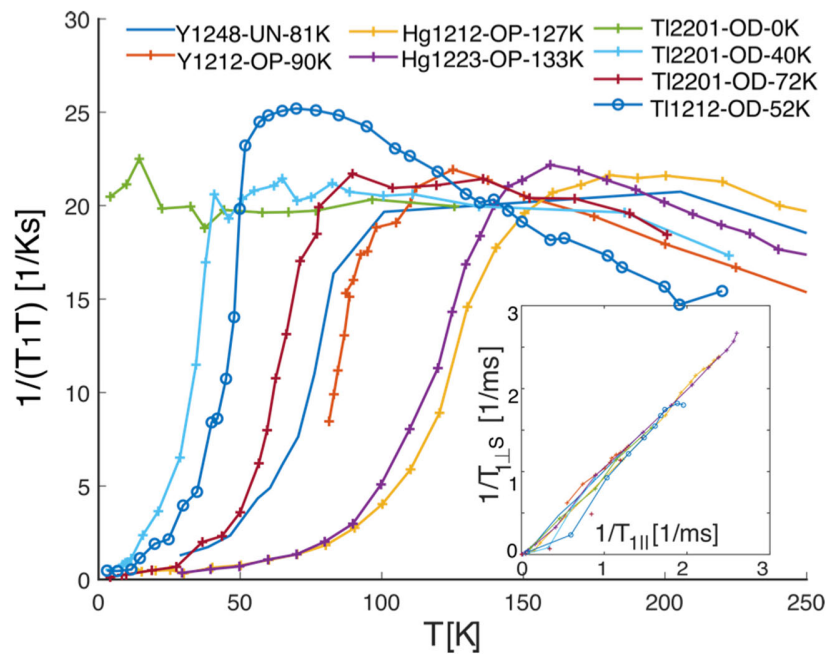
Fig. 4 ^{63}Cu NMR relaxation rates for various materials. Main panel: $1/T_{1\perp}T$ is very similar above T_c for all systems (even those that do not superconduct) and Fermi liquid–like, i.e., $1/T_{1\perp}T = $ const. above T_c and disappears below T_c from singlet pairing. From Korringa's relation and a Knight shift of 0.8% (cf. Fig. 3), one finds $1/(T_1 T) \approx 20$ /Ks. Inset: $(1/T_{1\perp})/(s \cdot (1/T_{1\parallel}))$ of the same materials with T-independent proportionality factor $s = 3.3, 3.1, 2.0, 1.9, 1.0, 1.5, 1.5, 1.7$ for the systems according to their appearance in the legend at the top. The rates are proportional to each other above T_c where the orientational dependence of the field is expected to be irrelevant for the fluid; even below T_c, only a couple of strongly overdoped materials show a slight deviation

Interestingly, the anisotropy takes on only special values (reminding one of selection rules, rather than a crossover).

Below T_c, the relaxation rates for both directions of the field drop rapidly, probably from spin singlet pairing. Both rates are nearly proportional to each other. Interestingly, the perpendicular shift, $K_\perp(T)$, that approaches a common value for all cuprates appears to be nearly proportional to $1/(T_{1\parallel,\perp}T)$. However, the proportionality factor depends on the maximum shift for that material, as can be seen in Fig. 5. This tells us that the shifts for materials that are located in the lower left part of Fig. 3 are suppressed compared with those in the upper right section of the plot that is reached for certain families and at high doping levels.

It is not quite obvious whether it is just the doping level that would bring all cuprates in the upper right corner of Fig. 3. We also know that there is a correlation between the sharing of the charge in the CuO$_2$ plane and the maximum T_c, which is not apparent in terms of the total doping (the sum of the planar Cu and O holes), which proves that doping is not the key parameter for all properties. Therefore, we introduce a parameter ζ (that clearly depends on doping) to be the cause of the changes of the uniform response, in addition to T, i.e., we write $\chi_0(\zeta, T)$.

The question arises how one can reconcile a robust and material-independent relaxation with a suppressed high-temperature shift. Of course, the uniform response, $\chi_0(T)$, can be very different from the wavevector (q)-dependent imaginary part of the susceptibility, $\chi''(q, T)$. For example, a sinusoidal modulation of the spatial spin response will reduce the uniform response of the system but can leave the local fluctuations that set relaxation unchanged.

We do know from experiments on a number of different cuprates [16–18, 20] that a single electronic spin component cannot explain the shift data, rather at least two components appear to be necessary, and couple to the nucleus with different hyperfine coupling constants to the electronic excitations. Therefore, a simple uniform $\chi_0(\zeta, T)$ is not sufficient to explain the data, that is why we propose a simple two-component model.

3 Simple Two-Component Description

In the most simple two-component model, the nuclear spin couples to two electronic spin components with the susceptibilities χ_A and χ_B. These spin components will then have different T dependences in general. We write,

$$K_{\parallel,\perp}(\zeta, T) = B_{\parallel,\perp} \cdot \chi_B(\zeta, T) + A_{\parallel,\perp} \cdot \chi_A(\zeta, T) \tag{1}$$

In other words, the magnetic field (B_0) induces the two electronic spin components $\langle S_A \rangle$ and $\langle S_B \rangle$ ($\gamma_e \hbar \langle S_j \rangle = \chi_j B_0$), which are not proportional to each other as a function
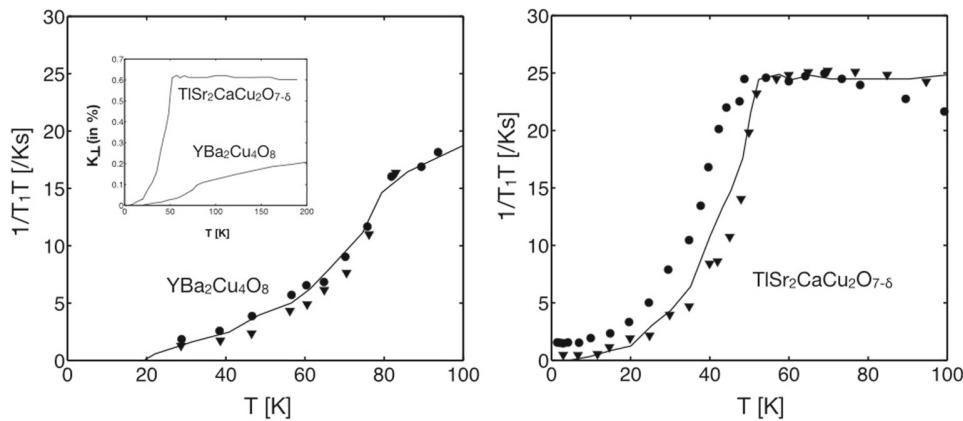
Fig. 5 Comparison of $K_\perp$ and $1/(T_{1\perp,\parallel}T)$ below T_c for an underdoped and overdoped material. The relaxation rates for $c \parallel B_0$ (circles) and $c \perp B_0$ (diamonds) are plotted as a function of temperature for the YBa$_2$Cu$_4$O$_8$ ($T_c \approx 81$ K) and TlSr$_2$CaCu$_2$O$_{7-\delta}$ ($T_c \approx 52$ K); note that

$1/T_{1\parallel}$ is multiplied by the proportionality constants above T_c given in Fig. 4 (1.5 for TlSr$_2$CaCu$_2$O$_{7-\delta}$ and 3.3 YBa$_2$Cu$_4$O$_8$). The original shifts shown in the inset are scaled in the main panel by a ratio of 15/4 to fit the relaxation curves

of temperature. The Cu nucleus experiences changes in the local field through the corresponding hyperfine coefficients $B_{\parallel,\perp}$ and $A_{\parallel,\perp}$.

Now, we denote with B the apparently isotropic hyperfine coefficient that arises as a function of ζ in Fig. 3 (we do not invoke the factor of 4, as opposed to the old literature). Then, there must also be an anisotropic local field contribution. In a minimalistic model, we seek this component in terms of the partially unfilled $3d(x^2 - y^2)$ orbital. As in the early literature, we denote this coefficient with $A_{\parallel,\perp}$. It is also known from reliable estimates, as well as experiment [3] that

$$|A_\parallel| \gtrsim 6|A_\perp| \quad \text{and} \quad A_\parallel = -|A_\parallel|, \tag{2}$$

i.e., the anisotropic hyperfine coefficient is negative and must lead to a negative shift for a positive spin moment. We will neglect the smaller $|A_\perp|$, and we have with (1),

$$\begin{aligned} K_\perp(T) &= B \cdot \langle S_B \rangle(T), \\ K_\parallel(T) &= B \cdot \langle S_B \rangle(T) + A \cdot \langle S_A \rangle(T), \end{aligned} \tag{3}$$

where $A \equiv A_\parallel$. Again, we seek to explain the NMR shift with these two equations that follow from the experimental observation that $\delta_T K_\perp(T)$ is not proportional to $\delta_T K_\parallel(T)$, and the fact that we need two different hyperfine coefficients, plus the assumption that one coefficient is isotropic and the second is related to the partially filled $3d(x^2 - y^2)$ orbital.

If two spin components are present, we must allow for a coupling between them [20]. Thus, each spin component is the sum of two terms, and we use the simplified notation,

$$\langle S_B \rangle \equiv b + c, \quad \langle S_A \rangle \equiv a + c, \tag{4}$$

where the spin components are denoted by $a(\zeta, T)$, $b(\zeta, T)$ and the coupling term by $c(\zeta, T)$.

That is, we have to analyze the shifts in Fig. 3 with the following two equations,

$$\begin{aligned} K_\perp(\zeta, T) &= B \left[b(\zeta, T) + c(\zeta, T) \right] \\ K_\parallel(\zeta, T) &= A[a(\zeta, T) + c(\zeta, T)] + B[b(\zeta, T) + c(\zeta, T)], \end{aligned} \tag{5}$$

where T is the temperature, and ζ takes care of the material-related property.

We now investigate some consequences in this simple picture, and we begin with the low temperature shifts for $c \perp B_0$. We remember that $\hat{K}_\perp(T \to 0) \approx 0.35\%$ is rather similar for all cuprates, and second, it agrees reasonably well with first-principle calculations that predict 0.30% [22]. Therefore, we make the fundamental assumption that $\hat{K}_\perp(T = 0) = K_{L\perp}$ is the orbital shift for this orientation of the field, i.e., the spin shift is zero (singlet pairing). We then conclude with (5),

$$b(\zeta, T \to 0) + c(\zeta, T \to 0) \approx 0. \tag{6}$$

Note that we only know the sum $(b + c)$ vanishes at low temperature, not each component separately.

Next, we address the isotropic shift lines that appear at high temperatures in Fig. 3. They demand that the changes in the shifts induced by ζ, i.e., $\delta_\zeta K_\alpha$, are nearly proportional to each other, i.e.,

$$\delta_\zeta K_\perp \approx \delta_\zeta K_\parallel, \tag{7}$$

and it follows with (5),

$$\delta_\zeta (a + c) \approx 0. \tag{8}$$

That means, the material-related shift variations at high T are given by $\delta_\zeta K_{\perp,\parallel} = B \delta_\zeta(b+c)$, i.e., for both orientations of the field.

With (6), we assumed the orbital shift for $c \perp B_0$ to be given by $K_{L\perp} \approx 0.35\%$ (as in the old model for the hyperfine scenario). Since the orbital shift anisotropy of 2.4

calculated from first principles is a rather reliable number [22], we conclude that $K_{L\parallel} \approx 0.84\%$ is a reliable orbital shift value for $c \parallel B_0$, as well. This is very different from the old scenario where the orbital shift for $c \parallel B_0$ was defined by the YBa$_2$Cu$_3$O$_{6+y}$ low T shift.

In our two-component analysis, at the (virtual) intersection of an isotropic shift line with $K_{L\perp} \approx 0.35\%$, which defines $\zeta \equiv \zeta_\Lambda$, we have,

$$K_\parallel(\zeta_\Lambda, T_h) = A\left[a(\zeta, T_h) + c(\zeta, T_h)\right], \tag{9}$$

where T_h was introduced to denote a sufficiently high T, i.e., $T \gg T_c$. This is the material-independent offset of the isotropic shift lines in Fig. 3. Near the intersection ζ_Λ, we have with (5) that $K_\perp(\zeta_\Lambda, T) = B\left[b(\zeta_\Lambda, T) + c(\zeta_\Lambda, T)\right]$, where $K_\perp(T)$ is very small even at high T. Thus, $c(\zeta_\Lambda) = -b(\zeta_\Lambda)$ holds to a good approximation for all T. We thus have in addition to (9),

$$K_\parallel(\zeta_\Lambda, T_h) = A\left[a(\zeta_\Lambda, T_h) + c(\zeta_\Lambda)\right]$$
$$K_\parallel(\zeta_\Lambda, T_h) = A\left[a(\zeta_\Lambda, T_h) - b(\zeta_\Lambda)\right]. \tag{10}$$

With $K_{L\parallel} = 0.84\%$ we have,

$$K_\parallel(\zeta_\Lambda, T_h) = 0.21\%. \tag{11}$$

Clearly, there could be differences between the materials in terms of $[a(\zeta) + c(\zeta)]$, but also the orbital shifts could vary slightly. However, it must be the negative coupling term $c(\zeta, T)$ that is responsible for the positive offset in the spin shifts of the cuprates for $c \parallel B_0$. In other words, there is an effective negative spin in the $3d(x^2 - y^2)$ orbital, while component a itself is positive, and at high temperatures, $a + c$ does not change with ζ.

We note that the maximum shift variation above the intersection defined by ζ_Λ is about 0.8%, and we conclude that

$$B \cdot (b(\zeta_{\max}, T_h) - b(\zeta_\Lambda, T_h)) \approx 0.8\%. \tag{12}$$

Roughly, there is a factor of 4 between $K_\parallel(\zeta_\Lambda, T_h)$ and the maximum ζ-related shift change. Note that an isotropic shift of about 0.8% is in agreement with the observed universal

relaxation rate just above T_c, i.e., it follows from Korringa's law for a simple Fermi liquid.

Based on the above discussion, we present in Fig. 6 a possible decomposition of the high T shifts, and the ensuing shift-shift plot, inspired by a large b term from a robust Fermi liquid–like fluid, a negative coupling c that tries to align positive spin components a and b antiferromagnetically.

Now, we turn to the temperature dependence of the shifts. The fact that basically all shift data lie below the isotropic shift lines in Fig. 3 tells us that as the shifts depart from the isotropic shift lines with $\delta_T K_\perp \leq \delta_T K_\parallel$. It follows with (5),

$$\delta_T\left[A(a + c)\right] \gtrsim 0$$
$$\delta_T(a + c) \lesssim 0, \tag{13}$$

since A is negative. This says that by lowering the temperature, $A\left(a(T) + c(T)\right)$ becomes more positive so that $K_\parallel$ stays to the right of the isotropic shift lines in Fig. 3. The nearly equal sign refers to points very near the isotropic shift line.

In Fig. 3, we pointed to certain slopes in the low-temperature behavior of the shift anisotropies (for a more detailed discussion, see [19]).

First, we have $\delta_T K_\perp / \delta_T K_\parallel \approx 1$, similar to the isotropic shift lines, but now as a function of T. We conclude $\delta_T(a + c) \approx 0$. This slope is observed, in particular, for overdoped systems where, after an initial steep drop of $K_\perp$ at T_c, the system holds $(a + c) = $ const. as T drops further (cf. Fig. 3). We do know that $(b + c)$ varies in this range of T since $K_\perp$ changes.

Second, we find in Fig. 3 the steep slope, i.e., $\delta_T K_\perp / \delta_T K_\parallel \gtrsim 10$. It can be found for the strongly doped systems at T_c for a given range of T, but also for other materials, e.g., YBa$_2$Cu$_4$O$_8$ in the whole range of T. This includes the variation in the NMR pseudogap region, but not for all materials. For example, HgBa$_2$CuO$_{4+\delta}$ takes on the slope of $\approx 5/2$ as it departs from the isotropic shift line at T_c, or in the pseudogap region. With $\delta_T K_\parallel \approx 0$, we conclude that

$$B\,\delta_T(b + c) \approx -A\,\delta_T(a + c). \tag{14}$$

Fig. 6 Left, possible decomposition of the high-T shifts as function of the material-related parameter ζ and the spin components a, b, and the coupling c (cf. (5)). Right, resulting shift-shift plot according to (5) for $B = 1$ and $A = -3/5B$
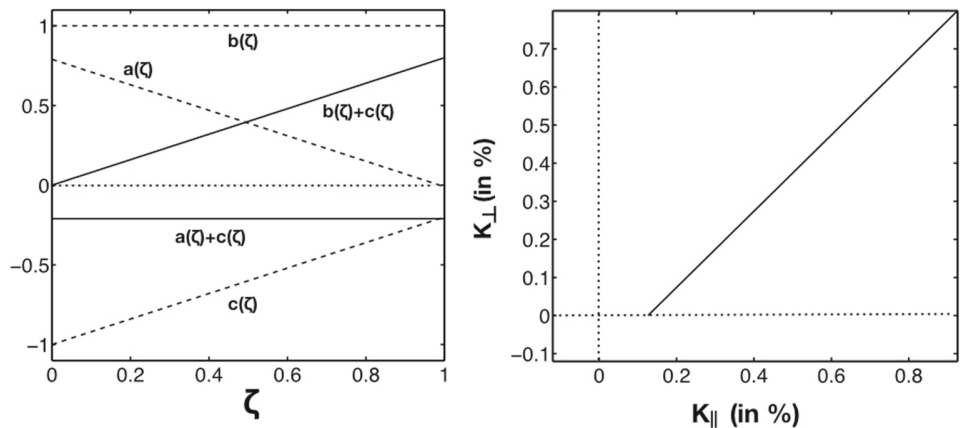
If only c became T-dependent, $A = -B$ would follow, which is the known argument in the old literature (our definition of B is that of $4B'$ in those papers).

Third, we observe a typical slope of $\delta_T K_\perp / \delta_T K_\parallel \approx 5/2$. This leads to the equation,

$$B\, \delta_T(b + c) \approx -\frac{5}{3} A\, \delta_T(a + c). \tag{15}$$

For example, if we assume that only c changes as a function of T for those slopes, we conclude that $B \approx -5/3A$. This is perhaps a reasonable conclusion, and the T-dependent NMR pseudogap feature is caused by a T-dependent $c(\zeta)$. Then, in order to generate, e.g., the steep slope, we find $3\delta_T b = 2\delta_T a - \delta_T c$.

The behavior of the shifts at low temperatures is perhaps more complicated. One must also be aware of the fact that the measurements were not pursued with the appropriate rigor since such behavior was not suspected. In addition, the penetration depth of the r.f. decreases rapidly and signal-to-noise can become a limiting factor, certainly for single crystals. Perhaps, $K_{L\perp} = 0.35\%$ is somewhat higher than the calculated 0.30%. We cannot be sure that all $\hat{K}_\parallel(\zeta)(T = 0)$ in Fig. 3 are the true low-T shifts for this orientation. If so, we clearly need negative spin $a + c$, i.e., $K_\parallel = -|A|(b - a)$ if $c = -b$. For example, the single-layer HgBa$_2$CuO$_{4+\delta}$ [7] has a $T = 0$ shift of $K_\parallel = +0.6\%$, and we conclude that $A(a + c)$ increased 3-fold compared with the ζ_Λ value of 0.21%.

How can one reconcile the variations of shift and relaxation? First, we focus on the largest ζ materials, which show Fermi liquid–like behavior with an isotropic $1/T_1 T$ of about 20 /Ks. This value follows from the Korringa relation for a simple Fermi liquid. Note that $(1/T_{1\perp})/(1/T_{1\parallel}) \approx 1$ is expected for relaxation dominated by fluctuations through B. Thus, the largest ζ systems are easily understood.

As ζ decreases, the shifts decrease isotropically with decreasing ζ, but remain T-independent above T_c. The relaxation is strictly proportional to T and even remains very similar, except that the anisotropy changes to $(1/T_{1\perp})/(1/T_{1\parallel}) = 1.5$. By decreasing the temperature, T_c is encountered and the shifts suddenly drop. First, $K_\perp$ begins to change, the initial steep drop in Fig. 3. It is followed by a nearly proportional decrease of both shifts along isotropic shift lines, now as a function of T. The initial drop can be rather large, followed by a short isotropic shift line to reach $K_{L\perp}(0) \approx 0.35\%$. Systems with a small initial drop have a longer isotropic shift line since it ends at $K_{L\perp}$. Consequently, in the latter case, a smaller shift ($K_\parallel(T = 0)$) remains at the lowest T. While the changes in the shifts are more complex, both relaxation rates drop almost proportionally to $K_\perp$ below T_c (and they are nearly proportional to each other). This is expected for singlet

pairing, here as vanishing of $b + c$. $1/(T_{1\perp,\parallel}T)$ is nearly proportional to $K_\perp(T)$ below T_c (cf. Fig. 5). We conclude that the relaxation must be dominated by the isotropic spin component, and only the coupling to the liquid has acquired a small anisotropy.

As we move to lower ζ and approach optimal doping, the systems tend to depart from the isotropic shift line with an initial slope of about 5/2, e.g., HgBa$_2$CuO$_{4+\delta}$. In particular, materials with the highest T_c appear to have the 5/2 slope (cf. inset in Fig. 3). The changes of the shifts at the lowest temperature are not well documented experimentally, and they cannot be discussed with certainty (some details are given in [19]). The nuclear relaxation remains rather similar for $c \perp B_0$, but the anisotropy of the relaxation changes.

It is obvious from Fig. 5 that $K_\perp$ is nearly proportional to $1/(T_{1\perp,\parallel}T)$; however, while $1/(T_{1\perp}T)$ drops from about 17 /Ks and 25 /Ks to zero for both systems, respectively, the shifts have to be rescaled. For TlSr$_2$CaCu$_2$O$_{7-\delta}$, the shift drops from about 0.6% to zero, cf. inset in Fig. 5, and for YBa$_2$Cu$_4$O$_8$ from about 0.1%. From the Korringa relation, one would expect $1/(T_{1\perp}T)$ of 9.6 /Ks and 0.26 Ks, respectively, very different values. The used scaling ratio between the two shifts in the main panel is 15/4, almost a factor of 4. Again, we observe a further suppression of the shifts compared with relaxation.

In a classical scenario, one expects that the relaxation governing local field fluctuations are perpendicular to the orientation of the magnetic field. Thus, in-plane fluctuations set $1/T_{1\parallel}$, while $1/T_{1\perp}$ (measured with the field in the plane) is determined by both kinds of fluctuations, i.e., parallel and perpendicular to the plane. Of course, the mean values of the shifts (proportional to χ_0) do not determine their r.m.s. averages that are set by χ'' at the nuclear frequency, but they might be a good first guess for seeking a relation. For example, $K_\parallel$ is on average much larger than $K_\perp$, but there are exceptions to that rule, e.g., in terms of $(1/T_{1\perp}T)/(1/T_{1\parallel}T)$ [21]. In addition, we do not see a simple way to derive the special proportionality constants for $(1/T_{1\perp}T)/(1/T_{1\parallel}T)$ that hint at matrix element effects, so that we do not pursue this model any further.

In Fig. 7, we illustrate a scenario of two coupled spins that we believe captures main elements observed.

There are very few systems that do not fit the general shift scenario, among them La$_{2-x}$Sr$_x$CuO$_4$ [19]. This is also true for the relaxation [21], where an additional mechanism increases the relaxation above T_c, but both rates stay proportional to each other. Therefore, we also do not pursue these few outlier systems here.

The very low-ζ materials are in general not investigated with great detail. It is known that the NMR signal can be lost, probably due to spin-glass behavior [23]. Greater material dependencies can be expected.
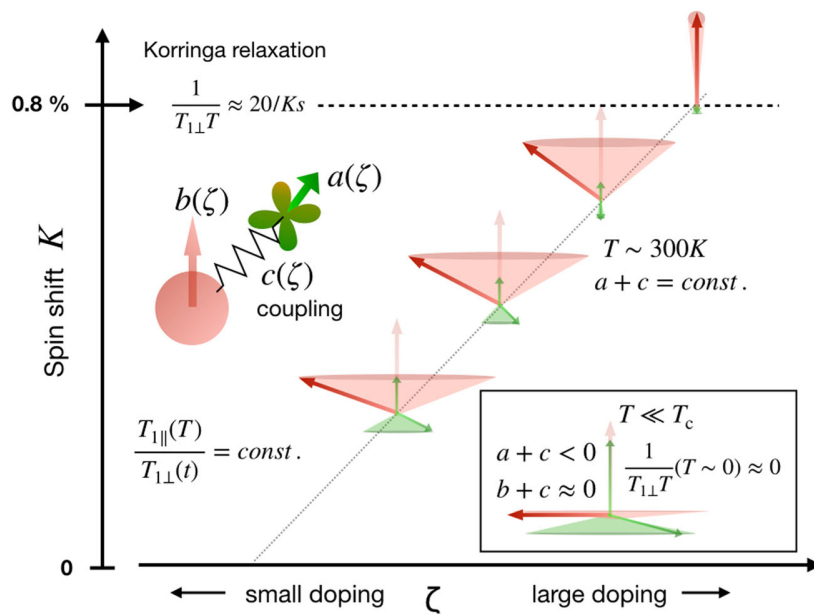
Fig. 7 Shift and relaxation scenario in the cuprates: two coupled ($c(\zeta)$) electronic spins ($a(\zeta)$ and $b(\zeta)$) precess about the external magnetic field and determine the nuclear spin shift ($K(\zeta)$). The parameter ζ determines the high-T shifts as a function of doping and material. Near room temperature, $c(\zeta)$ is found to be temperature-independent, causing isotropic changes in the NMR shifts. The largest shifts ($\sim 0.8\%$) are observed for the largest ζ, in agreement with Korringa-like relaxation (~ 20 /Ks). While the relaxation is hardly affected by the coupling (only the relaxation anisotropy $(1/T_{1\perp})/(1/T_{1\parallel})$ changes), the shifts become increasingly suppressed for smaller ζ, thus appear to violate the Korringa law. The coupled spins possess s- and $d(x^2 - y^2)$-like orbital symmetry, and with the corresponding hyperfine coefficients, the negative coupling explains the unexpected spin shifts observed in the cuprates. Deep in the condensed state $b + c = 0$ and relaxation disappears, but $a + c$ can be finite. The changes in ζ must be related to the pseudogap

4 Conclusions

From literature analysis, an almost universal planar Cu relaxation above and below T_c is found. It is Fermi liquid–like and changes only in terms of its anisotropy and T_c. Its doping independence rules out strong enhancement due to spin fluctuations. It is contrasted to the drastic variations of the Cu NMR shifts between different materials, as a function of doping or temperature above T_c that were reported recently [19]. Shifts for materials with the highest doping obey the Korringa law when compared with their relaxation. So it must be concluded that for most cuprates that do not obey the Korringa law, the shifts are suppressed, and it is not the relaxation that is enhanced.

The differences are explained with a simple two-component model that has two electronic spin components, $a(\zeta, T)$ and $b(\zeta, T)$ that depend on temperature (T) and a material parameter ζ that depends on doping. One of the electronic spin components, $b(\zeta, T)$, couples through an isotropic hyperfine constant, B, with the nuclei, while an anisotropic hyperfine constant, $A \equiv -|A_\parallel|, A_\parallel \gg A_\perp$, as known for the $3d(x^2 - y^2)$ orbital is responsible for anisotropic term, $a(\zeta, T)$. A negative coupling, $c(\zeta, T)$, between both spin components, a and b, leads to the reduction of the shifts while allowing for a largely unchanged relaxation above T_c. This negative coupling

can also resolve the long-standing discrepancy between calculated and presumed experimental orbital shifts.

For large ζ, we find a Fermi liquid–like fluid with isotropic coupling to the nuclei, as given by the Korringa relation with shift $K(\zeta)$. As ζ decreases, $a(\zeta)$ increases, but the magnitude of the negative coupling $c(\zeta)$ suppresses the shifts (while T_c increases). Thus, $c(\zeta)$ must be related to the pseudogap. In a possible scenario, $c(\zeta)$ becomes T-dependent above T_c and causes the NMR pseudogap phenomenon, i.e., it suppresses the shifts as a function of T already above T_c. In this case, we can conclude for the hyperfine coefficients that $A \approx -3/5B$.

We think it is established with NMR, now, that there is a nearly universal fluid that is Fermi liquid–like in the cuprates. This was found with NMR in 2009 [20], but also with an increasing number of other probes, e.g., [24–26]. Then, the most simplistic scenario suggested by our data is that the electronic spin of this liquid is coupled to the spin component in the $3d(x^2 - y^2)$ orbital. Of course, the latter spin could be part of the nearly universal liquid, as well. The term $b + c$ could be associated with quasiparticles in the nodal region of the Fermi surface [27–30], while the term $a + c$ represents the antinodal region with perhaps antiferromagnetic properties [31, 32]. For lower values of ζ, antinodal regions could be large [33] and below T_c antiferromagnetic correlations could exist with pairing. This

could explain the reduction of shift being more gradual, in comparison with overdoped samples with a smaller k-space region. Then, c is perhaps responsible for driving the k-space anisotropy, seen by ARPES and other techniques. Neutron scattering will mostly be determined by the a component and its coupling to b, while the response from b is likely to be distributed in reciprocal space and might escape detection.

Perhaps, a Fermi liquid could reside in a separate band and inter-band coupling is responsible for the high T_c [34]. The residual shift (that may be moments [19]) could be related to time reversal symmetry breaking, but whether loop currents [35] could be involved in the suppression of the shifts has to be seen. A two-component model involving hidden fermions [36, 37] should relate to our findings.

Finally, we would like to mention from an NMR point of view that the evolution of the intra-unit cell charge ordering that is now well documented also by NMR [8] could be connected to the coupling scenario.

Appendix

A collection of abbreviations used for the various compounds is given in Table 1.

Table 1 List of abbreviations with full stoichiometric formula and reference for the original data

Symbol	System	Ref.
Y1248-UN-92K	$YBa_2Cu_4O_8$	[12][1]
Y1212-OP-90K	$YBa_2Cu_3O_{6.92}$	[38][1]
Tl1212-OV-10K,-52K,-70K	$TlSr_2CaCu_2O_{7-\delta}$	[39][1]
Tl2201-OV-0K,-40K,-72K	$Tl_2Ba_2CuO_{6+y}$	[40, 41][1]
Tl2212-OP-112K	$Tl_2Ba_2CaCu_2O_{8-\delta}$	[42][1]
Hg1201-UN-45K,-74K	$HgBa_2CuO_{4+\delta}$	[18]
Hg1201-OP-97K,-OV-85K	$HgBa_2CuO_{4+\delta}$	[18]
Hg1223-OP-133K(IP)	$HgBa_2Ca_2Cu_3O_{8+\delta}$	[43, 44][1]
Hg1212-OP-127K	$HgBa_2CaCu_2O_{6+\delta}$	[45][1]
Ba0223-OP-120K(OP), (IP)	$Ba_2Ca_2Cu_3O_6(F,O)_2$	[46][1,2,3]
Ba0212-OP102K,-OP105K	$Ba_2CaCu_2O_6(F,O)_2$	[46][1]

[1]For the corresponding shift corrections, cf. [19]

[2]OP or IP in parentheses refer to the outer and inner plane of the triple-layer systems, respectively

[3]In Fig. 3, the orange curve corresponds to (IP) and the yellow curve to (OP), different from Ref. [46]

References

1. Slichter, C.P.: In: Schrieffer, J.R., Brooks, J.S. (eds.) Handbook of High-temperature Superconductivity, pp. 215–256. Springer, New York (2007)
2. Walstedt, R.E. The NMR Probe of High-Tc Materials, 1st edn. Springer, Berlin (2007)
3. Pennington, C.H., Durand, D.J., Slichter, C.P., Rice, J.P., Bukowski, E.D., Ginsberg, D.M.: Phys. Rev. B 39, 2902 (1989)
4. Zheng, G.Q., Mito, T., Kitaoka, Y., Asayama, K., Kodama, Y. Phys. C Supercond. 243, 337 (1995)
5. Haase, J., Sushkov, O.P., Horsch, P., Williams, G.V.M.: Phys. Rev. B 69, 94504 (2004)
6. Jurkutat, M., Rybicki, D., Sushkov, O.P., Williams, G.V.M., Erb, A., Haase, J.: Phys. Rev. B 90, 140504 (2014)
7. Rybicki, D., Jurkutat, M., Reichardt, S., Kapusta, C., Haase, J.: Nat. Commun. 7, 1 (2016)
8. Reichardt, S., Jurkutat, M., Guehne, R., Kohlrautz, J., Erb, A., Haase, J.: Condens. Matter 3(3), 23 (2018)
9. Takigawa, M., Hammel, P.C., Heffner, R.H., Fisk, Z.: Phys. Rev. B 39(10), 7371 (1989)
10. Takigawa, M., Reyes, A.P., Hammel, P.C., Thompson, J.D., Heffner, R.H., Fisk, Z., Ott, K.C.: Phys. Rev. B 43, 247 (1991)
11. Alloul, H., Ohno, T., Mendels, P.: Phys. Rev. Lett. 63, 1700 (1989)
12. Bankay, M., Mali, M., Roos, J., Brinkmann, D.: Phys. Rev. B 50, 6416 (1994)
13. Walstedt, R.E., Warren, J., Bell, R.F., Brennert, G.F., Espinosa, G.P., Cava, R.J., Schneemeyer, L.F., Waszczak, J.V.: Phys. Rev. B 38(13), 9299 (1988)
14. Berthier, C., Julien, M.H., Bakharev, O., Horvatić, M., Ségransan, P.: Physica C: Superconductivity and its Applications 282, 227 (1997)
15. Haase, J., Slichter, C.P., Williams, G.V.M.: J. Phys. Condens. Matter 21, 455702 (2009)
16. Meissner, T., Goh, S.K., Haase, J., Williams, G.V.M., Littlewood, P.B.: Phys. Rev. B 83, 220517 (2011)
17. Haase, J., Rybicki, D., Slichter, C.P., Greven, M., Yu, G., Li, Y., Zhao, X.: Phys. Rev. B 85, 104517 (2012)
18. Rybicki, D., Kohlrautz, J., Haase, J., Greven, M., Zhao, X., Chan, M.K., Dorow, C.J., Veit, M.J.: Phys. Rev. B 92, 081115 (2015)
19. Haase, J., Jurkutat, M., Kohlrautz, J.: Condens. Matter 2(2), 16 (2017)
20. Haase, J., Goh, S.K., Meissner, T., Alireza, P.L., Rybicki, D.: Rev. Sci. Instrum. 80(7), 073905 (2009)
21. Jurkutat, M., Avramovska, M., Williams, G.V.M., Dernbach, D., Pavicevic, D., Haase, J.: arXiv:1902.10625v1 (2018)
22. Renold, S., Heine, T., Weber, J., Meier, P.F.: Phys. Rev. B 67(2), 24501 (2003)
23. Hunt, A.W., Singer, P.P.M., Cederström, A.F., Imai, T.: Phys. Rev. B 64, 134525 (2001)
24. Doiron-Leyraud, N., Proust, C., LeBoeuf, D., Levallois, J., Bonnemaison, J.B., Liang, R., Bonn, D.A., Hardy, W.N., Taillefer, L.: Nature 447(7144), 565 (2007)
25. Sebastian, S.E., Harrison, N., Palm, E., Murphy, T.P., Mielke, C.H., Liang, R., Bonn, D.A., Hardy, W.N., Lonzarich, G.G.: Nature 454(7201), 200 (2008)
26. Barivsić, N., Badoux, S., Chan, M.K., Dorow, C., Tabis, W., Vignolle, B., Yu, G., Béard, J., Zhao, X., Proust, C., Li, Y.: Nat. Phys. 9(12), 761 (2013)
27. Kanigel, A., Norman, M.R., Randeria, M., Chatterjee, U., Souma, S., Kaminski, A., Fretwell, H.M., Rosenkranz, S., Shi, M., Sato, T., Takahashi, T., Li, Z.Z., Raffy, H., Kadowaki, K., Hinks, D., Ozyuzer, L., Campuzano, J.C.: Nat. Phys. 2(7), 447 (2006)

28. Fournier, D., Levy, G., Pennec, Y., McChesney, J.L., Bostwick, A., Rotenberg, E., Liang, R., Hardy, W.N., Bonn, D.A., Elfimov, I.S., Damascelli, A.: Nat. Phys. **6**, 905 (2010)
29. Proust, C., Vignolle, B., Levallois, J., Adachi, S., Hussey, N.E.: Proc. Natl. Acad. Sci. USA **113**(48), 13654 (2016)
30. Schmidt, A.R., Fujita, K., Kim, E.A., Lawler, M.J., Eisaki, H., Uchida, S., Lee, D.H., Davis, J.C.: New J. Phys. **13**(6), 65014 (2011)
31. Cilento, F., Dal Conte, S., Coslovich, G., Peli, S., Nembrini, N., Mor, S., Banfi, F., Ferrini, G., Eisaki, H., Chan, M.K., Dorow, C.J., Veit, M.J., Greven, M., van der Marel, D., Comin, R., Damascelli, A., Rettig, L., Bovensiepen, U., Capone, M., Giannetti, C., Parmigiani, F.: Nat. Commun. **5**, 4353 (2014)
32. Cilento, F., Manzoni, G., Sterzi, A., Peli, S., Ronchi, A., Crepaldi, A., Boschini, F., Cacho, C., Chapman, R., Springate, E., Eisaki, H., Li, Y., Berciu, M., Kemper, A.F., Damascelli, A., Capone, M., Giannetti, C., Parmigiani, F.: Sci. Adv. **4**(2), 1 (2018)
33. Kaminski, A., Kondo, T., Takeuchi, T., Gu, G.: Philos. Mag. **95**(5-6), 453 (2015)
34. Bussmann-Holder, A., Köhler, J., Simon, A., Whangbo, M.H., Bianconi, A., Perali, A.: Condens. Matter **2**, 1 (2017)
35. Varma, C.M.: Phys. Rev. B **55**(21), 14554 (1997)
36. Sakai, S., Civelli, M., Imada, M.: Phys. Rev. Lett. **116**(5), 696 (2016)
37. Imada, M., Suzuki, T.J.: J. Phys. Soc. Japan **88**(2), 024701 (2019)
38. Auler, T., Horvatić, M., Gillet, J.A., Berthier, C., Berthier, Y., Carretta, P., Kitaoka, Y., Ségransan, P., Henry, J.Y.: Phys. C: Supercond. **313**(3), 255 (1999)
39. Magishi, K., Kitaoka, Y., Zheng, G.Q., Asayama, K., Kondo, T., Shimakawa, Y., Manako, T., Kubo, Y.: Phys. Rev. B **54**(14), 10131 (1996)
40. Fujiwara, K., Kitaoka, Y., Ishida, K., Asayama, K., Shimakawa, Y., Manako, T., Kubo, Y.: Phys. C: Supercond. **184**(4-6), 207 (1991)
41. Kambe, S., Yasuoka, H., Hayashi, A., Ueda, Y.: Phys. Rev. B **47**(5), 2825 (1993)
42. Gerashchenko, A.P., Mikhalev, K.N., Verkhovskii, S.V., Piskunov, Y.V., Anan'ev, K.A., Okulova, A.Y., Yakubovskii, L.D., Shustov, J.: Exp. Theor. Phys. **88**, 545 (1999)
43. Magishi, K., Kitaoka, Y., Zheng, G.Q., Asayama, K., Tokiwa, K., Iyo, A., Ihara, H.: J. Phys. Soc. Japan **64**(12), 4561 (1995)
44. Julien, M.H., Carretta, P., Horvatić, M., Berthier, C., Berthier, Y., Ségransan, P., Carrington, A., Colson, D.: Phys. Rev. Lett. **76**(22), 4238 (1996)
45. Itoh, Y., Machi, T., Yamamoto, A.: Phys. Rev. B **95**, 094501 (2017)
46. Shimizu, S., Iwai, S., Tabata, S.i., Mukuda, H., Kitaoka, Y., Shirage, P.M., Kito, H., Iyo, A.: Phys. Rev. B **83**(14), 144523 (2011)

REVIEW

Phenomenology of ^{63}Cu Nuclear Relaxation in Cuprate Superconductors

Michael Jurkutat[1] · Marija Avramovska[1] · Grant V. M. Williams[2] · Daniel Dernbach[1] ·
Danica Pavićević[1] · Jürgen Haase[1] (ID)

Abstract

Nuclear relaxation is an important thermodynamic probe of electronic excitations, in particular in conducting and superconducting systems. Here, an empirical phenomenology based on all available literature data for planar Cu in hole-doped cuprates is developed. It is found that most of the seemingly different relaxation rates among the systems are due to a temperature-independent anisotropy that affects mostly measured $1/T_{1\parallel}$, the rate with an external magnetic field along the crystal c-axis, while $1/T_{1\perp}$ is largely independent on doping and material above the critical temperature of superconductivity (T_c). This includes very strongly overdoped systems that show Fermi liquid behavior and obey the Korringa law. Below T_c, the relaxation rates are similar, as well, if plotted against the reduced temperature T/T_c. Thus, planar Cu nuclear relaxation is governed by a simple, dominant mechanism that couples the nuclei with varying anisotropy to a rather ubiquitous bath of electronic excitations that appear Fermi liquid-like irrespective of doping and family. In particular, there is no significant enhancement of the relaxation due to electronic spin fluctuations, different from earlier conclusions. Only the $La_{2-x}Sr_xCuO_4$ family appears to be an outlier as additional relaxation is present; however, the anisotropy remains temperature independent. Also systems with very low doping levels, for which there is a lack of data, may behave differently.

✉ Jürgen Haase
j.haase@physik.uni-leipzig.de

Michael Jurkutat
jurkutat@physik.uni-leipzig.de

Marija Avramovska
marija.avramovska@hotmail.com

Grant V. M. Williams
grantw7@gmail.com

Daniel Dernbach
daniel.dernbach14@gmail.com

Danica Pavićević
danicas.dp@gmail.com

1   Felix Bloch Institute for Solid State Physics, University
     of Leipzig, Linnéstr. 5, 04103, Leipzig, Germany

2   Victoria University of Wellington, The MacDiarmid Institute
     for Advanced Materials and Nanotechnology, SCPS,
     PO Box 600, Wellington, 6140, New Zealand

1 Introduction

Nuclear relaxation is a fundamental probe in condensed matter physics [1]. In conducting materials, it is often determined by the electronic excitations, as was predicted [2] long before the techniques of nuclear magnetic resonance (NMR) became available. The heat transfer that establishes the (electronic) lattice temperature for a nuclear spin system can be conveniently measured in an external magnetic field, but also in zero field. It is characterized by the spin-lattice relaxation rate $1/T_1$. For Fermi liquids, this scattering of nuclear spin off electrons is not only proportional to the square of the electronic density of states and the hyperfine coefficients, but also proportional to the temperature (T), i.e., $1/T_1 \propto T$. The famous Korringa relation [3] is very useful for simple Fermi liquids since the electronic Pauli susceptibility leads to the NMR Knight shift (K_S) that is also proportional to the electronic density of states and the hyperfine coefficients, so that $1/(TT_1) = (\gamma_n/\gamma_e)^2(4\pi k_B/\hbar) \cdot \rho K_S^2$. The gyromagnetic ratios of the electron (γ_e) and nucleus under study (γ_n), as well as k_B

and $\hbar$, are known, and ρ is introduced to account for slight deviations (e.g., due to electronic correlations).

Another hallmark relation, of relevance here, comes from the first proof of BCS theory of superconductivity [4]. The relaxation rate $1/T_1$ was shown to disappear below the critical temperature of superconductivity (T_c), but the opening of the gap also led to a coherence peak (Hebel-Slichter peak of NMR [5]), both predicted by BCS for singlet pairing.

Thus, nuclear relaxation, as a bulk sensor of electron thermodynamic properties is a very important probe, and the typical temperature dependence of $1/T_1$ for a classical superconductor is sketched in Fig. 1.

With the discovery of cuprate high-temperature superconductors [6], there was immediate interest in measuring the nuclear relaxation rate, in particular for Cu and O nuclei in the ubiquitous CuO_2 plane where the nuclei must couple strongly to the electronic degrees of freedom. Early experiments focussed on the $YBa_2Cu_3O_{6+y}$ family of materials. The results showed more complicated dependences above and below T_c, even for the apparently overdoped $YBa_2Cu_3O_7$ that should be closer to a Fermi liquid. Nevertheless, the relaxation did disappear even as $1/(T_1T)$ at low T for the latter material in agreement with spin-singlet pairing. The actual decrease of $1/(T_1T)$ as a function of T below T_c was weaker than what follows from a symmetric s-wave gap. Furthermore, a Hebel-Slichter coherence peak could not be found (it can can also be absent [7] or broadened [8] for non-cuprate superconductors).

While relaxation measurements are quite robust, they can be difficult in the cuprates. The large unit cell gives rise to various resonances, and the $^{63,65}Cu$ and ^{17}O nuclei have quadrupole moments. Not only does this lead to even more

Fig. 1 Sketch of the temperature dependence of the nuclear relaxation rate from coupling to a Fermi liquid. The relaxation rate is proportional to temperature, above T_c. Below T_c, the rate drops for spin-singlet pairing and may show a Hebel-Slichter peak just below T_c (dotted line) before it disappears as T approaches zero

resonances from angular dependent splittings but also one finds large line broadenings that prove extensive variations of the local electric field gradient (EFG) at Cu and O nuclei, which are in fact charge density variations as proven more recently [9–11]. In addition, there are many nuclear reservoirs and quadrupolar relaxation could be present, as well. Also, broad resonances that cannot be uniformly excited with radio frequency pulses can give misleading relaxation data if spectral diffusion takes place [12], which is perhaps the case for $La_{2-x}Sr_xCuO_4$ (see below). Furthermore, large single crystals were not readily available and difficult to measure due to penetration depth effects. So, most early measurements were performed on (c-axis aligned) microcrystalline powders with NMR or NQR (nuclear quadrupole resonance), which is the reason that most studies focussed on $1/T_{1\parallel}$, the rate measured if the crystal c-axis is parallel to the external field, which is also measured with NQR. The strongly underdoped systems were not investigated very much. This is due to the fact not only that optimally doped materials have been of greatest interest but also since underdoped cuprates show Cu signal wipe-out [13], and one cannot assure that the measured signal represents the average material.

Nevertheless, while this all hampered rapid progress with NMR of cuprates, the nuclear relaxation data can be considered quite reliable for most systems.

In early NMR measurements on nearly optimally doped $YBa_2Cu_3O_{6+y}$ ($y \approx 0.95$), one had to assign the two different Cu sites, in the chains and plains, to two sets of NMR signals. Walstedt et al. in 1987 [14] showed that one Cu site exhibited Fermi liquid-like relaxation above T_c, while the other showed significant deviations at higher temperatures. Then, since yttrium (Y) atoms that are sandwiched between the two CuO_2 planes in this double-layer material, and since Markert et al. [15] had reported Fermi liquid-like relaxation above T_c for Y, it was reasonable to assume [14] that the Cu nuclei with Fermi liquid relaxation must be located in the plane. However, later, it was shown from various experiments [16, 17] that the opposite assignment was correct, which was put forward early on by Mali et al. [18].

Later, Walstedt et al. [19] discovered a nearly temperature independent anisotropy of relaxation ($T_{1\parallel}/T_{1\perp} \approx 3.4$) for planar Cu in $YBa_2Cu_3O_7$ above and below T_c (which we will show to be a unique property of the cuprates, only the proportionality factor can be material dependent). More importantly, it was concluded [20] that the Korringa ratio is violated by comparing with shift data, in the sense that the relaxation is enhanced by an order of magnitude for planar Cu (and a factor of about 2.8 for planar O), which was taken as proof for enhanced antiferromagnetic spin fluctuations (that tend to cancel at planar O if the electron spins are located at planar Cu).
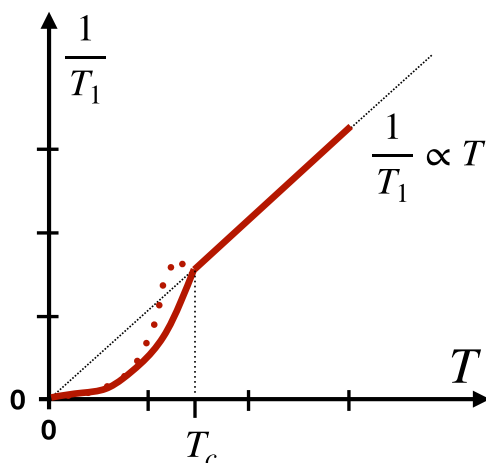
Despite the fact that only a very limited number of systems was investigated [21–27], numerous models were developed to understand the nuclear relaxation, which will not be reviewed here. Note that the mysterious cancellation of the Cu NMR shift for one orientation of the magnetic field ($c \parallel B_0$) was explained by an accidental cancellation of the on-site and transferred hyperfine coefficients ($A_\parallel + 4B \approx 0$). Later, when systems were discovered that had a substantial shift also for $c \parallel B_0$ (as much as 30% of that for $c \perp B_0$), this explanation was not questioned widely, while the corresponding changes in the hyperfine scenario appear unrealistic given the ubiquitous chemistry of the CuO$_2$ plane. With more thorough investigations of more systems, the then prevailing explanation did not grow more solid [28–32], rather, the failure of the hyperfine scenario became apparent [33]. This questions, at the same time, any quantitative discussion of nuclear relaxation, which hinges on the hyperfine scenario that can filter out certain wave vectors from fluctuating modes that are relevant to nuclear relaxation.

Here we will take a fresh look at all available planar Cu NMR relaxation data of hole-doped cuprates to establish what we think is a new, but reliable phenomenology that may change the way one views some properties of the cuprates.

By only plotting literature data, we will establish that the relaxation in the cuprates is surprisingly simple and universal. It turns out that the large differences between different systems concern predominantly the relaxation measured with the external field along the crystal c-axis ($1/T_{1\parallel}$). However, since we also find that the relaxation anisotropy ($\alpha_{\rm ani}$) is T independent for all cuprates, i.e., $\alpha_{\rm ani} = T_{1\perp}/T_{1\parallel}$ above and below T_c, it is predominantly $\alpha_{\rm ani}$ that changes between different systems, i.e., it is the anisotropy of coupling to the electronic reservoir that varies, not the reservoir itself. Other than that, relaxation is material and doping independent and very similar to that for the most overdoped systems that are very close to Fermi liquids. Also below T_c, the relaxation is very similar if plotted against T/T_c, the reduced temperature. Thus, there is no room for relaxation enhancement from spin fluctuations (except perhaps for the very underdoped systems for which we have no data).

2 Results and Discussion

In Table 1, we list all cuprates, sorted by family, for which we could find data for both directions of the field. More information about data extraction and processing are given in the Appendix, together with a discussion of this representative selection of data. Throughout the manuscript, data points are uniquely labelled as defined in

Table 1 Summary of materials used for this review [26, 34–46]. Materials are listed with reference (Ref.), the apparent doping level (dop.), the T_c, the relaxation anisotropy ($\alpha_{\rm ani}$), and a colored symbol that is used throughout the manuscript

Material	Ref.	dop.	T_c[K]	$\alpha_{\rm ani}^*$	Symb.
La$_{2-x}$Sr$_x$CuO$_4$	34	0.13	34	2.3	—○—
	34	0.18	35	2.3	—●—
YBa$_2$Cu$_3$O$_{6+y}$	35	0.92	90	3.1	—■—
YBa$_2$Cu$_3$O$_7$	26	UD	86	3.4	—■—
YBa$_2$Cu$_4$O$_8$	36	UD	81	3.3	—■—
TlSr$_2$CaCu$_2$O$_{7-\delta}$	37	OD	70	1.5	—▲—
	37	OD	52	1.5	—▲—
	37	OD	10	/	—▲—
Tl$_2$Ba$_2$CuO$_{6+y}$	38	OD	72	1.7	—▼—
	38	OD	40	1.5	—▼—
	38	OD	0	1.0	—▼—
Tl$_2$Ba$_2$Ca$_2$Cu$_3$O$_{10}$	39	OP	115	1.7	—▶—
Tl$_2$Ba$_2$CaCu$_2$O$_{8-\delta}$	40b	UD	102	2.8	—▷—
	40b	OP	112	2.5	—▷—
	40b	OD	104	2.4	—▶—
HgBa$_2$CaCu$_2$O$_{6+\delta}$	41	OP	127	2.0	—◆—
HgBa$_2$Ca$_2$Cu$_3$O$_{8+\delta}$	42	OP	133	1.9	—◆—
HgBa$_2$CuO$_{4+\delta}$	43a	UD	72	/	/
	43a	OD	89	/	/
Cu$_{0.6}$Ca$_{0.4}$Ba$_2$-Ca$_3$Cu$_4$O$_{12+y}$	44	UD	117	/	—●—
Bi$_2$Sr$_2$CaCu$_2$O$_8$	45	OP	85	1.8	—●—
Tl$_{0.5}$Pb$_{0.5}$Sr$_2$-Ca$_{1-x}$Y$_x$Cu$_2$O$_{7-\delta}$	46c	0.1	70	/	/
	46c	0.25	107	/	/
	46c	0.5	80	/	/

[a]Data contradictory to our own experimental data;

[b]$T_{1\perp}$ not measured, but deduced from spin echo decay;

[c]T_1 determination unclear and/or limited spectral resolution to measure site-specific T_1

*The error on $\alpha_{\rm ani}$ is typically less than ± 0.08

Table 1. Furthermore, all displayed data points represent experimental data points from the literature, except for Fig. 3 where we had to interpolate data points to be able to plot the data with T as an implicit parameter. A few sets of data are excluded from our discussion; nonetheless, they are listed in Table 1 (see Appendix).

Note that we assume magnetic, frequency-independent spin-lattice relaxation, as data were taken at different fields. This was proven a few times, but not for all data sets. We could not find significant differences between zero-field NQR and high-field $1/T_{1\parallel}$ data (for the same system).

2.1 General Overview

An overview of all relaxation data as a function of temperature is given in Fig. 2, for two directions of the external field with respect to the crystal c-axis: (a) upper panel, $1/T_{1\perp}$ for $c \perp B_0$, and (b) lower panel, $1/T_{1\parallel}$ for $c \parallel B_0$.
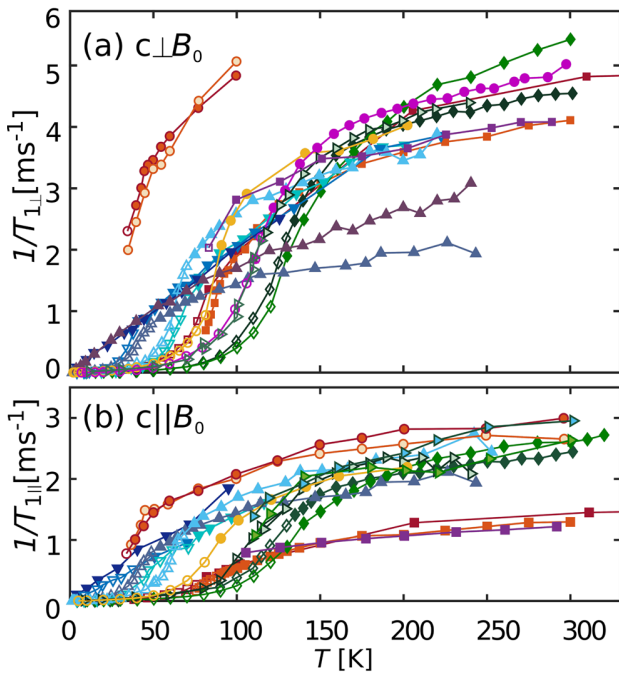
Fig. 2 ^{63}Cu nuclear relaxation rates as a function of temperature: **a** $1/T_{1\perp}$ and **b** $1/T_{1\parallel}$. For the used symbols see Table 1. Note that filled symbols indicate data above T_c and open symbols data below T_c. For more explanations, see text

Fig. 3 Main panel: $1/T_{1\perp}$ plotted vs. $1/T_{1\parallel}$ for each cuprate listed in Table 1 (T is implicit parameter). Dotted lines are fits to the data for each cuprate with slopes given by Eq. (1). The blue-dotted line is a diagonal with slope $\alpha_{\mathrm{ani}} = 1$. Inset: $1/T_{1\perp} \cdot 1/\alpha_{\mathrm{ani}}$ vs. $1/T_{1\parallel}$. All relaxation data can be explained by a single dominant relaxation process with a T-independent anisotropy

We would like to emphasize that it is more revealing to plot the relaxation rates against temperature (T), rather than plotting $1/(T_1 T)$ as a function of T. For a Fermi liquid, $1/T_1 \propto T$, and both plots carry the same information. However, if other mechanisms are present, they carry a T-dependent weight if one plots $1/(T_1 T)$, which complicates establishing a simple phenomenology.

While the plots are rather crowded, one can conclude on some general behavior, already. (i) Except for a couple of outliers (that will be discussed later), both panels show similar dependences, i.e., starting from $T = 0$ where relaxation has disappeared, the rates rise slowly below T_c. Above T_c, the rates are similar and begin to lag behind a Fermi liquid behavior, eventually. (ii) The data in panel (b) for $1/T_{1\parallel}$, while considerably smaller than for the other direction, show greater variations for different materials, which is somewhat surprising as the anisotropy of the hyperfine coupling coefficients is not expected to change. (iii) For $1/T_{1\perp}$ (panel (a)), one can identify Fermi liquid-like relaxation for many systems, without or with a T_c. In fact, one could imagine that if one would suppress T_c, $1/T_{1\perp}$ is not far from Fermi liquid behavior, with deviations mostly at higher temperatures (that can be caused by a more complicated band structure and has been observed in Fermi liquids [8]).

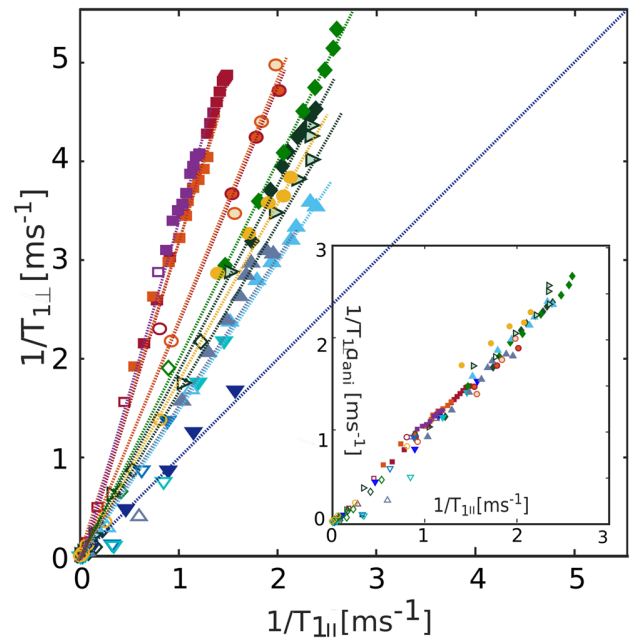We will now discuss salient features observed in the data in more detail.

2.2 Temperature-Independent T_1 Anisotropy

A salient feature in cuprate nuclear relaxation is a rather temperature-independent anisotropy,

$$\alpha_{\mathrm{ani}} = \frac{1/T_{1\perp}}{1/T_{1\parallel}} \equiv \frac{T_{1\parallel}}{T_{1\perp}}. \qquad (1)$$

That is, if we plot $1/T_{1\perp}$ vs. $1/T_{1\parallel}$ as in the main panel of Fig. 3, we find straight lines intersecting the origin, with slopes depending on the material. If one normalizes the slopes by the material specific α_{ani}, that is given in Table 1, all relaxation data collapse and fall on a single line as shown in the inset of Fig. 3.

Interestingly, these slopes take on special values for various materials and/or doping levels, and α_{ani} appears to increase as the doping decreases, but this is by no means a strict trend. The smallest $\alpha_{\mathrm{ani}} = 1$ (isotropic behavior) is observed for the highest doping levels, and the largest of 3.4 for YBa$_2$Cu$_3$O$_7$. For the underdoped, stoichiometric YBa$_2$Cu$_4$O$_8$, we find $\alpha_{\mathrm{ani}} = 3.33 \pm 0.02$, with rather high precision (this is one of the few cuprates that has very narrow linewidths). Indeed, it appears that α_{ani} takes on special values rather than showing a smooth dependence.

Since both rates are proportional to each other, above and below T_c, one concludes on a single, dominant relaxation
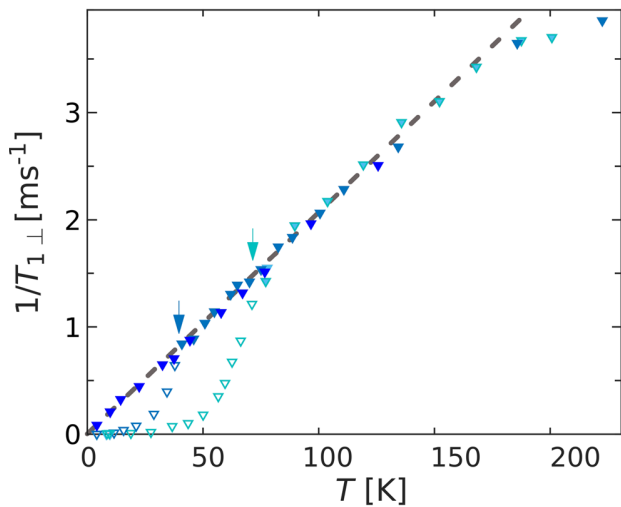
Fig. 4 Temperature dependence of the spin-lattice relaxation rates $1/T_{1\perp}$ for differently overdoped $Tl_2Ba_2CuO_{6+y}$ materials with $T_c =$ 0, 40, and 72 K (arrows). The grey-dashed line has a slope of 21/Ks which follows from Korringa's law for the Knight shift of about 0.89% for a simple Fermi liquid found for the highest doping level [33]

mechanism with excitations that are present at the highest temperatures and that decrease as T is lowered, similar to what happens for a Fermi liquid. Below T_c, the changes are more rapid but still show a rather fixed α_{ani} (note that the field's influence on T_c is anisotropic, as well, but those effects are mostly within the error bars here).

One would argue that the electronic liquid behaves quite similar in all cuprates and that it is the anisotropy of the coupling of the nuclei to this electronic reservoir that changes with doping and material. Furthermore, if the anisotropic relaxation mechanism does not share the crystal symmetry exactly, the differences in panel (a) of Fig. 2 could even be less.

Changes of the anisotropy of the hyperfine coefficients could lead to such behavior, but it is difficult to understand why this would produce only certain ratios and such large differences. While the spin response in the cuprates is believed

to be rather isotropic (except for strongly underdoped systems), dynamic correlations on short-length scales that can exist (as one knows from other probes) can contribute to such a behavior as well.

2.3 Fermi Liquid in Overdoped $Tl_2Ba_2CuO_{6+y}$

We now turn to the most overdoped cuprates in our data set, the $Tl_2Ba_2CuO_{6+y}$ family of materials. In Fig. 4, we plot $1/T_{1\perp}$ as a function of temperature for different doping levels with T_c of 0, 40, and 72 K (the same data are also present in Fig. 2). The dashed line is given by $1/T_{1\perp} = \sigma \times T$, with $\sigma = 21 /Ks$ as for a Fermi liquid with a Knight shift of 0.89% if one assumes $\rho = 1$ in Korringa's formula, which is close to what has been measured [33]. As can already be seen in Fig. 2, the data lag behind the Fermi liquid dependence only above about 200 K.

Clearly, this is hallmark Fermi liquid behavior for the most overdoped system (below 200 K). This is also true for the other two systems, except for a slight change in the anisotropies (there is no a priori reason to expect isotropic coupling). Below T_c, we observe spin-singlet pairing without a significant enhancement from coherent scattering (Hebel-Slichter peak). Again, from these plots one would assume that these three systems are well-behaved Fermi liquids, at least below about 200 K.

If one revisits Fig. 2, panel (a), with this important information, one is forced to conclude that the cuprate relaxation behaves rather Fermi liquid-like below about 200 K apart from the differences due to T_c for all doping levels and materials.

2.4 Doping Dependence of Nuclear Relaxation

In order to see how different doping levels affect the apparent relaxation, we plot in Fig. 5 the same data as in Fig. 2, but we emphasize in each of three panels a different doping range: (a) underdoped, (b) optimally doped, and (c) overdoped. Also shown is the dashed Fermi liquid line from Fig. 4.
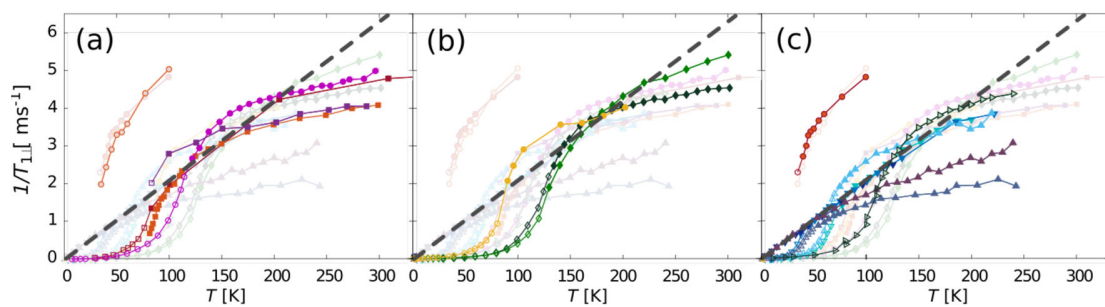

Fig. 5 Relaxation rate $1/T_{1\perp}$ vs. T (the same Fig. 2), with emphasis to three different regions of the phase diagram: (a) underdoped, (b) optimally doped, and (c) overdoped materials. In addition, each panel shows the same dashed line according to a Fermi liquid with 0.89% Knight shift

Apart form the differences in T_c, we do not see a particular trend in terms of doping dependence. It appears that no matter what the doping level is, whenever a material leaves the superconducting state, i.e., just above T_c, the relaxation is quite unique and very similar to the Fermi liquid value found for the very much overdoped systems. Also independent on doping, at higher temperatures, the relaxation rate starts to lag behind the Fermi liquid temperature dependence. $La_{2-x}Sr_xCuO_4$ appears to be an outlier independent on doping, as well.

Note that we do not have data for the very underdoped materials so that the findings above may not be valid there.

2.5 $La_{2-x}Sr_xCuO_4$

A significantly larger $1/T_{1\perp}$ compared with all other materials is found for the $La_{2-x}Sr_xCuO_4$ family. Such high rates [47] of $1/T_{1\perp}$ in $La_{2-x}Sr_xCuO_4$ have been reported repeatedly. It was discussed that these rates show a doping-dependent paramagnetic contribution, i.e., $1/T_1(T) =$ const., as well as an antiferromagnetic contribution, $T_1T \propto (T + T_N)$.[48]

Also, it was reported that $1/T_1$ converges at rather high T (above 700K) to a doping-independent value consistent with paramagnetic state of a Heisenberg antiferromagnet [49].

Given the additive nature of independent relaxation channels, it appears that $La_{2-x}Sr_xCuO_4$ may well have a similar component as all the other cuprates, i.e., one that is proportional to T, but also a second contribution that causes the special relaxation behavior. Also in terms of other (NMR) parameters, $La_{2-x}Sr_xCuO_4$ appears to be somewhat of an outlier: local charges on planars O and Cu measured by NMR clearly show that it has by far the least covalent in-plane bonding, such that its inherent hole is almost entirely localized in Cu $3d_{x^2-y^2}$ [50].

In terms of Cu shift, it also shows a special phenomenology, displaying no temperature or doping dependence of the shift for $c \parallel B_0$, and a comparatively strong dependence for $c \perp B_0$ [33].

2.6 Relaxation Below T_c

In order to see more clearly whether there is special behavior below T_c, we plot in Fig. 6 the relaxation $1/(T_{1\perp}T)$ as a function of the reduced temperature T/T_c. We restrict the plot to $T/T_c \lesssim 1.5$ since one cannot expect the reduced T to be meaningful at higher T.

When one tries to evaluate this plot, one must keep in mind that the reported T_c, which is used for the scaling in Fig. 6, might not be the best choice for the actual, local energy scale ($k_B T_c$). For example, T_c could be suppressed by sample quality, or it might differ due to different definitions when measured with different techniques.
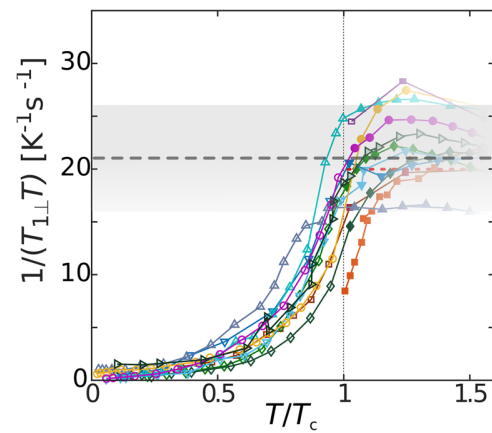

Fig. 6 $(T_{1\perp}T)^{-1}$ in $c \perp B_0$ for all materials listed in Table 1 as function of temperature scaled by the respective T_c. Also shown is $(T_1T)^{-1}(T) = 21 \pm 5$ $s^{-1}K^{-1}$ (dashed gray line with shaded background)

Furthermore, any additional relaxation mechanism is scaled by T_c, as well, and may introduce differences in samples with very high vs. very low T_c. Finally, since we use only $1/T_{1\perp}$ a slight change in anisotropy could also affect this value.

Despite possible uncertainties, inspection of Fig. 6 shows rather unique behavior for $T < T_c$. Just above T_c almost all cuprates come up to a similar relaxation rate, as we recognized earlier. This points to the same mechanism in the superconducting region independent on material and doping. Also, within the small variation of dependences, there is no clear trend as a function of the actual T_c or doping. Again, the most underdoped systems are almost indistinguishable from the most overdoped materials.

Worth mentioning is also that no cuprate shows an increased relaxation at the lowest temperatures in the $1/(T_1T)$ plot, where the low T rates are multiplied by increasingly large inverse T. So all excitations from this dominant mechanism are becoming gapped, which is true for d- and s-wave singlet pairing.

Whether the broad maximum in $1/(T_{1\perp}T)(T > T_c)$ seen in many materials signifies a vastly broadened coherence peak can unfortunately not be judged from the data available.

3 Conclusions

A review of all available planar Cu nuclear relaxation data in hole-doped cuprates offers a different understanding of the relevant electronic excitations.

The nuclear relaxation, when the external field lies in the CuO_2 plane, $1/T_{1\perp}$, is found to be rather independent on family and doping—from the weakly underdoped to

even those very strongly overdoped systems that are close to an ideal Fermi liquid, for which Korringa's law holds and to which the nuclei couple isotropcially. The material dependent and more often investigated $1/T_{1\parallel}$ is proportional to $1/T_{1\perp}$, above and below T_c, and thus only defines a material-dependent anisotropy of the nuclear coupling to the electronic bath. Thus, the nuclei appear to experience rather ubiquitous electronic excitations that begin to freeze below T_c. Therefore, the bath itself appears Fermi liquid-like throughout the whole phase diagram for all systems. At higher temperatures, the rates lag behind what is expected from a simple Fermi liquid (similar for all systems).

We also find universal behavior below T_c, i.e., the relaxation rates as a function of the reduced temperature (T/T_c) are rather similar.

All this points to a single, dominant relaxation mechanism due to electronic excitations that change significantly only below T_c due to spin singlet pairing.

In particular, no special electronic spin fluctuations were found to enhance nuclear relaxation. Furthermore, the pseudogap does not seem to affect the Cu relaxation, while it was shown that it is important for the suppression of the NMR shifts [51]. It was noticed before [52] that the Cu relaxation is in disagreement with neutron scattering results.

While we cannot say anything about the behavior of strongly underdoped systems, since there are no data available, it appear that only the $La_{2-x}Sr_xCuO_4$ family of materials is an outlier to the discussed scenario, as it appears to show additional relaxation for $1/T_{1\perp}$.

Author Contributions Data collection was performed equally by D.D and M.J.; independent verification of collected data was equally performed by M.A. and J.H.; discussion of data with equal help from D.P. and G.V.M.W.; preparation of the manuscript was equally performed by M.A., M.J., J.H.; J.H. also performed the data analysis and led the overall project.

Appendix: Literature data processing

For the review of relaxation data, we have collected all available literature data of $^{63}T_1$ of planar Cu. That means data for two orientations of the magnetic field with respect to the crystal c-axis, $c \parallel B_0$ and $c \perp B_0$, i.e. $1/T_{1\parallel}$ and $1/T_{1\perp}$, respectively. Furthermore, nuclear quadrupole resonance (NQR) were gathered, as well. The set comprises about 54 materials for $1/T_{1\parallel}$. The discussion in this manuscript, however, is limited to the 24 systems listed in Table 1, for which data for both directions of the field are available. Nevertheless, this (significant) subset we

are discussing is representative of all the data in terms of amplitude and different temperature dependences of relaxation, as we can judge from all $1/T_{1\parallel}$ data.

As remarked in the main text, the higher abundance of $1/T_{1\parallel}$ data is due to the use of c-axis aligned powders and NQR.

We have excluded data on electron-doped cuprates where $1/T_1$ in most cases is affected by rare earth magnetism in the charge reservoir layer, data on antiferromagnetic inner layers in triple and higher layered materials and data where it was unclear what definition for the T_1 was used [46]. We have also excluded $HgBa_2CuO_{4+\delta}$, for which our data are contradictory to results by Gippius et al. [43], as well as $Tl_2Ba_2CaCu_2O_{8-\delta}$, since $^{63}T_{1\perp}$ was not actually measured by Gerashenko et al. [40], but deduced from the spin-echo decay.

The data were extracted using the online software "WebPlotDigitzier", for which screenshots from graphs from the referenced papers were imported and the data extracted using the software tools.

In Fig. 3, the temperature is an implicit parameter, owing to the limited availability of $1/T_{1\alpha}(T)$ data for both orientations at identical temperatures, we used a linear interpolation.

References

1. Slichter, C.P. Principles of Magnetic Resonance, 3rd edn. Springer, Berlin (1990)
2. Heitler, W., Teller, E.: Proc. R. Soc. A Math. Phys. Eng. Sci. **155**, 629 (1936)
3. Korringa, J.: Physica **16**, 601 (1950)
4. Bardeen, J., Cooper, L.N., Schrieffer, J.R.: Phys. Rev. **106**, 162 (1957)
5. Hebel, L.C., Slichter, C.P.: Phys. Rev. **113**, 1504 (1959)
6. Bednorz, J.G., Müller, K.A.: Z. Phys. B Condens. Matter **193**, 189 (1986)
7. Kotegawa, H., Ishida, K., Kitaoka, Y., Muranaka, T., Akimitsu, J.: Phys. Rev. Lett. **87**(12), 127001 (2001)
8. Silbernagle, B.G., Weger, M., Clark, W.G., Wernick, J.H.: Phys. Rev. **153**, 535 (1967)
9. Rybicki, D., Haase, J., Greven, M., Yu, G., Li, Y., Cho, Y., Zhao, X.: J. Supercond. Nov. Magn. **22**, 179 (2009)
10. Jurkutat, M., Haase, J., Erb, A.: J. Supercond. Nov. Magn. **26**, 2685 (2013)
11. Reichardt, S., Jurkutat, M., Guehne, R., Kohlrautz, J., Erb, A., Haase, J.: Condens. Matter **3**(3), 23 (2018)
12. Singer, P.M., Hunt, A.W., Imai, T.: Phys. Rev. Lett. **88**, 047602 (2002)
13. Hunt, A.W., Singer, P.P.M., Cederström, A.F., Imai, T.: Phys. Rev. B **64**, 134525 (2001)
14. Walstedt, R.E., Warren, W.W., Bell, R.F., Brennert, G.F., Espinosa, G.P., Remeika, J.P., Cava, R.J., Rietman, E.A.: Phys. Rev. B **36**(10), 5727 (1987)
15. Markert, J.T., Noh, T.W., Russek, S.E., Cotts, R.M.: Solid State Commun. **63**(9), 847 (1987)
16. Kitaoka, Y., Hiramatsu, S., Kondo, T., Asayama, K.: J. Phys. Soc. Jpn. **57**(1), 30 (1988)

17. Shimizu, T., Yasuoka, H., Imai, T., Tsuda, T., Takabatake, T., Nakazawa, Y., Ishikawa, M.: J. Phys. Soc. Jpn. **57**(7), 2494 (1988)
18. Mali, M., Brinkmann, D., Pauli, L., Roos, J., mann, H., Hulliger, J.: Phys. Lett. A **124**(1-2), 112 (1987)
19. Walstedt, R.E., Warren, W.W., Bell, R.F., Brennert, G.F., Espinosa, G.P., Cava, R.J., Schneemeyer, L.F., Waszczak, J.V.: Phys. Rev. B **38**(13), 9299 (1988)
20. Walstedt, R.E., Warren, W.W.: Phys. B: Condens. Matter **163**(1), 75 (1990)
21. Pennington, C.H., Durand, D.J., Zax, D.B., Slichter, C.P., Rice, J.P., Ginsberg, D.M.: Phys. Rev. B **37**(1), 7944 (1988)
22. Imai, T., Shimizu, T., Yasuoka, H., Ueda, Y., Kosuge, K., Phys, J.: Soc. Jpn. **57**(7), 2280 (1988)
23. Pennington, C.H., Durand, D.J., Slichter, C.P., Rice, J.P., Bukowski, E.D., Ginsberg, D.M.: Phys. Rev. B **39**, 2902 (1989)
24. Takigawa, M., Hammel, P.C., Heffner, R.H., Fisk, Z.: Phys. Rev. B **39**(10), 7371 (1989)
25. Takigawa, M., Hammel, P.C., Heffner, R.H., Fisk, Z., Smith, J.L., Schwarz, R.B.: Phys. Rev. B **39**, 300 (1989)
26. Walstedt, R.E., Warren, W.W., Bell, R.F., Espinosa, G.P.: Phys. Rev. B **40**(4), 2572 (1989)
27. Barrett, S.E., Martindale, J.A., Durand, D.J., Pennington, C.H., Slichter, C.P., Friedmann, T.A., Rice, J.P., Ginsberg, D.M.: Phys. Rev. Lett. **66**(1), 108 (1991)
28. Slichter, C.P.: In: Schrieffer, J.R., Brooks, J.S. (eds.) Handbook of High-Temperature Superconductivity, pp. 215–256. Springer, New York (2007)
29. Haase, J., Goh, S.K., Meissner, T., Alireza, P.L., Rybicki, D.: Rev. Sci. Instrum. **80**(7), 073905 (2009)
30. Meissner, T., Goh, S.K., Haase, J., Williams, G.V.M., Littlewood, P.B.: Phys. Rev. B **83**, 220517(R) (2011)
31. Haase, J., Rybicki, D., Slichter, C.P., Greven, M., Yu, G., Li, Y., Zhao, X.: Phys. Rev. B **85**, 104517 (2012)
32. Rybicki, D., Kohlrautz, J., Haase, J., Greven, M., Zhao, X., Chan, M.K., Dorow, C.J., Veit, M.J.: Phys. Rev. B **92**, 081115(R) (2015)
33. Haase, J., Jurkutat, M., Kohlrautz, J.: Condens. Matter **2**(2), 16 (2017)
34. Itoh, Y., Machi, T., Fukuoka, A., Tanabe, K., Yasuoka, H.: J. Phys. Soc. Jpn. **65**, 3751 (1996)
35. Auler, T., Horvatić, M., Gillet, J.A., Berthier, C., Berthier, Y., Carretta, P., Kitaoka, Y., Ségransan, P., Henry, J.Y.: Phys. C:, Supercond. **313**(3), 255 (1999)
36. Zimmermann, H., Mali, M., Bankay, M., Brinkmann, D.: Phys. C:, Supercond. **185–189**, 1145 (1991)
37. Magishi, K., Kitaoka, Y., Zheng, G.Q., Asayama, K., Kondo, T., Shimakawa, Y., Manako, T., Kubo, Y.: Phys. Rev. B **54**(14), 10131 (1996)
38. Fujiwara, K., Kitaoka, Y., Ishida, K., Asayama, K., Shimakawa, Y., Manako, T., Kubo, Y.: Phys. C:, Supercond. **184**(4-6), 207 (1991)
39. Zheng, G.Q., Kitaoka, Y., Asayama, K., Hamada, K., Yamauchi, H., Tanaka, S.: Phys. C:, Supercond. **260**(3–4), 197 (1996)
40. Gerashenko, A., Piskunov, Y., Mikhalev, K., Ananyev, A., Okulova, K., Verkhovskii, S., Yakubovskii, A., Shustov, L., Trokiner, A.: Phys. C:, Supercond. **328**(3-4), 163 (1999)
41. Itoh, Y., Machi, T., Yamamoto, A.: Phys. Rev. B **95**, 094501 (2017)
42. Magishi, K., Kitaoka, Y., Zheng, G.Q., Asayama, K., Tokiwa, K., Iyo, A., Ihara, H.: J. Phys. Soc. Japan **64**(12), 4561 (1995)
43. Gippius, A.A., Antipov, E.V., Hoffmann, W., Lüders, K., Buntkowsky, G.: Phys. Rev. B **59**(1), 654 (1999)
44. Tokunaga, Y., Ishida, K., Kitaoka, Y., Asayama, K., Tokiwa, K., Iyo, A., Ihara, H.: Phys. Rev. B **61**(14), 9707 (2000)
45. Walstedt, R.E., Bell, R.F., Mitzi, D.B.: Phys. Rev. B **44**(14), 7760 (1991)
46. Bogdanovich, A., Zhdanov, Y.I., Mikhalyov, K., Lavrentjev, V., Aleksashin, B., Verkovskij, S., Winzek, N., Gergen, P., Gross, J., Mehring, M., et al.: Phys. C:, Supercond. **215**(3-4), 253 (1993)
47. Ohsugi, S., Kitaoka, Y., Ishida, K., Zheng, G.Q., Asayama, K.: J. Phys. Soc. Jpn. **63**, 700 (1994)
48. Gor'kov, L.P., Teitel'baum, G.B.: J. Exp. Theor. Phys. Lett. **80**(3), 195 (2004)
49. Imai, T., Slichter, C.P., Yoshimura, K., Katoh, M., Kosuge, K.: Phys. B Condens. Matter **197**(1-4), 601 (1994)
50. Jurkutat, M., Rybicki, D., Sushkov, O.P., Williams, G.V.M., Erb, A., Haase, J.: Phys. Rev. B **90**(R), 140504 (2014)
51. Avramovska, M., Pavicevic, D., Haase, J.: Supercond. Nov. Magn. (2019). https://doi.org/10.1007/s10948-019-05174-w
52. Berthier, C., Julien, M.H., Bakharev, O., Horvatić, M., Ségransan, P.: Phys. C **282**, 227 (1997)

ORIGINAL PAPER

NMR Shift and Relaxation and the Electronic Spin of Superconducting Cuprates

Marija Avramovska[1] · Danica Pavićević[1] · Jürgen Haase[1]

Abstract

Very recently, by inspecting large sets of data across all families of superconducting cuprates, it became obvious that the prevailing nuclear magnetic resonance (NMR) interpretation of cuprate properties is not adequate, as it does not account for the differences between the families, as well as common characteristics beyond simple temperature dependence. From the most abundant planar Cu shift data, one concludes readily on two electronic spin components with different doping and temperature dependencies. Their uniform response that causes NMR spin shifts consists of a doping-dependent component due to planar O, and another due to spin in the planar copper $3d(x^2 - y^2)$ orbital, where the latter points opposite the field direction. Planar Cu relaxation was found to be rather ubiquitous (except for $La_{2-x}Sr_xCuO_4$), and Fermi liquid-like, i.e., independent of doping and material, apart from the sudden drop at the superconducting transition temperature, T_c. Only the relaxation anisotropy is doping and material dependent. We showed previously that one can understand the shifts within a two-component scenario, but we failed with a model to account for the relaxation. Here, we suggest a slightly different shift scenario, still based on the two components, by introducing different hyperfine couplings, and, importantly, we are able to account for the Cu nuclear relaxation and its anisotropy for all materials, including also $La_{2-x}Sr_xCuO_4$. The results represent a solid framework for theory.

Keywords Cuprates · NMR · Electronic properties

1 Introduction

Nuclear magnetic resonance (NMR) is a powerful local, bulk probe of material properties [1]. This concerns the chemical as well as electronic structure of materials, which can be studied locally at various nuclear sites in the unit cell. The changes in the NMR shifts and relaxation from the modification of the density of states due to the opening of a superconducting gap in conventional superconductors are famous examples [2, 3]. Not surprisingly, after the discovery of cuprate superconductivity [4], NMR experiments focused

✉ Marija Avramovska
marija.avramovska@uni-leipzig.de

Danica Pavićević
danicas.dp@gmail.com

Jürgen Haase
j.haase@physik.uni-leipzig.de

[1] Felix Bloch Institute for Solid State Physics,
University of Leipzig, Linnéstr. 5, 04103, Leipzig, Germany

in particular on planar Cu and O in these type II materials (for reviews of cuprate NMR, see [5, 6]). However, with the early focus on only a few systems and a lack of established theory, the NMR data interpretation ceased to evolve with a number of questions unanswered. Fortunately, more and more NMR studies of different materials appeared in the literature over the years.

During the last 10 years, with special NMR experiments on $La_{1.85}S_{0.15}CuO_4$ [7], $YBa_2Cu_4O_8$ [8], and samples of the $HgBa_2CuO_{4+\delta}$ family of materials [9, 10], a cornerstone of the old interpretation was questioned and shown to be not correct: a single temperature-dependent electronic spin component, $s(T)$, that follows from the uniform spin susceptibility, i.e., $s(T) = \chi(T) \cdot B_0$, in an external field B_0, is *not* capable of describing the temperature-dependent NMR spin shifts, $^nK_d(T) = {}^nH_d \cdot \chi(T)$. Since $^nK_d(T)$ can be measured at various nuclei (n), or for any orientation (d) of the external field with respect to the crystal axes, with ^nH_d being the corresponding hyperfine constant, one demands from different experiments that $\Delta^nK_d \propto \Delta^mK_e$, which was clearly *not* observed in general, only in certain ranges of temperature [7–10].

Also during the last decade, the understanding of the charge sharing in the CuO_2 plane advanced significantly from a more qualitative [11] into a quantitative model [12, 27]. It became apparent that, e.g., the maximum temperature of superconductivity correlates with the sharing of the inherent hole between planar Cu and O, the higher the oxygen hole content the higher $T_{c, max}$ [13]. Other cuprate properties depend on the charge sharing, as well. This mostly family-dependent behavior stimulated some of us to inspect also a larger body of NMR shifts and relaxation for material-dependent differences or common characteristics.

In the first step, all available ^{63}Cu NMR shifts that are rather abundant and reliable were gathered [14]. And, indeed, by just plotting these shifts a new phenomenology emerged, and points immediately to a more complicated uniform response that cannot be explained with a simple $\chi(T)$. In the second step, all available ^{63}Cu NMR relaxation rates were collected [15, 16] and, again, simple plots revealed a surprisingly different scenario. Here, a rather material- and doping-independent relaxation was revealed with spin fluctuations similar, but not in excess to what one expects from a simple Fermi liquid. Only the relaxation anisotropy depends on the materials and decreases with increasing doping.

Then, in a first attempt, we tried to reconcile these findings [15]. We could show that a two-component description, as introduced earlier [7] (with two spin components that couple with two different hyperfine coefficients, $^{n}H_{1d}$ and $^{n}H_{2d}$, to each nuclear spin, n), is indeed sufficient to understand the planar Cu shifts (with the $La_{2-x}Sr_xCuO_4$ family being some kind of outlier, cf. Fig. 1). Two spin susceptibilities (χ_1, χ_2) demand a third term from a coupling between the two electronic spin components. That is, one has to write, $\chi_1 = \chi_{11} + \chi_{12}$, $\chi_2 = \chi_{22} + \chi_{21}$ ($\chi_{12} = \chi_{21}$), and,

$$^{n}K_{\parallel,\perp} = {^{n}H_{1\parallel,\perp}} \cdot (a + c) + {^{n}H_{2\parallel,\perp}} \cdot (b + c) \quad (1)$$

with $a = \chi_{11}B_0$, $b = \chi_{22}B_0$, and $c = \chi_{12}B_0$, and the magnetic field parallel and perpendicular to the crystal c-axis.

In order to independently test the important conclusion of two spin components with different doping and temperature dependencies, we investigated the planar O data [20], very recently. We found that, indeed, planar O shifts demand two spin components, as well, where one of them is doping dependent. This encouraged us to search for a better understanding of the very reliable Cu data, in particular of the nuclear relaxation and its anisotropy, which we failed to deliver previously [15].

By plotting a large set of literature Cu relaxation data [15], we found generic behavior, as well, with the exception of just one family, $La_{2-x}Sr_xCuO_4$. In fact, all other cuprates have rather similar relaxation rates, $1/T_{1\perp}$ [16], i.e., if measured with the magnetic field perpendicular to the crystal c-axis, $c \perp B_0$, cf. Fig. 2. In particular, just above T_c the value of $1/T_{1\perp}T_c \sim 20/Ks$ for all cuprates, while T_c can be very different, or even close to zero for strongly overdoped systems. There is no particular doping dependence of $1/T_{1\perp}$ as one might naively expect if electronic spin fluctuations beyond those of a more regular Fermi liquid were to increase toward lower doping levels (there are hardly data available at very low doping). In fact, a value of 20/Ks follows with the Korringa relation [22] from those cuprates with the highest shifts, i.e., the upper right corner of the shaded triangle in Fig. 1 [15], which suggests that the shifts have the tendency to be suppressed if the Korringa relation fails, and it is not due to an increased relaxation. The situation is somewhat different for $1/T_{1\parallel}$ since for this direction of measurement ($c \parallel B_0$) the rates differ between families and have the tendency to increase with decreasing doping. However, it was demonstrated that the ratio, $[1/T_{1\perp}(T)] / [1/T_{1\parallel}(T)]$, is temperature independent for all cuprates, and is the same above and below T_c; i.e., both rates are proportional to each other [15, 16].

Interestingly, the $La_{2-x}Sr_xCuO_4$ family of materials is the only outlier to this phenomenology, cf. Fig. 2. However, the anisotropy ratio is also temperature independent and has a value of about 2.3, very similar to that of some other cuprates.

In our first attempt at reconciling shift and relaxation [15], we could only explain the shift suppression, but failed to present a microscopic model that also explains the relaxation and its anisotropy. Here, we discuss and modify our previously suggested two-component scenario [15] in that we introduce somewhat different hyperfine coefficients, together with a new notation, still based on the identification of the two electronic components as being due to planar Cu $3d(x^2 - y^2)$ and likely planar O $2p_\sigma$ spin densities. Most importantly, we are able to present a simple, yet fundamental, model of nuclear relaxation in terms of these two components that fits all planar Cu relaxation data, even including the outlier $La_{2-x}Sr_xCuO_4$.

2 Planar Cu Shifts

Dissimilar from our previous attempt to understand all planar Cu shift data [15], we will be using a somewhat different nomenclature and hyperfine coupling coefficients here. Therefore, we repeat the basic arguments leading to the description, now.

The total magnetic shift for planar Cu, $^{63}\hat{K}_{\parallel,\perp}$, is the sum of an orbital and spin shift component, and we have for
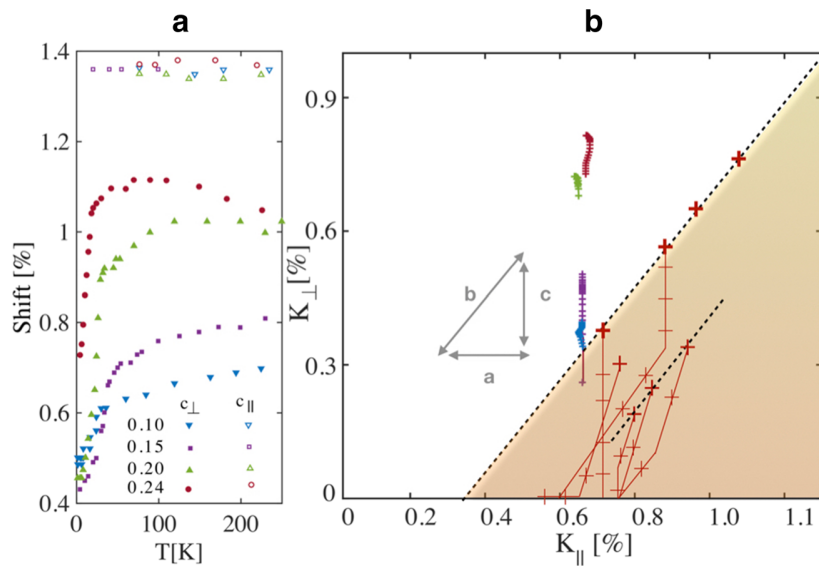
Fig. 1 **a** Total ^{63}Cu shifts vs. temperature, $\hat{K}_{\parallel,\perp}(T)$, for 4 doping levels of La$_{2-x}$Sr$_x$CuO$_4$ and two directions ($c \parallel B_0$, $c\perp B_0$) of the external field B_0 with respect to the crystal c-axis (adopted from [17]). $K_\parallel$ is T independent and similar for all doping levels. $K_\perp$ shows a much larger spread with doping and decreases rapidly near T_c. **b** Sketch of the spin shift $K_\perp(T)$ vs $K_\parallel(T)$ plot valid for other cuprates [14], with real data from the 4 doping levels of La$_{2-x}$Sr$_x$CuO$_4$ (with temperature as an implicit parameter). The shaded area is where the rest of the many cuprates can be found (the shaded triangle has a hypotenuse of slope $\approx$ 1), only typical data are shown by crosses. Data

lie on straight line segments (lines) with a few slopes only: a slope $\approx$ 1 (dashed lines); a very steep slope (vertical lines); a slope of 2.5. For example, a slope of 2.5 is typical for HgBa$_2$CuO$_{4+\delta}$ (at higher T), a steep slope for YBa$_2$Cu$_4$O$_8$, and for symmetry reasons we use a slope of 1 for some Tl-based compounds, as well as for overdoped HgBa$_2$CuO$_{4+\delta}$ at low T. La$_{2-x}$Sr$_x$CuO$_4$ is a clear outlier with only the steep slope. In the simple two-component description, cf. (5), (6), a change in one of the components a, b, or the coupling c leads to the indicated slopes in the middle of (**b**); for the subtraction of the orbital shifts, see main text

the two orientations ($c \parallel B_0$, $c\perp B_0$) of the magnetic field B_0 with respect to the crystal c-axis,

$$\hat{K}_{\parallel,\perp}(T) = K_{L\parallel,\perp} + K_{\parallel,\perp}(T). \tag{2}$$

It is of particular use to plot the total shifts $\hat{K}_\perp(T)$ vs. $\hat{K}_\perp(T)$ [14] with temperature as an implicit parameter, i.e., one does not make assumptions about $K_{L\parallel,\perp}$. Such a plot brings out a number of remarkable trends [14, 15]. A sketch of such a plot is presented in Fig. 1b, and we repeat some conclusions [15], but also include new ones, below.

A fundamental assumption is [14, 15],

$$K_{L\perp} \approx 0.30\%, \tag{3}$$

since all cuprates show a rather similar low temperature shift for $c\perp B_0$ with $\hat{K}_\perp(T \to 0) \approx 0.30\%$. Therefore, this value appears to be reliable. It is the same assumption made early on [5]. We note that this value is backed by first principle calculations [19] (while this is not the case for $K_{L\parallel}$).

Second, except for La$_{2-x}$Sr$_x$CuO$_4$, all data points in that plot are found in the lower right triangle that has

Fig. 2 **a** Planar ^{63}Cu relaxation rates of the cuprates (data from [16]); $1/T_{1\perp}$ of La$_{2-x}$Sr$_x$CuO$_4$ in comparison is about twice as high as that of other cuprates. **b** $1/T_{1\perp}$ vs $1/T_{1\parallel}$, which is ≈ 2.3 for La$_{2-x}$Sr$_x$CuO$_4$ (highlighted), is very similar to what is found for other cuprates (data [16]). It is mostly $1/T_{1\parallel}$ that changes with doping and material, but remains proportional to $1/T_{1\perp}$ (at all temperatures)
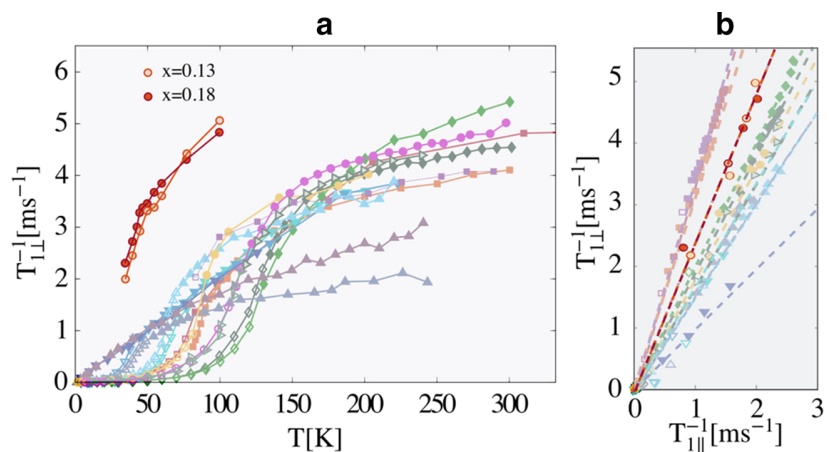
as hypothenuse a line of slope 1, i.e., $\Delta \hat{K}_\perp / \Delta \hat{K}_\parallel(T) \approx 1$. This line points immediately to an isotropic hyperfine coefficient, while the fact that $\hat{K}_\parallel(T) > \hat{K}_\perp(T)$ (all data in the lower, right triangle) demands a second, very anisotropic hyperfine coefficient that acts mostly for $c \parallel B_0$. Very similar arguments as put forward in the old literature let us choose $A_{\perp,\parallel}$ and B: note that there must be spin in the $3d(x^2 - y^2)$ orbital, and it is very likely that there will also be an isotropic coupling term. Then, the NMR shifts demand, however, that the spin polarization in the $3d(x^2 - y^2)$ orbital must be *negative*, as pointed out recently [14, 15], for we know that $A_\parallel$ is negative, and $|A_\parallel| \gg A_\perp$ [23].

Thus, we write with (1),

$$K_{\parallel\perp} = A_{\parallel,\perp} \cdot (a + 4c_j) + B \cdot 4(b_j + c_j). \tag{4}$$

For symmetry reasons, we take $(b_j + c_j)$ from each of the 4 neighbors to be the same, i.e., from spin in the planar O $2p_\sigma$ orbitals, cf. Fig. 3. As before [15], we will neglect $A_\perp$ and simply write:

$$K_\parallel = A_\parallel(a + 4c_j) + B \cdot 4(b_j + c_j) \tag{5}$$
$$K_\perp \approx B \cdot 4(b_j + c_j). \tag{6}$$

This is a different notation from before [15] where we used $b = 4b_j$.
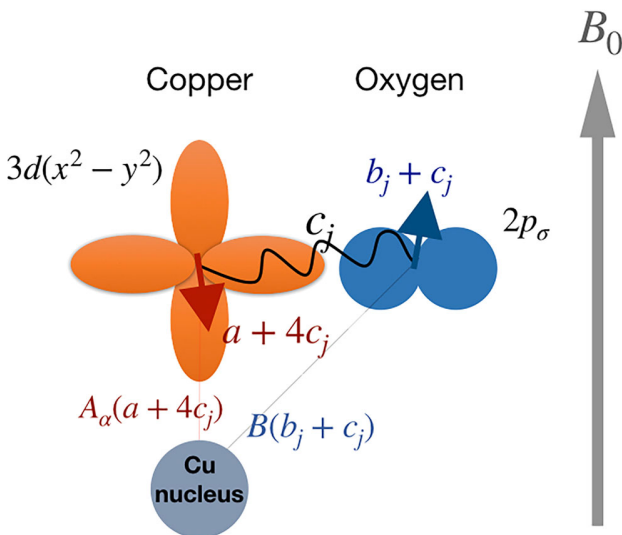

Fig. 3 In an external magnetic field B_0 two spin components a and b_j appear, originating from the planar Cu $3d(x^2 - y^2)$ and the four surrounding O $2p_\sigma$ orbitals, respectively. Due to a coupling (c), the effective components are $(a + 4c_j)$ and $(b_j + c_j)$. While $(b_j + c_j)$ is positive for the cuprates, $(a + 4c_j)$ turns out to be negative. The hyperfine coefficients A_d and B lead to orientation-dependent (d) NMR shifts $K_d = A_d(a + 4c_j) + B(b_j + c_j)$ at the Cu nucleus

A zero spin shift, our first, fundamental assumption means that $\sum_j (b_j + c_j) = 0$, and we have for the other orientation:

$$\hat{K}_\parallel(T \to 0) = K_{L\parallel} + A_\parallel(a + 4c_j). \tag{7}$$

In order to estimate the orbital shift, $K_{L\parallel}$, for this orientation of the field, as before [15], the most reliable approach is to use (3) together with calculations of the orbital shift anisotropy, since the latter is mostly determined by matrix elements involving the orbital bonding wave functions of Cu and O [18, 19]. In fact, we use the suggested value of 2.4 from [19]:

$$^{63}K_{L\parallel} = 2.4 \cdot {}^{63}K_{L\perp} \approx 0.72\%. \tag{8}$$

Note that this value could vary between families, but since the orbital shift for $c \perp B_0$ does not change significantly between families, we do not expect a large effect for $c \parallel B_0$, as well. This is important as it means that most cuprates have a non-vanishing spin shift for $c \parallel B_0$ from a negative spin polarization in the $3d(x^2 - y^2)$ orbital, even at the lowest temperatures.

As mentioned earlier, a few special slopes govern the shift-shift plot presented in their figure 7 [14], and we highlighted them in Fig. 2b, again. These are segments defined by temperature or doping for which the ratio of changes in both shifts is constant, $\Delta \hat{K}_\perp(T) / \Delta \hat{K}_\parallel(T) = \kappa$, and one finds 4 slopes, $\kappa \approx 0, 1, 2.5, \infty$. For example, $\kappa = 1$ denotes isotropic shift lines and readily follows from a mere change of b_j only, as it enters both terms in (5) and (6). Then, $\kappa \approx 0$ in this approximation is realized by a change in a, only, since we neglected the rather small $A_\perp$. Note that term c operates on both shifts, $K_\perp$ and $K_\parallel$, and must be involved in the special slopes $\kappa = 2.5$ and $\kappa \approx \infty$. While not favored before [15], we believe that $\kappa \approx \infty$ is caused by a mere change in c. The reasoning is as follows: not a single material in the shift-shift plot shows a negative slope, i.e., a slope to the right of $\kappa \approx \infty$. This is remarkable and must mean that the component a cannot significantly be involved in shift changes.

With this assumption that c_j causes $\kappa \approx \infty$, we note that (5) and (6) require:

$$A_\parallel \approx -B, \tag{9}$$

and we have with (5) and (6):

$$K_\parallel \approx B(4b_j - a) \tag{10}$$
$$K_\perp \approx B4(b_j + c_j). \tag{11}$$

Note that in this approximation, c effectively acts only for $c \perp B_0$. Then, the slope of $\kappa \approx 2.5$ is given by a concomitant change of b_j and c_j, e.g., $\Delta b_j = 1.5 \Delta c_j$ if both terms change proportionally.

To summarize, in the above model, the individual changes of a, b_j, and c_j correspond to slopes of $\kappa = 0, 1,$

and ∞, respectively, in Fig. 1 (if all b_j and c_j are the same). Even if this is not precisely what happens, we think that (10) and (11) still capture the fundamental aspects of the planar Cu shifts.

With these results in mind, we can look at the data for $La_{2-x}Sr_xCuO_4$ again.

The high temperature shifts for $La_{2-x}Sr_xCuO_4$, $K_\perp$, are much larger than what we expect from its $K_\parallel = B(4b_j - a)$ values. In one scenario, a larger a and larger b_j could position this family at larger $K_\perp$ (for given c_j). The action of a temperature-dependent c_j then leads to the $\kappa \approx \infty$ slope. Alternatively, c_j could be much larger for $La_{2-x}Sr_xCuO_4$, i.e., much more positive, at high temperatures. This also leads to a much larger $B(b_j + c_j)$. Again, a drop in c_j then makes $(b_j + c_j)$ disappear.

To conclude, while $La_{2-x}Sr_xCuO_4$ is an outlier in the shifts, the position in Fig. 1 can be understood within the two-component scenario, as well.

3 Planar Cu Relaxation

The nuclear relaxation rate $1/T_{1\parallel}$ measures the in-plane fluctuating magnetic fields, $\langle h_\perp^2 \rangle$, from electronic spin fluctuations, while $1/T_{1\perp}$ is affected by both, in-plane, $\langle h_\perp^2 \rangle$, as well as out-of-plane, $\langle h_\parallel^2 \rangle$, fields (only fluctuating field components perpendicular to the nuclear quantization axis lead to nuclear spin flips, required for spin-lattice relaxation).

Phonons will cause nuclear relaxation for quadrupolar nuclei ($I > 1/2$, like Cu and O) as they modulate the electric field gradient, but it has been shown that the magnetic fluctuations dominate in most situations [24, 25], and the recent analysis of all Cu relaxation data shows that a simple magnetic mechanism appears to capture the overall behavior quite well [15, 16].

In a straightforward approach, one would assume nearly isotropic spin fluctuations filtered by the nuclear hyperfine coefficients, which can then lead to a relaxation anisotropy. The electronic correlation time (τ_0) of electronic spin fluctuations is expected to be very fast compared with the slow precession of the nuclei. Thus, the nuclear relaxation rates can be written as [18]:

$$\frac{1}{T_{1\parallel}} = \frac{3}{2}\gamma^2 \cdot 2\langle h_\perp^2 \rangle \tau_0 \tag{12}$$

$$\frac{1}{T_{1\perp}} = \frac{3}{2}\gamma^2 \left[\langle h_\perp^2 \rangle + \langle h_\parallel^2 \rangle \right] \tau_0, \tag{13}$$

from which the relaxation anisotropy follows:

$$\frac{1/T_{1\perp}}{1/T_{1\parallel}} = \frac{1}{2} + \frac{\langle h_\parallel^2 \rangle}{2\langle h_\perp^2 \rangle}. \tag{14}$$

Given that the shifts demand two different electronic spin components coupled to the nuclei through an anisotropic constant $A_{\parallel,\perp}$ and an isotropic constant B, one should allow for two different fluctuating spin densities α and $\beta = \sum_j \beta_j$, as well. Furthermore, since the fluctuations are caused by rapid exchange, the correlation time τ_0 should be the same for both components.

We thus write:

$$\langle h_{\perp,\parallel}^2 \rangle \approx \langle (\sum_j B\beta_j + A_{\perp,\parallel}\alpha)^2 \rangle \tag{15}$$

$$\langle h_\parallel^2 \rangle \approx B^2 \langle (\sum_j \beta_j - \alpha)^2 \rangle, \tag{16}$$

$$\langle h_\perp^2 \rangle \approx B^2 \langle (\sum_j \beta_j + f\alpha)^2 \rangle, \tag{17}$$

where we introduced $f = A_\perp/B \approx -A_\perp/A_\parallel$ if $A_\perp \alpha$ is not negligible (see below).

With these expressions for the fluctuating field components, we seek to explain a rather doping- and material-independent $1/T_{1\perp}$ (it only increases marginally with decreasing doping) and a material- and doping-dependent $1/T_{1\parallel}$ that explain the temperature-independent anisotropy (14), as well as the exceptional behavior found for $La_{2-x}Sr_xCuO_4$.

In the first scenario, one might be interested to see what would be the consequences of totally uncorrelated spin fluctuations for the 5 spin components, i.e., $\langle \beta_i \beta_j \rangle = \langle \beta_0^2 \rangle \delta_{ij}$, and $\langle \beta_j \alpha \rangle = 0$, cf. Fig. 4. We then have $\langle h_\perp^2 \rangle = 4\langle \beta_0^2 \rangle$ and $\langle h_\parallel^2 \rangle = 4\langle \beta_0^2 \rangle + \langle \alpha^2 \rangle$, thus with (12) and (13) for uncorrelated (u) fluctuations:

$$\frac{1}{T_{1\parallel,u}} = \frac{3}{2}\gamma^2 B^2 \cdot 8\langle \beta_0^2 \rangle \tau_0 \tag{18}$$

$$\frac{1}{T_{1\perp,u}} = \frac{3}{2}\gamma^2 B^2 \cdot \left[8\langle \beta_0^2 \rangle + \langle \alpha^2 \rangle \right] \tau_0, \tag{19}$$

and it follows for the anisotropy:

$$\frac{1/T_{1\perp,u}}{1/T_{1\parallel,u}} = 1 + \frac{\langle \alpha^2 \rangle}{8\langle \beta_0^2 \rangle}. \tag{20}$$

Clearly, for $\langle \alpha^2 \rangle \lesssim \langle \beta_0^2 \rangle$, we find near isotropic relaxation, and in order to explain the largest anisotropy of about 3.3 [16], we conclude $\langle \alpha^2 \rangle \approx 18.4\langle \beta_0^2 \rangle$. This implies, however, rather large changes of α and β for meeting the experimental observations, i.e., the change in relaxation between materials and different doping levels, which appears to be difficult to meet in this approach (we do notice that a large α could be present, which demands that we do not neglect $A_\perp$ for the modeling of nuclear relaxation).

In the second scenario, cf. Fig. 4, we assume that all spins are aligned; i.e., the 5 fluctuating spin components are correlated, with $\langle \beta_i \beta_j \rangle = \langle \beta_0^2 \rangle$ and $\langle \beta_j \alpha \rangle = \pm\alpha\beta_0$. We note

Fig. 4 Fluctuating spins α and β_0, respectively located in the Cu $3d(x^2-y^2)$ and O $2p_\sigma$ orbital. **a**, all 5 spin components fluctuate independently, i.e., $\langle\alpha\beta_0\rangle = 0$, $\langle\beta_i\beta_j\rangle = \beta_0^2\delta_{ij}$, **b**, the fluctuations are fully correlated, i.e., $\langle\alpha\beta_0\rangle = \alpha\beta_0$, $\langle\beta_i\beta_j\rangle = \beta_0^2$
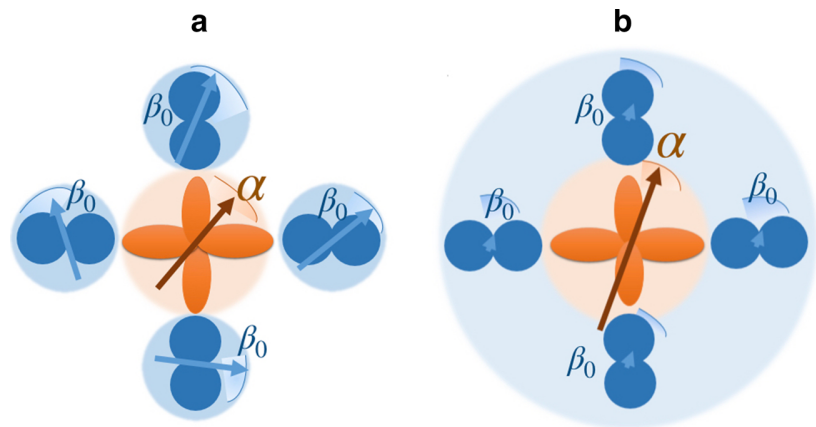
that the field fluctuations $\langle h_\perp^2\rangle \approx B^2\langle(\sum_j\beta_j + f\alpha)^2\rangle$ that enter (12) and $\langle h_\parallel^2\rangle \approx B^2\langle(\sum_j\beta_j - \alpha)^2\rangle$ that determine (13) are both quadratic in the resulting local spin densities. Therefore, in order to find a rather flat dependence for the relaxation for $c\perp B_0$ on β_0, as demanded by the experiment, we need to be close to its minimum, while at the same time, the parabola must be shifted by a negative α compared with the other parabola in order to meet a smaller but varying relaxation rate for $c \parallel B_0$. The results of simple calculations according to (12), (13) with (16) and (17) are shown in Fig. 5. We observe that there is only a special region with solutions that fit the experiments, for $\beta_0/\alpha = 0.04$ to 0.11 according to anisotropies ranging from 3.3 to 1.0, respectively, cf. Fig. 5.

Furthermore, an increase of α by a factor of about 1.3, at an anisotropy ratio of 2.3, increases the relaxation rates in both directions by about a factor of 2, cf. Fig. 5, which readily explains the data found for $La_{2-x}Sr_xCuO_4$. We thus conclude that the two components β_0 and α are crucial for the cuprates, but appear to be very similar for most of the materials.

4 Discussion

It seems out of question that a two-component scenario describes the shifts and relaxation in the cuprates quite well. It has spin density located in the Cu $3d(x^2-y^2)$ orbital, which couples to the nucleus through the rather anisotropic hyperfine constant $A_{\parallel,\perp}$, and, most likely, the planar O $2p_\sigma$ orbital, leading to an isotropic hyperfine interaction given by (4).

The spin density α is much larger than β_0, as one expects from the overall material properties; however, the uniform response of both spins is quite different, also due to the coupling term c_j.

The special slopes observed in the shift-shift plot, cf. Fig. 1, are caused by changes of the individual spin

components as a function of doping or temperature, except for the slope $\kappa \approx 2.5$ that must stem from a concomitant change of b_j and c_j. This leads to the simple conclusion that $A_\parallel \approx -B$ (while $A_\perp \approx 0.15A_\parallel$ [23]), and it leaves us with a straightforward description of the spin shifts of the cuprates in terms of (10) and (11), i.e., $K_\parallel \approx B(4b_j - a)$ and $K_\perp \approx B4(b_j + c_j)$ (in these equations, we also adopted a different notation in terms of b_j compared with our earlier analysis [15]). We note that the conclusion that $A_\parallel \approx -B$ has a similar origin as in the old interpretation.
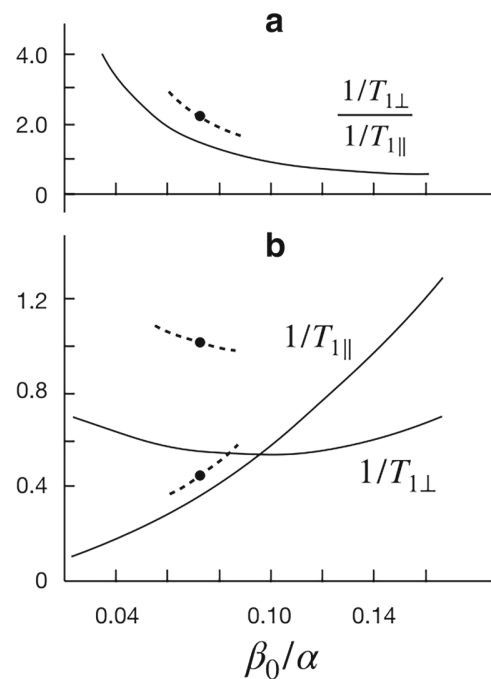

Fig. 5 a Calculated nuclear relaxation rates for $c \parallel B_0$ ($1/T_{1\parallel}$) and $c\perp B_0$ ($1/T_{1\perp}$) as a function of the ratio of the two spin components $\beta_0 \equiv \beta_j$ and α (β_0/α), according to (12), (13) with (16) and (17), in arbitrary units. **b** The anisotropy of the relaxation (14) varies between 4 and 0.5 in the same range of β_0/α. Corresponding line segments for $La_{2-x}Sr_xCuO_4$ with an anisotropy of about 2.3 are indicated, as well

Looking again at Fig. 1b, the cuprates are sorted in this shift-shift plot effectively by the high-temperature b_j, the component that grows with increasing doping (toward the upper right in Fig. 1b). As the temperature is lowered, at a given temperature, which can be above or at T_c, this term begins to disappear due to the action of c_j (both components c_j and b_j can fall together, as well). It is the coupling to a that sets c_j (and effectively couples different a terms, as well). The component a appears to be temperature independent. It emerges that either b_j or c_j can be exhausted independently indicated by changes in slope at lower temperatures. However, all cuprates seem to reach the same $(b_j + c_j) = 0$, which we define as zero spin shift. Importantly, there is no evidence that there is a different mechanism as one passes through T_c if the shift began to change already far above T_c (NMR pseudogap), but c_j can traverse the region below T_c at a much higher rate for given steps in temperature.

The earlier conclusion [14, 15] that the spin shift for $c \parallel B_0$ does not disappear at low temperatures, here takes the formulation that $(4b_j - a) \neq 0$ and says that the positive spin density b_j and the negative spin density a_j can remain temperature independent for systems with $\kappa \approx \infty$, or b_j can also drop with c_j as for the systems with slope $\kappa \approx 2.5$; i.e., it does not change in the condensed state, while relaxation ceases.

In terms of a simple fluctuating field model, we can explain the cuprate relaxation rather well. Fast electronic, Fermi liquid-like spin fluctuations act through two different hyperfine coefficients with two different electronic spin densities on the Cu nucleus (or, these densities are part of that ubiquitous fluid). The corresponding fluctuations from the 5 locations must be correlated, as one might have guessed due to the close proximity. The on-site $3d(x^2 - y^2)$ spin (α) is about 10 times as large as that due to one O neighbor (β_0). The spin density α appears to be the same for all cuprates; except for the $La_{2-x}Sr_xCuO_4$ family, it is 30% larger. The spin β_0 varies with doping and between materials and leads to the change in $1/T_{1\parallel}$ observed in the data. For large doping the relaxation anisotropy is about 1 and it increases to about 3.3 for $YBa_2Cu_4O_8$ (corresponding to a change in β_0 of about 3). For $La_{2-x}Sr_xCuO_4$ the anisotropy is 2.3 and thus also β_0 is about a factor of two larger.

Since the ^{63}Cu relaxation begins to disappear only at T_c, for all cuprates, the electronic, Fermi liquid-like spin fluctuations freeze out and the relaxation disappears. Thus, the pseudogap in the relaxation is just due to the correlations that for planar Cu do not change α and β_0 spin alignment. For planar O the situation is different as the nucleus couples to two α spins at adjacent Cu nuclei and their coupling changes, which leads to the pseudogap in the relaxation for nuclei that are affected by different a spins [26].

The relation between the spin densities α, β_0 and the uniform response of the system in terms of a, b_j, and c_j is not known. It appears that the response of α is rather small compared to that of β, which may not be surprising since different a should favor antiferromagnetic alignment (that is somehow affected by β).

It appears that the doping dependent spread in $K_\parallel$ varies among the cuprates. This reminds us of the way the charge carriers enter the CuO_2 plane [12]. For the $La_{2-x}Sr_xCuO_4$ family, the doped charges x enter almost exclusively the $2p_\sigma$ orbital (n_p) while for other systems the Cu $3d(x^2 - y^2)$ (n_d) is affected as well ($x = \Delta n_d + 2\Delta n_p$ [12, 27]), and the spread in doping appears to grow with Δn_d. The maximum achievable T_c, however, is set by the sharing of the parent material's hole content, i.e., $n_d^* + 2n_p^* = 1$ and $T_{c, max} \propto n_p^*$ [12, 13, 28]. Materials with the highest T_c appear to adopt $\kappa \approx 2.5$, only. However, the jumping between different slopes κ in different regions of the shift-shift plot that involves b_j and/or c_j below T_c is absent for optimally doped systems, which probably means that b_j and c_j are matched at optimal doping.

Finally, one may argue that the intra cell charge variation between neighboring planar O atoms that appears to be ubiquitous and that can respond to the external magnetic field [22, 29] could be involved in the two component scenario.

5 Conclusions

Two spin densities were shown to reside in the planar Cu $3d(x^2 - y^2)$ and likely the planar O $2p_\sigma$ orbitals, respectively, with hyperfine constants $A_{\parallel,\perp}$ and $B \approx -A_\parallel$. They connect the Cu nuclear spins with a rather ubiquitous Fermi liquid-like bath. The relaxation anisotropy is predominantly due to changes in the planar O spin density that increases with doping. Near T_c, these electronic fluctuations freeze out and the relaxation disappears.

The uniform response a and b_j of the two electronic spins on Cu and O is special in the sense that a is negative while b_j points along the field. The coupling term c_j between a and b_j sets the temperature dependence of the shift above (NMR pseudogap) and below T_c. Interestingly, at the lowest temperatures, $4(b_j + c_j)$ approaches the same value for all cuprates, probably zero, but a remains and most of b_j, as well, resulting in a non-vanishing spin shift for $c \parallel B_0$, $K_\parallel \approx (4b_j - a) \neq 0$.

The coupling term c_j must be related to a coupling between different spin components a_i on different Cu nuclei, and it is argued that the pseudogap phenomenon for planar O nuclear relaxation, and that of Y, is just a consequence of the temperature dependence of c_j, an effect that cannot be there in the Cu relaxation data.

This simple two-component scenario appears to fit all cuprates, in particular also the only outlier family so far, $La_{2-x}Sr_xCuO_4$, which must make it a reliable framework for theory.

References

1. Slichter, C.P. Principles of Magnetic Resonance, 3rd edn. Springer, Berlin (1990)
2. Hebel, L.C., Slichter, C.P.: Phys. Rev. **113**, 1504 (1959). https://doi.org/10.1103/PhysRev.113.1504
3. Yosida, K.: Phys. Rev. **110**, 769 (1958). https://doi.org/10.1103/PhysRev.110.769
4. Bednorz, J.G., Müller, K.A., Phys, Z., Condens, B.: Matter **193**, 189 (1986). https://doi.org/10.1007/BF01303701
5. Slichter, C.P.: In: Schrieffer, J.R., Brooks, J.S. (eds.) Handbook of High-Temperature Superconductivity, pp. 215–256. Springer, New York (2007). https://doi.org/10.1007/978-0-387-68734-6_5
6. Walstedt, R.E.: The NMR Probe of High-T_c Materials, 1st edn, Springer. https://doi.org/10.1007/978-3-540-75565-4 (2007)
7. Haase, J., Slichter, C.P., Williams, G.V.M.: J. Phys. Condens. Matter **21**, 455702 (2009). https://doi.org/10.1088/0953-8984/21/45/455702
8. Meissner, T., Goh, S.K., Haase, J., Williams, G.V.M., Littlewood, P.B.: Phys. Rev. B **83**, 220517 (2011). https://doi.org/10.1103/PhysRevB.83.220517
9. Haase, J., Rybicki, D., Slichter, C.P., Greven, M., Yu, G., Li, Y., Zhao, X.: Phys. Rev. B **85**, 104517 (2012). https://doi.org/10.1103/PhysRevB.85.104517
10. Rybicki, D., Kohlrautz, J., Haase, J., Greven, M., Zhao, X., Chan, M.K., Dorow, C.J., Veit, M.J.: Phys. Rev. B **92**, 081115 (2015). https://doi.org/10.1103/PhysRevB.92.081115
11. Zheng, G.Q., Mito, T., Kitaoka, Y., Asayama, K., Kodama, Y.: Phys. C Supercond. **243**, 337 (1995). https://doi.org/10.1016/0921-4534(95)00029-1
12. Jurkutat, M., Rybicki, D., Sushkov, O.P., Williams, G.V.M., Erb, A., Haase, J.: Phys. Rev. B **90**, 140504 (2014). https://doi.org/10.1103/PhysRevB.90.140504
13. Rybicki, D., Jurkutat, M., Reichardt, S., Kapusta, C., Haase, J.: Nat. Commun. **7**, 1 (2016). https://doi.org/10.1038/ncomms11413
14. Haase, J., Jurkutat, M., Kohlrautz, J.: Condens. Matter **2**(2), 16 (2017)
15. Avramovska, M., Pavićević, D., Haase, J.: J. Supercond Nov. Magn. **243**(3), 337 (2019)
16. Jurkutat, M., Avramovska, M., Williams, G.V.M., Dernbach, D., Pavićević, D., Haase, J.: J. Supercond Nov. Magn. **155**(12), 629 (2019)
17. Ohsugi, S., Kitaoka, Y., Ishida, K., Aheng, G.Q., Asayama, K.: J. Phys. Soc. Jpn. **63**, 700 (1994). https://doi.org/10.1143/JPSJ.63.700
18. Pennington, C.H., Durand, D.J., Slichter, C.P., Rice, J.P., Bukowski, E.D., Ginsberg, D.M.: Phys. Rev. B **39**, 2902 (1989). https://doi.org/10.1103/PhysRevB.39.2902
19. Renold, S., Heine, T., Weber, J., Meier, P.F.: Phys. Rev. B **67**(2), 24501 (2003). https://doi.org/10.1103/PhysRevB.67.024501
20. Pavićević, D., Avramovska, M., Haase, J.: arXiv.org (2019)
21. Haase, J.: Phys. Rev. Lett. **91**(18), 189701 (2003)
22. Korringa, J.: Physica **16**, 601 (1950). https://doi.org/10.1016/0031-8914(50)90105-4
23. Husser, P., Suter, H.U., Stoll, E.P., Meier, P.F.: Phys. Rev. B **61**(2), 1567 (2000)
24. Takigawa, M., Smith, J.L., Hults, W.L.: Phys. Rev. B **44**(14), 7764 (1991)
25. Suter, A., Mali, M., Roos, J., Brinkmann, D.: J. Magn. Reson. **143**(2), 266 (2000)
26. Avramovska, M., Pavićević, D., Haase, J. ((in preparation))
27. Haase, J., Sushkov, O.P., Horsch, P., Williams, G.V.M.: Phys. Rev. B **69**, 94504 (2004). https://doi.org/10.1103/PhysRevB.69.094504
28. Jurkutat, M., Erb, A., Haase, J.: Condens. Matter **4**(3), 67 (2019)
29. Reichardt, S., Jurkutat, M., Guehne, R., Kohlrautz, J., Erb, A., Haase, J.: Condens. Matter **3**(3), 23 (2018)

Publisher's Note Springer Nature remains neutral with regard to jurisdictional claims in published maps and institutional affiliations.

4.2   O NMR and the pseudogap

This subchapter presents two publications dealing with the O NMR data. The first publication centers on O relaxation and shift data for one direction of the magnetic field ($c \parallel B_0$). The O relaxation data in its totality showed some notable observations, e.g., the overdoped systems showed clear metallic behavior ($1/T_1 \propto T$), with a slope $\approx 0.36/Ks$ intersecting the origin. As doping is lowered, we observe the same slope but with an offset. This means that for the optimally doped and underdoped systems, increasing temperature adds states in the same way as in the overdoped systems. The offset points to the fact that low energy states are missing even at the highest temperatures. This is the action of a temperature-independent pseudogap and is very similar to what was pointed out also from electronic entropy, [Loram et al., 1998]. As doping is lowered, more low energy states are missing, i.e., the pseudogap size increases and shifts the parallel relaxation lines.

The O shifts similarly point to the presence of a temperature-independent pseudogap. The overdoped shifts are Fermi-liquid like, and the Korringa relation holds, but as doping is lowered we see the signature behavior where the shifts are offset and gain a temperature dependence above T_c. So, the O data could be explained by the presence of a temperature-independent pseudogap at the Fermi surface, where the states outside the gap are ubiquitous to all the cuprates, irrespective of doping and material and are metallic-like.

We presented a simple model to fit the data, where we used the Fermi function with a fixed density of states and calculated the NMR relaxation. Then we manually removed states near the Fermi surface, by assuming a U- or a V-shaped gap in the density of states. The model simulated the observed behavior in relaxation, i.e., parallel lines for different sizes of the pseudogap.

Similarly for the shifts, we find that using the same model, we are able to simulate the data, and even the hallmark pseudogap behavior—temperature dependence above T_c —seems to be a result of the temperature-independent pseudogap.

The second paper focuses on the O shift and relaxation anisotropy. We present shift data measured with the field along the Cu-O-Cu σ bond, $K_{\parallel\sigma}$, perpendicular to

the bond, $K_{\perp c}$, and along the crystal c-axis, $K_{\perp a}$. Additionally, for the O relaxation, we present only the anisotropy since the relaxation data are scarce with other field directions. First, we find that the measured O orbital shifts are in good agreement with theoretical predictions using first principle cluster calculations [Renold et al., 2003].

[Hüsser et al., 2000] calculated the O magnetic hyperfine coefficients from first principles. If there is only a single spin component susceptibility, then the shift anisotropies should follow from the ratios of the magnetic hyperfine coefficients, which is indeed the case. We note that both shift and relaxation anisotropies are in agreement with the calculated hyperfine coefficients. So, unlike the more complicated Cu data, the O shift and relaxation can be fully explained by assuming a single-spin component coupled to the nucleus with the theoretically predicted hyperfine coefficients.

Lastly, we also analyzed ^{89}Y data, which marked the early discovery of the pseudogap [Alloul et al., 1989] as the characteristic temperature dependence well above T_c. This data also showed the typical features of a temperature-independent pseudogap, similarly as the O data.

Temperature-Independent Cuprate Pseudogap from Planar Oxygen NMR

Jakob Nachtigal [1], Marija Avramovska [1], Andreas Erb [2], Danica Pavićević [1], Robin Guehne [1] and Jürgen Haase [1],*

[1] Felix Bloch Institute for Solid State Physics, University of Leipzig, Linnéstr. 5, 04103 Leipzig, Germany; jn43neti@studserv.uni-leipzig.de (J.N.); marija.avramovska@uni-leipzig.de (M.A.); danicas.dp@gmail.com (D.P.); r.guehne@physik.uni-leipzig.de (R.G.)

[2] Walther Meissner Institut, Bayerische Akademie der Wissenschaften, 85748 Garching, Germany; Andreas.Erb@wmi.badw.de

* Correspondence: j.haase@physik.uni-leipzig.de

Abstract: Planar oxygen nuclear magnetic resonance (NMR) relaxation and shift data from all cuprate superconductors available in the literature are analyzed. They reveal a temperature-independent pseudogap at the Fermi surface, which increases with decreasing doping in family-specific ways, i.e., for some materials, the pseudogap is substantial at optimal doping while for others it is nearly closed at optimal doping. The states above the pseudogap, or in its absence are similar for all cuprates and doping levels, and Fermi liquid-like. If the pseudogap is assumed exponential it can be as large as about 1500 K for the most underdoped systems, relating it to the exchange coupling. The pseudogap can vary substantially throughout a material, being the cause of cuprate inhomogeneity in terms of charge and spin, so consequences for the NMR analyses are discussed. This pseudogap appears to be in agreement with the specific heat data measured for the YBaCuO family of materials, long ago. Nuclear relaxation and shift show deviations from this scenario near T_c, possibly due to other in-gap states.

Keywords: NMR; cuprates; pseudogap

1. Introduction

Nuclear magnetic resonance (NMR) provides important local information about the electronic properties of materials [1], and it has played a key role in the characterization of cuprate high-temperature superconductors [2,3]. However, different from when NMR proved Bardeen-Cooper-Schrieffer (BCS) theory [4,5], for cuprates a full theoretical understanding is lacking, and thus, it is challenging to decipher NMR data.

In classical metals and superconductors, NMR is known for the local measurement of the electronic spin susceptibility [6–10], including the predicted changes in the density of states at the Fermi surface with a coherence peak in nuclear relaxation [5]. In the normal state, the high density of states near the Fermi surface leads to the distinctive, fast nuclear relaxation $(1/T_1)$ that is proportional to temperature $(1/T_1 \propto T)$ since temperature increases the available number of electronic states for scattering with nuclear spins. Quite to the contrary, the NMR spin shift that is proportional to the uniform electronic spin susceptibility is temperature-independent, as the increase in temperature also decreases the occupation difference.

These elements of observation were the backdrop against which the cuprate NMR data were discussed, early on. Unfortunately, the cuprates have large unit cells and the important nuclei in the plane, ^{63,65}Cu

and ^{17}O, have electric quadrupole moments and thus are affected by the local charges, as well. This leads to multiple resonances that have to be assigned to the chemical structure, and inhomogeneously broadened lines in the non-stoichiometric systems are the rule. This complicates measurement and interpretation. Fortunately, the cuprates are type-II materials and can be investigated in the mixed state below T_c at typical magnetic fields used for NMR, which gives access to the properties of the superfluid, but also complicates shift measurements from residual diamagnetism [11].

Early on, a number of more or less universal magnetic properties of the cuprates were derived, such as spin-singlet pairing, the pseudogap, and special spin fluctuations (for reviews see [2,3]). Here, we will not dwell on a more detailed discussion of previous conclusions, as we believe that while the data are undisputed, the prevailing view needs to be corrected.

In recent years, some of us were involved in special NMR shift experiments that raised suspicions about the description of the magnetic properties based on NMR [12–15]. During the same period of time, a comprehensive picture of the charge distribution in the CuO$_2$ plane was developed [16–18]. It fostered the understanding of charge sharing in electron and hole-doped cuprates, as it was found that $1 + x = n_{Cu} + 2n_O$, i.e., the charges measured with NMR in the planar Cu (n_{Cu}) and O (n_O) bonding orbitals add up to the total charge, inherent plus doped hole ($x > 0$) or electron ($x < 0$) content. An astonishing correlation appeared in this context, as the maximum T_c of a curpate system ($T_{c,max}$) is nearly proportional to n_O [18,19]. This explains the differences in $T_{c,max}$ between the various families that differ in charge sharing considerably, and it calls into question the usefulness of what one calls the cuprate phase diagram, rather, a phase diagram in terms of n_{Cu} and n_O appears advantageous [20].

These findings suggested that some cuprate properties might be family dependent, and that a broader look at NMR data might be useful, as well. Since planar O NMR requires the exchange of ^{16}O by ^{17}O, which is not easily performed for single crystals and can have consequences for the actual doping and its spatial distribution, the focus was on planar Cu data that appeared more abundant and more reliable.

Immediately, the overview of the Cu shifts across all families [21] demands different shift and hyperfine scenarios, as the changes in the shifts are not proportional to each other (similar to what was found with special NMR experiments before [12,14,15]). Likely, it involves two spin components, one that has a negative uniform response and is located at planar Cu, coupled to a second component (presumably on planar O) with the usual positive response. In the next step, all planar Cu relaxation data were gathered [22,23], and from the associated plots, it became obvious that, surprisingly, the Cu relaxation is quite ubiquitous, very different from what was concluded early on. It turns out that the relaxation rate measured with the magnetic field in the plane ($1/T_{1\perp}$) does neither change significantly between families, nor as a function of doping, with $1/T_{1\perp}T_c \approx 21/\text{Ks}$. Only the relaxation anisotropy changes by about a factor of three across all cuprates. Thus, no enhanced, special spin fluctuations are present in the underdoped systems. This leaves, as an explanation for the failure of the Korringa relaxation (discovered early on [3]), only a suppression of the NMR shifts [22]. This also means that there is no pseudogap effect in planar Cu relaxation, while the Cu shifts do have a temperature dependence above T_c presumably from pseudogap effects. Finally, it was shown that the planar Cu relaxation can be understood in terms of two spin components, as well [24], where a doping dependent correlation of the Cu spin with that of O explains the relaxation anisotropy. Furthermore, the unusual planar Cu shift component that is a function of doping and not necessarily temperature was found to be present in the planar O high temperature data [25], where it causes the hallmark asymmetry of the total quadrupole lineshape, observed long ago [26–28], but not understood.

Here, we present all temperature-dependent shift and relaxation data of planar ^{17}O collected in an intensive literature search (data points from about 80 publications were taken). The main conclusion from the data will be that planar O relaxation, different from Cu, is affected by the pseudogap that also dominates the planar O shifts. Here, the pseudogap represents itself as a loss in the density of

states close to the lowest energies (at the Fermi surface) for the underdoped materials, and this gap is temperature-independent, but set by doping, different from what is often assumed [29,30]. This scenario is in agreement with early specific heat data [31] that also discussed such a pseudogap in $YBa_2Cu_3O_{7-\delta}$. The largest found pseudogap is in agreement with a nodeless suppression of states of the size of the exchange coupling, 1500 K. It rapidly decreases with increasing doping, e.g., it is closed for $YBa_2Cu_3O_{7-\delta}$ at optimal doping, but not for optimally doped $La_{2-x}Sr_xCuO_4$.

2. Planar Oxygen Relaxation and Shift for $YBa_2Cu_3O_{6+y}$ and $YBa_2Cu_4O_8$

Nuclear relaxation of planar oxygen shows strikingly simple behavior in these most studied materials, and we will find the conclusions to be generic to the cuprates.

2.1. Planar Oxygen Relaxation

In Figure 1, next to a sketch of expected behavior for a Fermi liquid (**A**) we plot the relaxation rate ($1/T_1$) vs. temperature (T). It is apparent that optimally and overdoped $YBa_2Cu_3O_{7-\delta}$ (**B**) are Femi liquid-like: above T_c, an increase (decrease) in temperature adds (subtracts) additional states for nuclear scattering and even the density of states (DOS) seems to be rather constant up to about 250 K (above that temperature the relaxation appears to begin to lag behind the expected value [32]).

It is important to note that at high temperatures, changes in temperature (ΔT) lead to proportional changes in relaxation ($\Delta(1/T_1)$) with a slope of 0.36 /Ks that intersects the origin. In other words, the proportionality of the rate to temperature is only disturbed by the opening of the superconducting gap at T_c, below which relaxation drops more rapidly as pairing sets in (no Hebel–Slichter peak is observed). Thus, planar O relaxation of optimally and overdoped $YBa_2Cu_3O_{7-\delta}$ appears determined by Fermi liquid-like electrons, turning into a spin-singlet superconductor.

The underdoped materials behave distinctively different, Figure 1B. Here we observe a rapid change of relaxation with doping at a given temperature, but we find nearly the same high-temperature slope of about 0.36 /Ks, i.e., increasing the temperature adds states at the same rate as for optimally or overdoped systems. However, the shifted slopes signal an offset in temperature below which relaxation must disappear. This means, even at much larger temperatures one is aware of the lost low temperature states. This is exactly what one expects if a temperature-independent, low-energy gap in the DOS develops with doping (a gap that remains open at high temperatures). The same scenario applies to $YBa_2Cu_4O_8$, cf. Figure 1C, where the intercept of the high-temperature slope with the abscissa is about 70 K.

At lower temperatures, the rates for $YBa_2Cu_3O_{7-\delta}$ become rather doping-independent, below about 80 K. It appears that the special temperature dependence due to the superconducting gap and pseudogap merge, somewhat different from the behavior with $YBa_2Cu_4O_8$, but still similar in the sense that the relaxation begins to increase as it departs from the parallel lines.

Note, the relaxation ceases completely at the lowest temperatures for all materials. While electric contributions (electric quadrupole interaction) to the relaxation have been shown to exist and contribute at lower temperatures [33,34] their contribution vanishes, as well. The true magnetic relaxation dependencies might be systematically shifted to lower rates at lower temperatures compared to what is seen in Figure 1. Therefore, the apparent increase in relaxation could signal quadrupolar relaxation, as well. A thorough study of these effects might be in order.
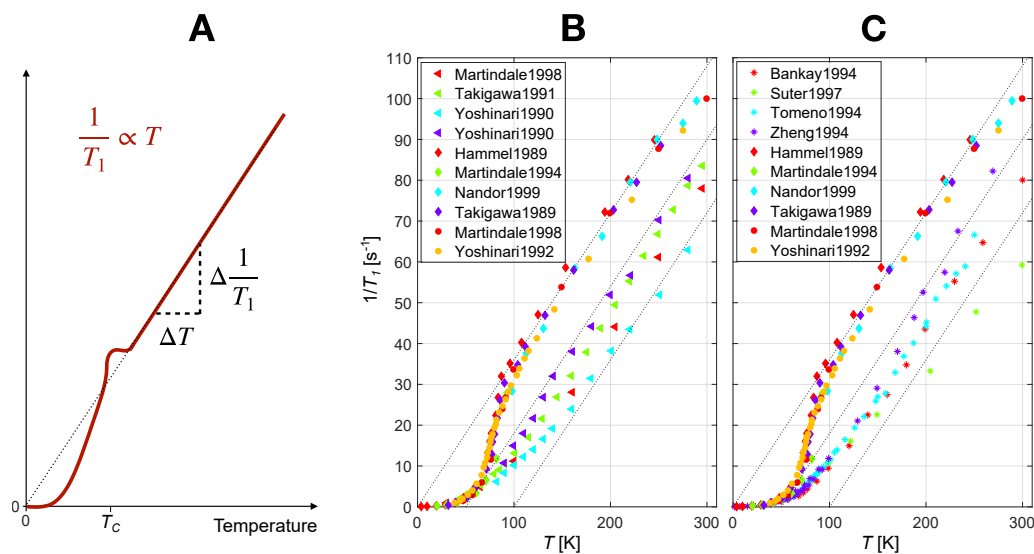
Figure 1. Nuclear Relaxation. (**A**) (sketch), above the critical temperature for superconductivity, T_c, in a Fermi liquid, the relaxation is proportional to temperature, i.e., the slope points to the origin of the plot; only just below T_c, the BCS gap for spin singlet pairing leads to a loss of states and relaxation (after the Hebel–Slichter coherence peak). (**B**), optimally doped $YBa_2Cu_3O_{6.96}$ (full circles) and overdoped $YBa_2Cu_3O_7$ (diamonds) behave Fermi liquid-like above T_c (dotted lines have slope $1/(T_1T) = 0.36/Ks$). Underdoped $YBa_2Cu_3O_{7-\delta}$ (triangles) show identical high-temperature behavior in the sense that as a function of temperature the relaxation increases with the same slope as found for optimally and underdoped systems, i.e., as the Fermi function opens with increasing temperature, it adds states at the same rate. However, the slope does not intersect the origin, which shows that even at high temperatures, low energy states are missing. This is the planar O pseudogap effect that rapidly evolves when the doping is lowered. (**C**), same as (**B**), except the relaxation data for the underdoped materials have been replaced by data for $YBa_2Cu_4O_8$ (starred points); this underdoped, stoichiometric material displays a very similar temperature dependence at higher temperatures. For the references see Appendix A.

2.2. Planar Oxygen Shifts

For planar O the orbital shift is almost negligible [26], making the spin shifts rather reliable with uncertainties arising only from the diamagnetic response below T_c. Shift referencing is simple, as well, as ordinary tap water can be used for ^{17}O NMR referencing (there is significant confusion about Cu shift referencing in the literature [21]). Nevertheless, there appear to be deviations between the shifts measured on similar samples, even for stoichiometric $YBa_2Cu_4O_8$ [35], and it is not always clear if shifts were corrected for the diamagnetic response. We will show the bare shifts without correction, in order to avoid introducing systematic errors. For example, it is possible that the uniform spin response from Cu^{2+} is negative [21,22] leading to a negative term for planar O at low temperatures.

Note that the diamagnetic response of the cuprates was experimentally determined with ^{89}Y NMR, early on [11], by assuming that this nucleus' spin shift is negligible at low temperatures (4.2K). A value of about 0.05% was derived [11]. This value appears to be rather large [36], and as experiments with ^{199}Hg NMR of $HgBa_2CuO_{4+\delta}$ showed [15], the diamagnetic response measured at ^{199}Hg is probably less than 0.01% (note that ^{199}Hg is located far from the plane and should not suffer from large spin shifts, different from ^{89}Y that might be affected by a negative term, as well).

For a Fermi liquid with a fixed DOS near the Fermi surface one expects a temperature-independent spin shift (K) above T_c, since an increase in temperature adds new states from an opening Fermi function, but the occupation decreases at the same rate, cf. Figure 2A. Now, in view of the planar O relaxation, a temperature-independent gap at the Fermi surface should be assumed. Then, qualitatively, we expect a behavior shown in Figure 2A: at the highest temperatures, far above the gap, low temperature states will still be missing, leading to a lower spin shift. As the temperature is lowered, the effect of the gap will be more severe. This is in agreement with data in Figure 2B,C. Below T_c, we note that there is no sudden loss of states as for optimally or overdoped materials, which one might naively expect if the same superconducting gap opens on the states still available. Quite to the opposite, a less rapid decrease of the shifts below T_c is observed (we noted a different low-temperature behavior for relaxation, as well).

Note that the Korringa relation is given by $T_1 T K^2 = (\gamma_e/\gamma_n)^2 \hbar/(4\pi k_B) \equiv S_0$ [8], and with $S_0 = 1.4 \cdot 10^{-5}$ Ks one estimates a spin shift of about $K = 0.23\%$ from the relaxation slope of 0.36 /Ks, not very different from what is observed for optimally or overdoped systems in Figure 2.
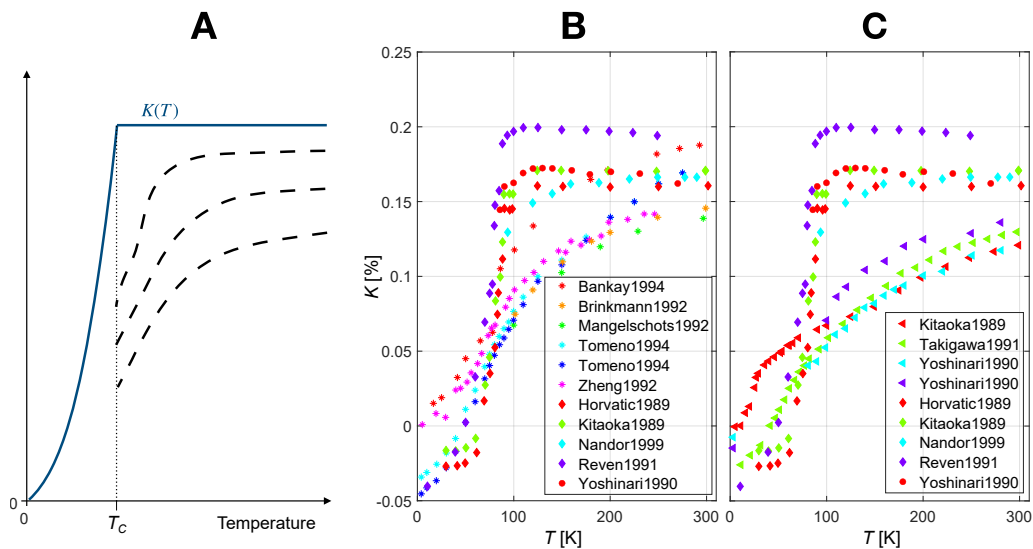

Figure 2. Planar ^{17}O nuclear magnetic resonance (NMR) Shifts. (**A**), (sketch) Fermi liquid behavior with spin singlet pairing at T_c is shown with the full blue line. The dashed lines indicate what one expects based on the relaxation data: above T_c, states are missing increasingly as the doping decreases, and as a function of temperature these lost states become more pronounced. (**B,C**), literature shift data. Optimally doped YBa$_2$Cu$_3$O$_{6.96}$ (circles) and overdoped YBa$_2$Cu$_3$O$_7$ (diamonds) behave Fermi liquid-like, but the underdoped materials YBa$_2$Cu$_3$O$_{7-\delta}$ (triangles), and YBa$_2$Cu$_4$O$_8$ (stars) show the expected high-temperature behavior. Below T_c, the shifts drop less dramatically for the underdoped systems. Some materials appear to show a negative spin shift at the lowest temperatures. For the references see Appendix A.

2.3. Numerical Analysis

The planar O relaxation data point to a pseudogap that is simply caused by missing low energy states. This gap is not temperature dependent, but rapidly increases with decreasing doping. In a very simple picture (that is very likely *not* to be correct, already in view of the planar Cu shift and relaxation data [21–24]),we use the Fermi function with fixed DOS and calculate the relaxation as being proportional

to the sum of the product of occupied states times empty states (the nuclear energy change is negligible for the electrons), i.e., $\sum_E p(E)[1 - p(E)]$, where

$$p(E, \mu) = 1/\left[1 + \exp(E - \mu)/k_B T\right].$$ (1)

As a result one finds the Heitler-Teller dependence [6], $1/T_1 \propto T$, cf. Figure 3.
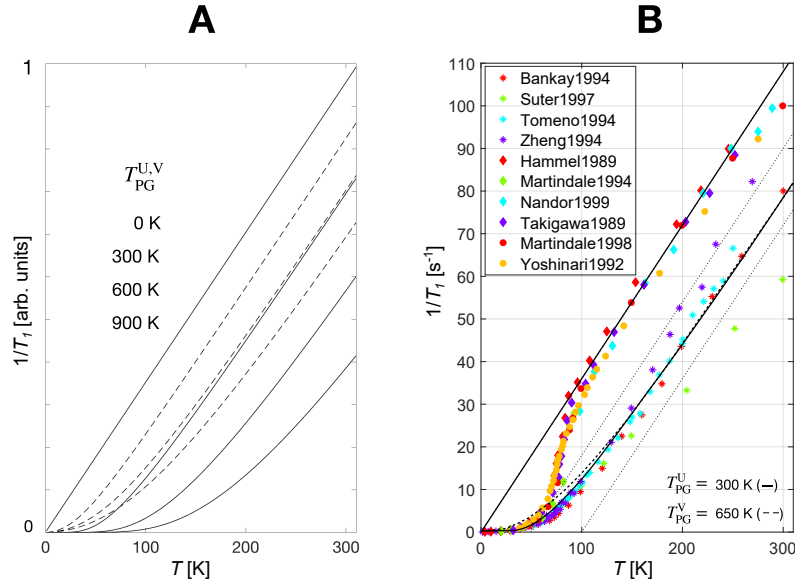

Figure 3. (**A**), model relaxation calculations with a U- and V-shaped gap ($T_{PG}^{U,V}$) in the density of states. (**B**), estimation of the pseudogap temperature by varying the gap size for YBa$_2$Cu$_4$O$_8$.

Now, one can remove manually states near the Fermi surface with a width ΔE given in temperature as defined by,

$$T_{PG}^{U,V} = \Delta E^{U,V}/k_B,$$ (2)

by assuming a U- or V-shaped gap in the DOS, respectively [31]. For the U-shaped gap all states within ΔE are removed (exponential decrease), for a V-shaped gap a linear decrease in DOS is assumed, vanishing at $E = \mu$. This simple scenario leads to the found behavior, i.e., we obtain nearly parallel high-temperature lines for different sizes of this pseudogap, cf. Figure 3A. For a given offset, the cutoff temperature is different for both gaps, cf. Figure 3B. With such an approach we find for YBa$_2$Cu$_4$O$_8$ a gap of about $T_{PG}^{U} \approx 300$ K ($T_{PG}^{V} \approx 650$ K). Obviously, one cannot decide on the shape of the gap. Note that the BCS gap is not included in the fit and that there are uncertainties from quadrupolar relaxation at lower temperatures.

Since the action of the gap is to cause a near parallel shift of the high-temperature dependence, any spatial inhomogeneity of the gap will lead to similar lines, as well, very different from how it affects the shifts that we will discuss now.

One can estimate what such a pseudogap will do for the NMR shifts (by assuming a slightly different μ for spin up and down). Examples are shown in Figure 4 for various T_{PG}^{U} (**A**), and T_{PG}^{V} (**B**). Clearly, for small gap sizes the shift will approach the Fermi liquid value (normalized to 1). The V-shaped gap has more total DOS and the action of the gap is weaker.

Above T_c, one should be able to fit the experimental shifts, and by comparing Figures 2 and 4 one finds qualitative agreement. However, a more quantitative determination of the gap appears difficult since

(i) there is a large spread in shifts already for similar samples, and (ii) at lower temperatures the shifts for the underdoped systems appear larger, cf. Figure 2, pointing to gap inhomogeneity. Note that the dashed lines in Figure 4 are the simple mean shifts of the shown temperature dependences. Thus, any spatial distribution of the pseudogap will change the actual temperature dependence as smaller gaps will lift the apparent shift at lower temperatures. We estimate gap sizes of $T_{PG}^{U} \approx 200$ K, $T_{PG}^{V} \approx 400$ K for $YBa_2Cu_4O_8$. These values are less than what relaxation shows, but sufficiently close for the assumed simple scenario and perhaps inhomogeneous samples (see below).
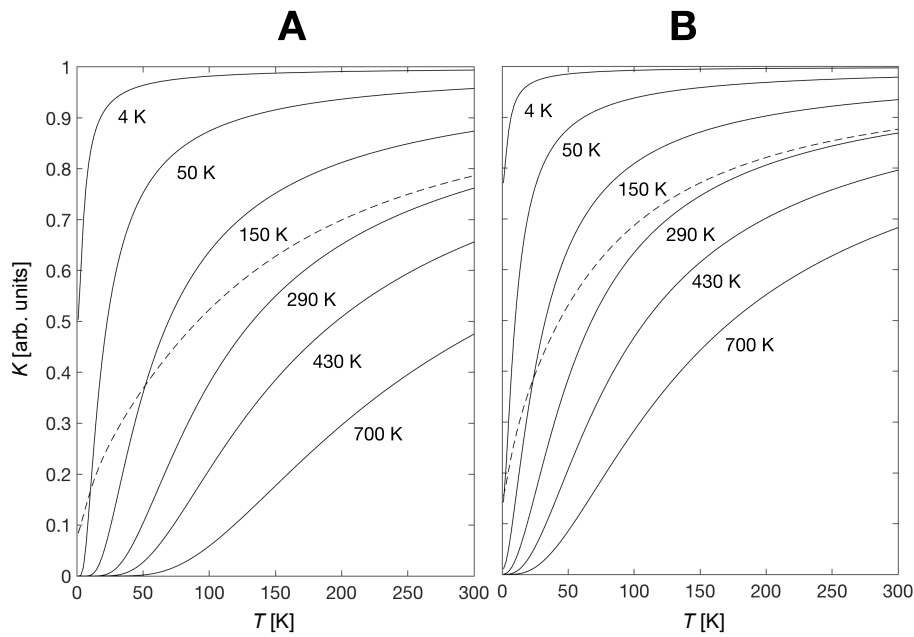

Figure 4. Model calculations of temperature-dependent shifts from a pseudogap at the Fermi surface with the indicated gap temperatures. (**A**), for a U-shaped gap, and, (**B**) for a V-shaped gap. The simple mean of the shifts is indicated by a dashed line, emphasizing that a gap inhomogeneity can cause a different temperature dependence of the apparent magnetic shift. The magnetic linewidths will also behave differently (the linewidths will grow as the temperature decreases, before it finally decreases).

An important feature of this pseudogap is a high-temperature shift offset. It arises from the fact that even far above the pseudogap energy one still misses the low energy states. Even if the shifts are temperature-independent, they can carry a doping dependence (as the pseudogap depends on doping), i.e., two variables are needed to describe the shifts ($K(x, T)$).

3. Planar Oxygen Relaxation in Other Cuprates

In Figure 5 we plot relaxation data from the literature for all other cuprates. Note that only the temperature axis is different (up to 600 K) compared to that in Figure 1B,C.

We note that the slope for optimally and overdoped $YBa_2Cu_3O_{7-\delta}$ (left dashed line) is similar to the dependencies found for the other overdoped cuprates. Thus, the CuO_2 plane appears to have this upper bound on the DOS. However, if we look at optimally doped $La_{2-x}Sr_xCuO_4$, it appears to still have a sizable pseudogap, in fact, similar to that of $YBa_2Cu_4O_8$. The largest gap is observed for the very underdoped $La_{2-x}Sr_xCuO_4$ ($x = 0.025$) with $T_{PG}^{U} \approx 1450$ K, the size of the exchange coupling in the cuprates. A V-shaped gap appears to better fit the low-temperature behavior. It could be the states near the

gap edge that are special (coherence peaks), also in-gap states could play a role in enhancing the relaxation at low temperature. Again, the loss of parts of the inhomogeneous sample with a large gap favors states from lower gap areas with increased relaxation. Quadrupolar relaxation plays some role, as well. Thus, the shape of the gap cannot be deduced from the low-temperature behavior. The gap rapidly closes with doping, as widely assumed.
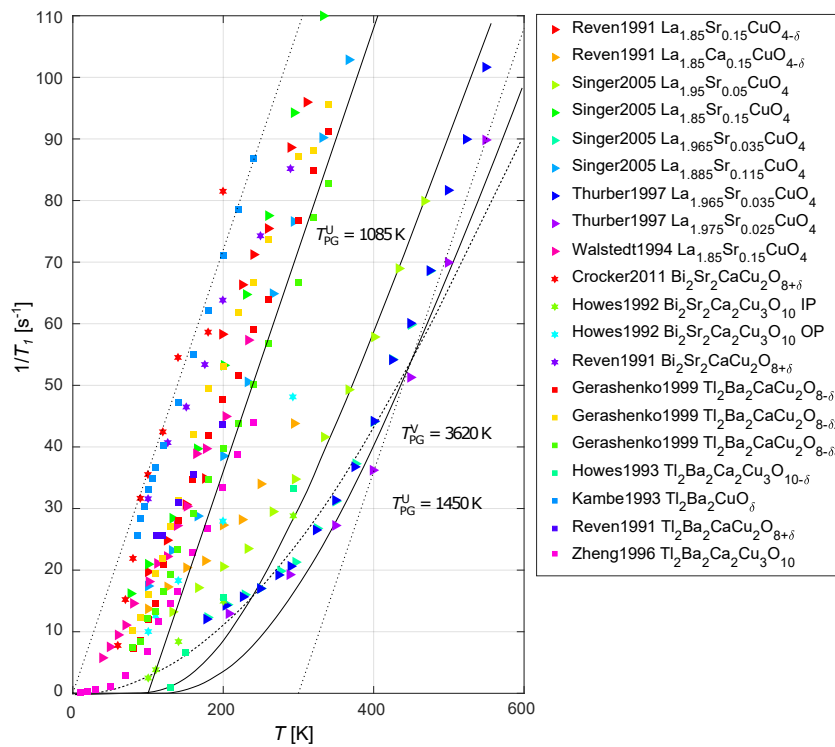

Figure 5. Planar O relaxation rates ($c \parallel B_0$) as a function of temperature for other cuprates. The slopes are rather similar to those observed for $YBa_2Cu_3O_{7-\delta}$ and $YBa_2Cu_4O_8$ in Figure 1 as the dotted lines show. The U-shaped gap closes rapidly with increasing doping where all low energy states are recovered. The maximum slope (DOS) appears to be a property of the CuO_2 plane, as well as the maximum size of the gap. For the references see Appendix B.

Note that the high-temperature behavior is similar for all materials, which does support the idea of a temperature-independent gap set by doping, and, importantly, very similar high-temperature Fermi liquid-like states.

To conclude, planar O NMR relaxation appears ubiquitous to the cuprates, and it defines and measures the pseudogap in a rather simple way (which is not the case for planar Cu relaxation and shift [22–24]).

4. Planar Oxygen Shifts in Other Cuprates

Shift data from all other materials are presented in Figure 6. The overall qualitative phenomenology is similar to what was found for $YBa_2Cu_3O_{7-\delta}$ and $YBa_2Cu_4O_8$. Except for a couple of overdoped materials, the shifts increase monotonously with temperature. Overdoped systems have nearly temperature-independent shifts, as for a Fermi liquid, and drop rapidly near T_c. In the pseudogap regime the shifts begin to show a temperature dependence above T_c, however, a temperature-independent

shift as for La$_{1.85}$Sr$_{0.15}$CuO$_4$ at high temperatures does not mean there is no pseudogap. Again, Fermi liquid-like shifts can be suppressed in the cuprates due to lost, low-energy states [22].

The superconducting gap is hardly noticeable, as there are no rapid changes in the shifts near T_c. Despite the scarcity of data below T_c, it appears that a number of materials could show a negative shift at the lowest temperatures.

The maximum observed shifts for overdoped materials are expected from the Korringa ratio by using the dominant slope in the relaxation plots ($1/T_1T \approx 0.36/Ks$). Samples with the largest pseudogap (La$_{1.965}$Sr$_{0.035}$CuO$_4$) also have the lowest high-temperature shifts. Obviously, the pseudogap can lead to doping-dependent, but not necessarily temperature-dependent spin shift ($K(x,T)$) since the low-energy states are still missing for small pseudogaps at high temperatures.
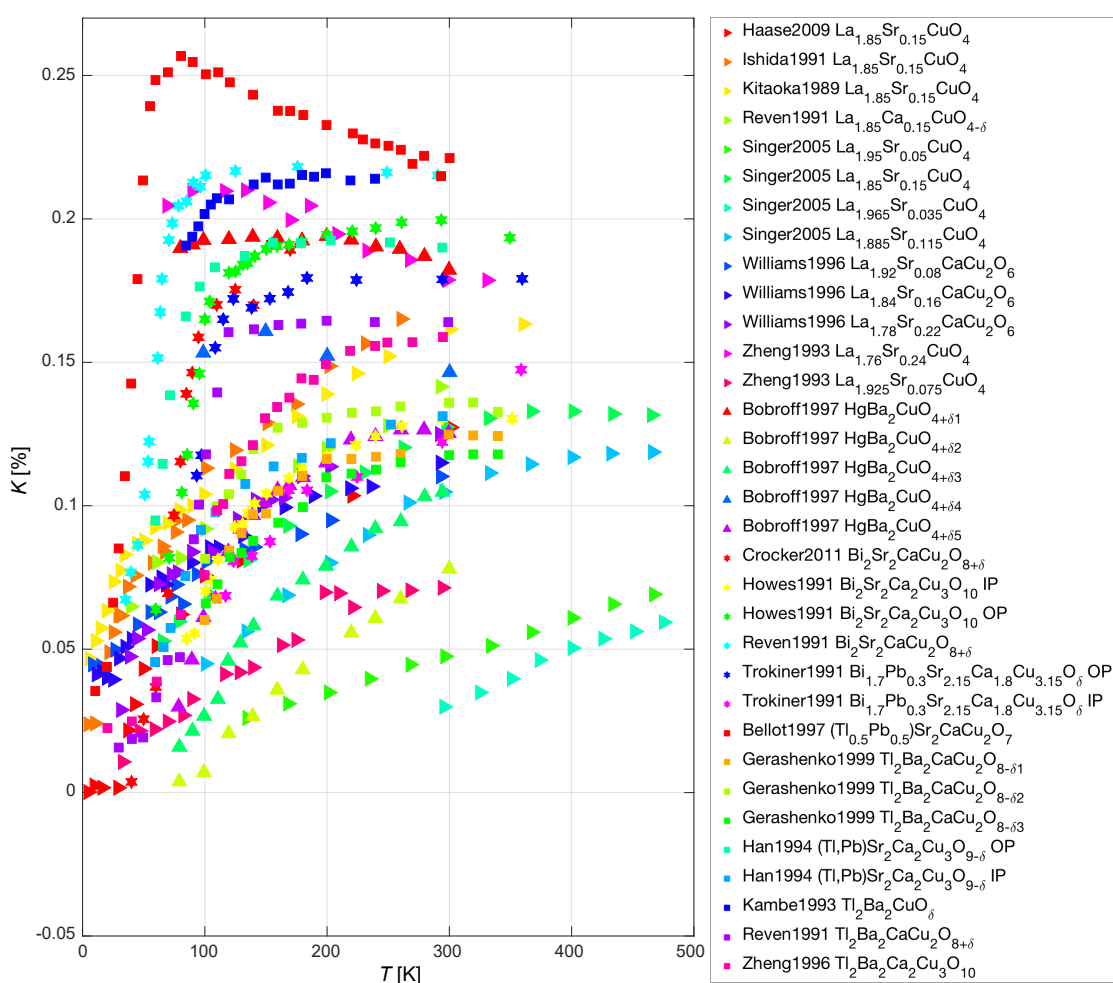

Figure 6. Planar ^{17}O NMR shifts for $c \parallel B_0$ for the other cuprates. Note that the temperature axis extends to 500 K. For more detailed plots see Figures 7 and 8. Note that a high-temperature-independent shift may still show lost states, as for optimally doped La$_{2-x}$Sr$_x$CuO$_4$. For references see Appendix B.

The true temperature dependence of the shifts in the pseudogap region is difficult to assess as sample inhomogeneity leads to a loss of the shift from areas that show a larger pseudogap as the temperature is lowered, cf. dashed lines in Figure 4.

It is also clear that optimally doped materials may have almost no pseudogap as for $YBa_2Cu_3O_{7-\delta}$, but it can be sizable as for $La_{2-x}Sr_xCuO_4$.
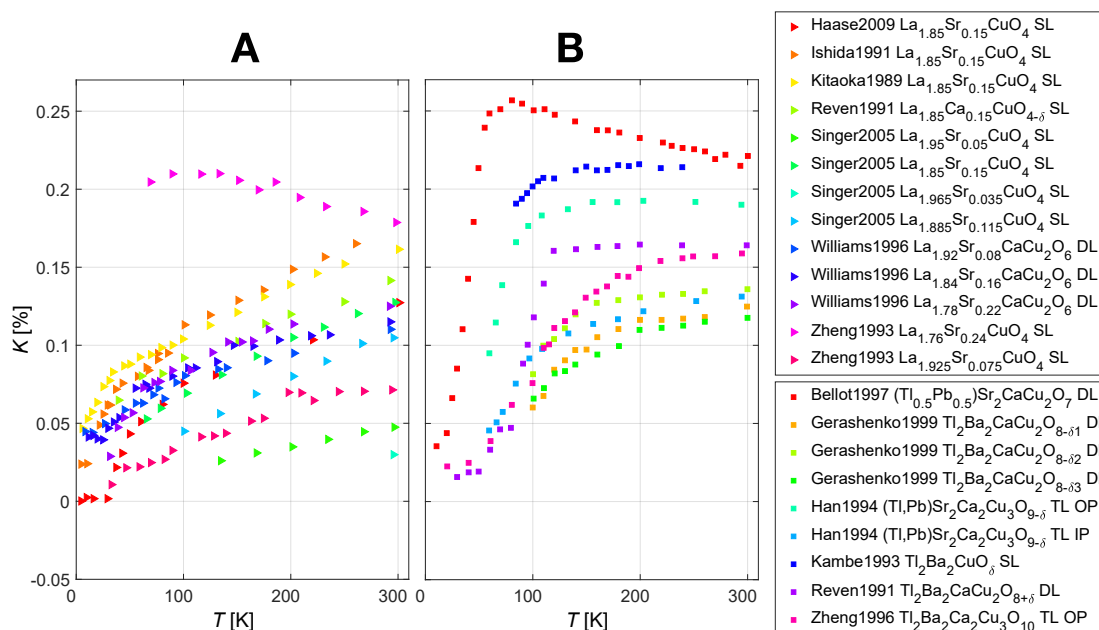

Figure 7. Planar ^{17}O NMR shifts for $c \parallel B_0$ for the other cuprates from Figure 6, separated for clarity. (**A**), La based cuprates, single and double layered. The doping ranges from x = 0.035, highly underdoped (lowest point near 300 K), to x = 0.24, highly overdoped. The shifts cover the range from 0.01% to 0.2%. The highly overdoped sample has the highest shift (there is some discrepancy between optimally doped data from different sources, probably due to inhomogeneity). (**B**), Tl based compounds. The overdoped samples have the highest and Fermi liquid-like shifts and also show an abrupt decrease near T_c. As doping is lowered the shifts become more suppressed. In the triple layer compound the inner plane (IP) has a larger pseudogap than the outer plane (OP).

5. Discussion and Conclusions

Planar O relaxation and spin shift data were collected and simple plots reveal that they demand a temperature-independent pseudogap at the Fermi surface with a size set by doping. The pseudogap rapidly opens, coming from the overdoped side by decreasing doping, and it approaches the size of the exchange coupling, J, for strongly underdoped systems. The states above the pseudogap, no matter what its size is, appear to be the same for all cuprates and carry even a more or less constant density, as perhaps expected from a two-dimensional surface. In fact, in the absence of this pseudogap, shift and relaxation for planar O are Fermi liquid-like and the Korringa relation holds. This supports the view that even in the presence of the pseudogap, the available states above it are the same Fermi liquid-like states. The doping level at which the pseudogap disappears can be different for different materials. For example, at optimal doping, there is a substantial pseudogap already present for $La_{2-x}Sr_xCuO_4$, while the pseudogap has vanished for optimally doped $YBa_2Cu_3O_{7-\delta}$. For triple-layer materials, the pseudogap is much larger for the inner layer. A plot of the pseudogap temperature for a U-shaped gap (T_{PG}^U) is shown in Figure 9.
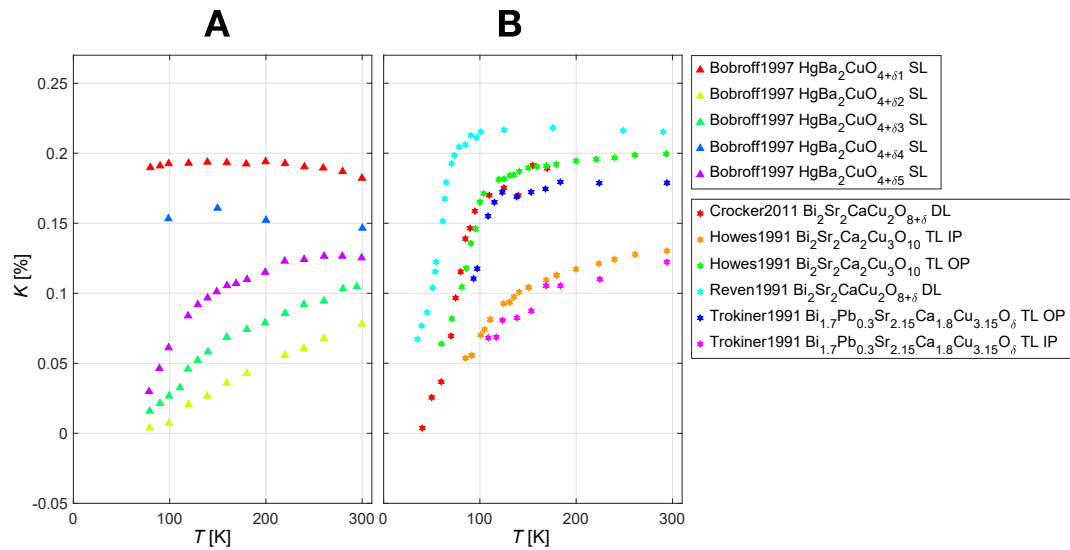
Figure 8. Planar ^{17}O NMR shifts for $c \parallel B_0$ for the other cuprates from Figure 6, separated for clarity. (**A**), single layer mercury based cuprates; the two overdoped samples have temperature-independent shifts. The pseudogap becomes apparent at optimal doping (purple triangles). (**B**), Bi based cuprates; the two double layered and overdoped samples have the highest and temperature-independent shifts, with an abrupt drop near T_c. The outer plane shifts from the two triple layered compounds show Fermi liquid-like behavior, whereas the inner plane (yellow and pink stars) show a large pseudogap.

An important consequence of the temperature-independent pseudogap is a doping dependent spin shift. At high temperatures where the shifts can be nearly temperature-independent (Fermi liquid-like), states can still be missing and thus the magnitude of shift can be suppressed. Consequently, the cuprate planar O spin shifts must carry at least two independent variables, one related to doping and the other to temperature, $K(x, T)$. This is effectively a two-component description. Whether this two-component description is sufficient is not clear (for planar Cu it is not [21]).

At lower energies, there are deviations from the simple behavior, but it is difficult to analyze given the possible influence of inhomogeneity and quadrupolar relaxation. Likely, states in the gap or near the gap edge are responsible for special behavior.

Very recently, it was shown from plots of literature shift data of planar Cu [21] that there is a doping-dependent spin shift at high temperatures, and comparison with planar Cu relaxation data [22,23]—that do not show a pseudogap—led to the conclusion of suppressed planar Cu spin shifts [22,24], as well. Thereafter, it was shown that this doping-dependent planar Cu spin shift explains the conundrum of the correlation of high-temperature spin shifts with the local charge [25], resulting in the hallmark asymmetric total planar O lineshapes (that include the quadrupolar satellites) of the cuprates [25,28].

Here, we argue that it is the doping dependence of the pseudogap that plays the dominant role in these effects. Then it follows that it is the pseudogap that can be spatially very inhomogeneous [25]. This distinction could not be made earlier [28], but it is in agreement with STM data [37]. With a large distribution of the pseudogap, shift and relaxation can be affected. An inhomogeneous broadening changes the apparent temperature dependence of the shift, cf. Figure 4, as small pseudogap areas contribute more to the shift at lower temperatures than those with large pseudogaps. For relaxation, the faster-relaxing regions,

i.e., those with a smaller pseudogap, may dominate throughout the whole temperature range, if spin diffusion is possible. Thus, one has to be very careful in analyzing shift and relaxation quantitatively [38].

The inhomogeneity of the pseudogap affects the apparent temperature dependence of the average shift, as discussed with the dashed lines in Figure 4, but also the observed linewidths depend on it. In view of Figure 4 one concludes that in case of inhomogeneity of the pseudogap the NMR linewidths grow towards lower temperatures before they finally decrease again, while the shift is decreasing monotonously. This is exactly what was found experimentally (for $YBa_2Cu_3O_{7-\delta}$ and $La_{2-x}Sr_xCuO_4$ [28]), and what was interpreted as proof for two different spin components [25].

The relation of this pseudogap to the intra-unit cell charge variation that was first proposed from NMR data [39] and very recently shown to exist in the bulk of the material [40] is not clear. However, the response of the local charge symmetry to an external magnetic field and pressure found with NMR [40,41], must bear similarities to the discussed charge ordering phenomena and special susceptibilities associated with the pseudogap [29,30], recently. The total charge involved in the ordering is small (1-2% of the total planar O hole content) and may come from states within the pseudogap.

Note that the superconducting transition temperature T_c appears to be not affected by this inhomogeneity, as it is nearly proportional to the average planar oxygen hole density of the parent compounds [18,19]. Then, with the size and distribution of the pseudogap set by doping, there appears no simple relation to the maximum T_c.
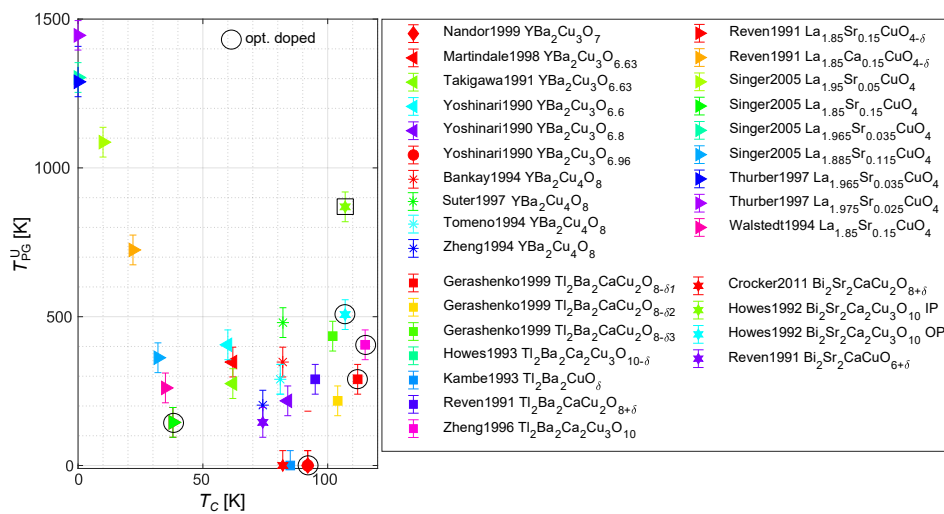

Figure 9. Values for a U-shaped gap, T_{PG}^U, as determined from the relaxation data, vs. the critical temperature, T_c. Optimally doped materials (denoted with circles) can have a vanishing pseudogap as for $YBa_2Cu_3O_{6.96}$ despite a rather high T_c, but it appears that materials with the highest T_c all have a substantial pseudogap, and their T_c increases with the pseudogap temperature. The inner layer of the triple layer system (denoted with a square) has a significantly larger pseudogap than the outer layers. These findings are in qualitative agreement with the shift data. The data can also be found in the tables in the appendices.

The pseudogap behavior was first reported with measurements above T_c for ^{89}Y NMR of $YBa_2Cu_3O_{7-\delta}$ [42], and these data show a high-temperature offset in the shifts, as well. So we believe that ^{89}Y NMR data are in agreement with what we found for planar O here.

A U-shaped gap in our simulation means that all states contributing to planar O relaxation vanish suddenly within the gap. With such an assumption the largest pseudogap appears to be set by the exchange coupling. Then, effectively, doping decreases the energy gap that needs to be overcome for electrons to flip the nuclear spin for relaxation. Of course, the true shape of the gap and the nature of the states within the gap are not known.

If the above scenario describes the essential electronic states involved in cuprate conductivity and superconductivity, it should leave its typical signature in electronic specific heat. Indeed, the $YBa_2Cu_3O_{7-\delta}$ family of materials appears to fit the specific heat data by Loram et al. [31] rather well [43]. Loram et al. [31] argue similarly in their specific heat investigations, as the specific heat is linear in temperature in the pseudogap range. Additional states are added by the temperature at the same rate as for overdoped systems where there is no gap. Thus, the specific heat of other materials should be similar in view of all analyzed planar O data.

Planar Cu relaxation was shown not to be affected by the pseudogap, at all [22,23], its relaxation is rather ubiquitous across all cuprates ($1/^{63}T_1T_c \approx 21/Ks$), independent on doping (the relaxation anisotropy changes with doping [24]). With the cuprate specific heat being in agreement with planar O relaxation, the heat involved with the states that relax planar Cu must be small (perhaps nodal particles). Not surprisingly, the planar Cu shifts, as a uniform response, do see the pseudogap. The maximum shift $^{63}K \approx 0.8\%$ is also similar to what follows from the Korringa relation. The details of a comparison between planar Cu and O NMR will be investigated in a forthcoming publication.

Unfortunately, we feel that it is difficult to conclude on the superconducting gap from the planar O data. An inhomogeneous pseudogap dominates the shifts and the relaxation may be partly electric [44] in the vicinity of T_c. The latter clearly points to the involvement of charge fluctuations [45,46], very different from the relaxation of planar Cu [23], which is also rather ubiquitous at low temperatures in the cuprates, when normalized by T_c [23]. Naively, one might assume that the states not already lost to the pseudogap disappear rapidly below T_c, further slowing down relaxation, but the opposite behavior is found, i.e., the rate appears to increase at lower temperature before it finally decreases. This could be due to additional quadrupolar relaxation, alternatively, the magnetic relaxation could show a special increase, but perhaps the inhomogeneity of the pseudogap is most important as regions with fast relaxation (small pseudogap) will dominate. Details of the spin shift, including the behavior below T_c, are difficult to evaluate, as well, not only due to the inhomogeneity, but also because of the uncertainty of the low-temperature data (loss of signal etc.). A small negative spin shift appears to be observed for a number of materials, which would be expected from the suggested shift scenario [21,22].

To conclude, the planar O data in their entirety reveal a simple temperature-independent pseudogap scenario. The gap can be as large as the exchange coupling and vanishes with increasing doping in a family-specific way. The states above the pseudogap are unique and Fermi liquid-like for all cuprates and have even constant density. This leads to a relaxation that increases at the same rate with temperature for all cuprates above the pseudogap, and to shifts that become temperature-independent. However, depending on the size of the pseudogap (located at lower energies), relaxation and shift can still be suppressed at these higher temperatures. This leads to the otherwise unexpected behavior of shift and relaxation found in NMR. The inhomogeneity of the pseudogap becomes apparent from comparison with the total planar O lineshapes and the planar Cu shifts. No simple relation of the pseudogap to the superconducting transition temperature is found. Note, however, that the planar Cu data do not fit this simple scenario with doping-independent relaxation and a two-component shift [21–24], while similarities exist and need to be explored.

discussions; R.G., J.N., J.H. worked mainly on the preparation of the manuscript. All authors have read and agreed to the published version of the manuscript.

Conflicts of Interest: The authors declare no conflict of interest.

Appendix A

List of all references for YBa$_2$Cu$_3$O$_{7-\delta}$ and YBa$_2$Cu$_4$O$_8$. We found about 36 publications on these materials, out of a total of about 80 papers on all cuprates. If the same data set appears in multiple papers, typically from the same group, we only show the last published account.

Table A1. References for YBCO literature accounts with critical temperature T_c, label as shown in figures, reference link, external magnetic field during measurement and the size of U-shaped gap from the numerical analysis. All samples were aligned powders, if not stated otherwise *.

Compound	T_c	Label	Ref.	Field	T_{PG}^{U}
YBa$_2$Cu$_4$O$_8$	82 K	Bankay1994	[47]	9.03 T	350 K
YBa$_2$Cu$_4$O$_8$	82 K	Brinkmann1992	[48]		
YBa$_2$Cu$_4$O$_8$	82 K	Mangelschots1992	[49]	9.129 T	
YBa$_2$Cu$_4$O$_8$	81 K	Suter1997	[33]	8.9945 T	490 K
YBa$_2$Cu$_4$O$_8$	81 K	Tomeno1994	[50]	5.71 T	290 K
YBa$_2$Cu$_4$O$_8$	74 K	Zheng1992	[51]	11 T	
YBa$_2$Cu$_4$O$_8$	74 K	Zheng1993	[52]	11 T	
YBa$_2$Cu$_4$O$_8$	74 K	Zheng1994	[53]	4.3/11 T	200 K
YBa$_2$Cu$_3$O$_7$	93 K	Hammel1989	[54]	7.0 T	
YBa$_2$Cu$_3$O$_7$	92 K	Horvatic1989	[55]	5.75 T	
YBa$_2$Cu$_3$O$_{6.65}$	61 K	Kitaoka1989	[56]	5.75 T	
YBa$_2$Cu$_3$O$_7$	92 K	Kitaoka1989	[56]	5.75T	
YBa$_2$Cu$_3$O$_7$	91.2 K	Martindale1993	[57]	0.67 T	
YBa$_2$Cu$_3$O$_7$	91.2 K	Martindale1993	[57]	8.30 T	
YBa$_2$Cu$_3$O$_7$	93 K	Martindale1994	[58]	0.67 T	
YBa$_2$Cu$_3$O$_7$	93 K	Martindale1994	[58]	8.30 T	0 K
YBa$_2$Cu$_3$O$_{6.63}$	62 K	Martindale1998	[59]	high field	350 K
YBa$_2$Cu$_3$O$_{6.96}$	92.2 K	Martindale1998	[59]	high field	
YBa$_2$Cu$_3$O$_7$ *	92 K	Nandor1999	[32]	9.05 T	0 K
YBa$_2$Cu$_3$O$_7$ *	92 K	Reven1991	[60]	8.45 T	
YBa$_2$Cu$_3$O$_7$	93 K	Takigawa1989	[26]		0K
YBa$_2$Cu$_3$O$_{6.63}$	62 K	Takigawa1991	[34]	6/7 T	280 K
YBa$_2$Cu$_3$O$_{6.60}$	60 K	Yoshinari1990	[61]	10 T	410 K
YBa$_2$Cu$_3$O$_{6.80}$	84 K	Yoshinari1990	[61]	10 T	22 K
YBa$_2$Cu$_3$O$_{6.96}$	92 K	Yoshinari1990	[61]	10 T	0 K
YBa$_2$Cu$_3$O$_{6.96}$	87 K	Yoshinari1992	[62]	8.97 T	0 K

Appendix B

Here we list the references for other cuprates, about 44 publications with relevant data. If a data set appeared in multiple papers, typically from the same group, we only show the last published account.

Table A2. References to literature accounts of data, with critical temperature T_c, label as shown in figures, reference link, sample type (a.p.(c.)—aligned powder (crystal); r.p.—randomly orientated powder; s.c.—single crystal), the external magnetic field for measurement, and the U-shaped gap size from the numerical analysis (i.p.—inner plain; o.p.—outer plane in case of the triple-layer compound).

Compound	T_c	Label	Ref.	Sample	Field	T_{PG}^U
$La_{1.85}Sr_{0.15}CuO_4$	38 K	Haase2009	[12]	a.p.	9 T	
$La_{1.85}Sr_{0.15}CuO_4$	38 K	Ishida1991	[63]	a.p.	11 T	
$La_{1.85}Sr_{0.15}CuO_4$		Kitaoka1989	[56]	a.p.	5.75 T	
$La_{1.85}Ca_{0.15}CuO_{4+\delta}$	22 K	Reven1991	[60]	a.c	8.45 T	720 K
$La_{1.85}Sr_{0.15}CuO_{4+\delta}$	38 K	Reven1991	[60]	a.c	8.45 T	140 K
$La_{1.95}Sr_{0.05}CuO_4$	~10 K	Singer2005	[64]	a.c.	9 T	1085 K
$La_{1.85}Sr_{0.15}CuO_4$	38 K	Singer2005	[64]	a.c.	9 T	140 K
$La_{1.965}Sr_{0.035}CuO_4$	0 K	Singer2005	[64]	a.c.	9 T	1300 K
$La_{1.885}Sr_{0.115}CuO_4$	~32 K	Singer2005	[64]	a.c.	9 T	360 K
$La_{1.965}Sr_{0.035}CuO_4$	0 K	Thurber1997	[65]	s.c.	9 T	1290 K
$La_{1.975}Sr_{0.025}CuO_4$	0 K	Thurber1997	[65]	s.c.	9 T	1450 K
$La_{1.85}Sr_{0.15}CuO_{4+\delta}$	35 K	Walstedt1994	[66]	a.p.		260 K
$La_{1.92}Sr_{0.08}CaCu_2O_6$	17.7 K	Williams1996	[67]	r.p.	8.45 T	
$La_{1.84}Sr_{0.16}CaCu_2O_6$	31.5 K	Williams1996	[67]	r.p.	8.45 T	
$La_{1.78}Sr_{0.22}CaCu_2O_6$	47 K	Williams1996	[67]	r.p.	8.45 T	
$La_{1.76}Sr_{0.24}CuO_4$	25 K	Zheng1993	[16]	a.c.		
$La_{1.925}Sr_{0.075}CuO_4$	20 K	Zheng1993	[16]	a.c.		
$HgBa_2CuO_{4+\delta1}$	61 K	Bobroff1997	[68]	a.c.	7.5 T	
$HgBa_2CuO_{4+\delta2}$	75 K	Bobroff1997	[68]	a.c.	7.5 T	
$HgBa_2CuO_{4+\delta3}$	87.8 K	Bobroff1997	[68]	a.p.	7.5 T	
$HgBa_2CuO_{4+\delta4}$	89 K	Bobroff1997	[68]	a.p.	7.5 T	
$HgBa_2CuO_{4+\delta5}$	95.7 K	Bobroff1997	[68]	a.p.	7.5 T	
$Bi_2Sr_2CaCu_2O_{8+\delta}$	82 K	Crocker2011	[69]	a.p.	9 T	0 K
$Bi_2Sr_2Ca_2Cu_3O_{10}$	107 K	Howes1991	[70]	a.p.	8.45 T	
$Bi_2Sr_2Ca_2Cu_3O_{10}$	107 K	Howes1992	[71]	r.p.	8.45 T	i.p. 870 K
$Bi_2Sr_2Ca_2Cu_3O_{10}$	107 K	Howes1992	[71]	r.p.	8.45 T	o.p. 510 K
$Bi_2Sr_2CaCu_2O_{8+\delta}$	74 K	Reven1991	[60]	r.p.	8.45 T	140 K
$Bi_2Sr_2CaCuO_{6+\delta}$	5.6 K	Reven1991	[60]	r.p.	8.45 T	
$Bi_{1.7}Pb_{0.3}Sr_{2.15}Ca_{1.8}Cu_{3.15}O_\delta$	110 K	Trokiner1991	[72]	r.p.		
$(Tl_{0.5}Pb_{0.5})Sr_2CaCu_2O_7$	65 K	Bellot1997	[73]	r.p.	7 T	
$Tl_2Ba_2CaCu_2O_{8-\delta1}$	112 K	Gerashenko1999	[74]	a.c.		290 K
$Tl_2Ba_2CaCu_2O_{8-\delta2}$	104 K	Gerashenko1999	[74]	a.c.		220 K
$Tl_2Ba_2CaCu_2O_{8-\delta3}$	102 K	Gerashenko1999	[74]	a.c.		430 K
$(Tl,Pb)Sr_2Ca_2Cu_3O_{9-\delta}$	124 K	Han1994	[75]	r.p.	8.45 T	
$Tl_2Ba_2CuO_7$	< 4.2 K	Kambe1991	[76]	a.c.		
$Tl_2Ba_2CuO_\delta$	85K	Kambe1993	[27]	a.c.	12 T	0 K
$Tl_2Ba_2Ca_2Cu_3O_{10-\delta}$	125 K	Howes1993	[77]	s.c.	8.45 T	870 K
$Tl_2Ba_2CaCu_2O_{8+\delta}$	95 K	Reven1991	[60]	r.p.	8.45 T	290 K
$Tl_2Ba_2Ca_2Cu_3O_{10}$	125 K	Zheng1995	[78]	a.p.	11 T	
$Tl_2Ba_2Ca_2Cu_3O_{10}$	125 K	Zheng1996	[79]	a.p.	11 T	410 K

References

1. Slichter, C.P. *Principles of Magnetic Resonance*, 3rd ed.; Springer: Berlin/Heidelberg, Germany, 1990.
2. Slichter, C.P. Magnetic Resonance Studies of High Temperature Superconductors. In *Handbook of High-Temperature Superconductivity*; Schrieffer, J.R., Brooks, J.S., Eds.; Springer: New York, USA, 2007; pp. 215–256. [CrossRef]
3. Walstedt, R.E. *The NMR Probe of High-T_c Materials*, 1st ed.; Springer: Berlin/Heidelberg, Germany, 2008. [CrossRef]

4. Bardeen, J.; Cooper, L.N.; Schrieffer, J.R. Microscopic theory of superconductivity. *Phys. Rev.* **1957**, *106*, 162–164. [CrossRef]

5. Hebel, L.C.; Slichter, C.P. Nuclear Spin Relaxation in Normal and Superconducting Aluminum. *Phys. Rev.* **1959**, *113*, 1504–1519. [CrossRef]

6. Heitler, W.; Teller, E. Time Effects in the Magnetic Cooling Method-I. *Proc. R. Soc. A Math. Phys. Eng. Sci.* **1936**, *155*, 629–639. [CrossRef]

7. Knight, W. Nuclear Magnetic Resonance Shift in Metals. *Phys. Rev.* **1949**, *76*, 1259–1260. [CrossRef]

8. Korringa, J. Nuclear magnetic relaxation and resonnance line shift in metals. *Physica* **1950**, *16*, 601–610. [CrossRef]

9. Schumacher, R.T.; Slichter, C.P. Electron Spin Paramagnetism of Lithium and Sodium. *Phys. Rev.* **1956**, *101*, 58–65. [CrossRef]

10. Yosida, K. Paramagnetic Susceptibility in Superconductors. *Phys. Rev.* **1958**, *110*, 769–770. [CrossRef]

11. Barrett, S.E.; Durand, D.J.; Pennington, C.H.; Slichter, C.P.; Friedmann, T.A.; Rice, J.P.; Ginsberg, D.M. ^{63}Cu Knight shifts in the superconducting state of YBa$_2$Cu$_3$O$_{7-\delta}$ (T$_c$ = 90 K). *Phys. Rev. B* **1990**, *41*, 6283–6296. [CrossRef] [PubMed]

12. Haase, J.; Slichter, C.P.; Williams, G.V.M. Evidence for two electronic components in high-temperature superconductivity from NMR. *J. Phys. Condens. Matter* **2009**, *21*, 455702. [CrossRef] [PubMed]

13. Meissner, T.; Goh, S.K.; Haase, J.; Williams, G.V.M.; Littlewood, P.B. High-pressure spin shifts in the pseudogap regime of superconducting YBa$_2$Cu$_4$O$_8$ as revealed by ^{17}O NMR. *Phys. Rev. B* **2011**, *83*, 220517. [CrossRef]

14. Haase, J.; Rybicki, D.; Slichter, C.P.; Greven, M.; Yu, G.; Li, Y.; Zhao, X. Two-component uniform spin susceptibility of superconducting HgBa$_2$CuO$_{4+\delta}$ single crystals measured using ^{63}Cu and ^{199}Hg nuclear magnetic resonance. *Phys. Rev. B* **2012**, *85*, 104517. [CrossRef]

15. Rybicki, D.; Kohlrautz, J.; Haase, J.; Greven, M.; Zhao, X.; Chan, M.K.; Dorow, C.J.; Veit, M.J. Electronic spin susceptibilities and superconductivity in HgBa$_2$CuO$_{4+\delta}$ from nuclear magnetic resonance. *Phys. Rev. B* **2015**, *92*, 081115. [CrossRef]

16. Zheng, G.Q.; Kuse, T.; Kitaoka, Y.; Ishida, K.; Ohsugi, S.; Asayama, K.; Yamada, Y. ^{17}O NMR study of La$_{2-x}$Sr$_x$CuO$_4$ in the lightly-and heavily-doped regions. *Phys. C Supercond.* **1993**, *208*, 339–346. [CrossRef]

17. Haase, J.; Sushkov, O.P.; Horsch, P.; Williams, G.V.M. Planar Cu and O hole densities in high-T_c cuprates determined with NMR. *Phys. Rev. B* **2004**, *69*, 94504. [CrossRef]

18. Jurkutat, M.; Rybicki, D.; Sushkov, O.P.; Williams, G.V.M.; Erb, A.; Haase, J. Distribution of electrons and holes in cuprate superconductors as determined from ^{17}O and ^{63}Cu nuclear magnetic resonance. *Phys. Rev. B* **2014**, *90*, 140504. [CrossRef]

19. Rybicki, D.; Jurkutat, M.; Reichardt, S.; Kapusta, C.; Haase, J. Perspective on the phase diagram of cuprate high-temperature superconductors. *Nat. Commun.* **2016**, *7*, 1–6. [CrossRef] [PubMed]

20. Jurkutat, M.; Erb, A.; Haase, J. Tc and Other Cuprate Properties in Relation to Planar Charges as Measured by NMR. *Condens. Matter* **2019**, *4*, 67. [CrossRef]

21. Haase, J.; Jurkutat, M.; Kohlrautz, J. Contrasting Phenomenology of NMR Shifts in Cuprate Superconductors. *Condens. Matter* **2017**, *2*, 16. [CrossRef]

22. Avramovska, M.; Pavićević, D.; Haase, J. Properties of the Electronic Fluid of Superconducting Cuprates from ^{63}Cu NMR Shift and Relaxation. *J. Supercond. Nov. Magn.* **2019**, *32*, 3761–3771. [CrossRef]

23. Jurkutat, M.; Avramovska, M.; Williams, G.V.M.; Dernbach, D.; Pavićević, D.; Haase, J. Phenomenology of ^{63}Cu Nuclear Relaxation in Cuprate Superconductors. *J. Supercond. Nov. Magn.* **2019**, *32*, 3369–3376. [CrossRef]

24. Avramovska, M.; Pavićević, D.; Haase, J. NMR Shift and Relaxation and the Electronic Spin of Superconducting Cuprates. *J. Supercond. Nov. Magn.* **2020**, *33*, 2621–2628. [CrossRef]

25. Pavićević, D.; Avramovska, M.; Haase, J. Unconventional ^{17}O and ^{63}Cu NMR shift components in cuprate superconductors. *Mod. Phys. Lett. B* **2020**, *34*, 2040047. [CrossRef]

26. Takigawa, M.; Hammel, P.; Heffner, R.; Fisk, Z.; Ott, K.; Thompson, J. ^{17}O NMR study of YBa$_2$Cu$_3$O$_{7-\delta}$. *Phys. C Supercond.* **1989**, *162–164*, 853–856. [CrossRef]

27. Kambe, S.; Yasuoka, H.; Hayashi, A.; Ueda, Y. NMR study of the spin dynamics in Tl$_2$Ba$_2$CuO$_y$ (Tc=85 K). *Phys. Rev. B* **1993**, *47*, 2825–2834. [CrossRef]

28. Haase, J.; Slichter, C.P.; Stern, R.; Milling, C.T.; Hinks, D.G. Spatial Modulation of the NMR Properties of the Cuprates. *Phys. C Supercond.* **2000**, *341*, 1727–1730. [CrossRef]

29. Mukhopadhyay, S.; Sharma, R.; Kim, C.K.; Edkins, S.D.; Hamidian, M.H.; Eisaki, H.; Uchida, S.I.; Kim, E.A.; Lawler, M.J.; Mackenzie, A.P.; et al. Evidence for a vestigial nematic state in the cuprate pseudogap phase. *Proc. Nat. Acad. Sci. USA* **2019**, *116*, 13249–13254. [CrossRef]

30. Sato, Y.; Kasahara, S.; Murayama, H.; Kasahara, Y.; Moon, E.G.; Nishizaki, T.; Loew, T.; Porras, J.; Keimer, B.; Shibauchi, T.; Matsuda, Y. Thermodynamic evidence for a nematic phase transition at the onset of the pseudogap in $YBa_2Cu_3O_y$. *Nat. Phys.* **2017**, *13*, 1074–1078. [CrossRef]

31. Loram, J.W.; Mirza, K.A.; Cooper, J.R.; Tallon, J.L. Specific heat evidence on the normal state pseudogap. *J. Phys. Chem. Solids* **1998**, *59*, 2091–2094. [CrossRef]

32. Nandor, V.A.; Martindale, J.A.; Groves, R.W.; Vyaselev, O.M.; Pennington, C.H.; Hults, L.; Smith, J.L. High-temperature ^{17}O and ^{89}YNMR of $YBa_2Cu_3O_{7-\delta}$. *Phys. Rev. B* **1999**, *60*, 6907–6915. [CrossRef]

33. Suter, A.; Mali, M.; Roos, J.; Brinkmann, D.; Karpinski, J.; Kaldis, E. Electronic crossover in the normal state of $YBa_2Cu_4O_8$. *Phys. Rev. B* **1997**, *56*, 5542–5551. [CrossRef]

34. Takigawa, M.; Reyes, A.P.; Hammel, P.C.; Thompson, J.D.; Heffner, R.H.; Fisk, Z.; Ott, K.C. Cu and O NMR studies of the magnetic properties of $YBa_2Cu_3O_{6.63}(T_c = 62K)$. *Phys. Rev. B* **1991**, *43*, 247–257. [CrossRef]

35. Brinkmann, D. The mysterious spin gap in high-temperature superconductors: New NMR/NQR studies. *Appl. Magn. Reson.* **1998**, *15*, 197–202. [CrossRef]

36. Oldfield, E.; Coretsopoulos, C.; Yang, S.; Reven, L.; Lee, H.C.; Shore, J.; Han, O.H.; Ramli, E.; Hinks, D. ^{17}O nuclear-magnetic-resonance spectroscopic study of high-T_c superconductors. *Phys. Rev. B* **1989**, *40*, 6832–6849. [CrossRef] [PubMed]

37. Pan, S.H.; O'Neal, J.P.; Badzey, R.L.; Chamon, C.; Ding, H.; Engelbrecht, J.R.; Wang, Z.; Eisaki, H.; Uchida, S.; Gupta, A.K.; et al. Microscopic electronic inhomogeneity in the high-Tc superconductor $Bi_2Sr_2CaCu_2O_{8+x}$. *Nature* **2001**, *413*, 282–285. [CrossRef] [PubMed]

38. Bussmann-Holder, A. Evidence for s+d Wave Pairing in Copper Oxide Superconductors from an Analysis of NMR and NQR Data. *J. Supercond. Nov. Magn.* **2011**, *25*, 155–157. [CrossRef]

39. Haase, J. Charge density variation in $YBa_2Cu_3O_{6+y}$. *Phys. Rev. Lett.* **2003**, *91*, 189701. [CrossRef]

40. Reichardt, S.; Jurkutat, M.; Guehne, R.; Kohlrautz, J.; Erb, A.; Haase, J. Bulk Charge Ordering in the CuO_2 Plane of the Cuprate Superconductor $YBa_2Cu_3O_{6.9}$ by High-Pressure NMR. *Condens. Matter* **2018**, *3*, 23. doi:10.3390/condmat3030023. [CrossRef]

41. Reichardt, S.; Jurkutat, M.; Erb, A.; Haase, J. Charge Variations in Cuprate Superconductors from Nuclear Magnetic Resonance. *J. Supercond. Nov. Magn.* **2016**, *29*, 3017–3022. [CrossRef]

42. Alloul, H.; Ohno, T.; Mendels, P. ^{89}Y NMR evidence for a Fermi-liquid behavior in $YBa_2Cu_3O_{6+x}$. *Phys. Rev. Lett.* **1989**, *63*, 1700–1703. [CrossRef]

43. Fine, B. (Institute of Physics and Technology, Moscow, Russia). Private communication with J.H, 2020.

44. Suter, A.; Mali, M.; Roos, J.; Brinkmann, D. Charge degree of freedom and the single-spin fluid model in $YBa_2Cu_4O_8$. *Phys. Rev. Lett.* **2000**, *84*, 4938–4941. [CrossRef]

45. Olson Reichhardt, C.J.; Reichhardt, C.; Bishop, A.R. Fibrillar Templates and Soft Phases in Systems with Short-Range Dipolar and Long-Range Interactions. *Phys. Rev. Lett.* **2004**, *92*, 016801. [CrossRef] [PubMed]

46. Mazumdar, S. Valence transition model of the pseudogap, charge order, and superconductivity in electron-doped and hole-doped copper oxides. *Phys. Rev. B* **2018**, *98*, 205153.[CrossRef]

47. Bankay, M.; Mali, M.; Roos, J.; Brinkmann, D. Single-spin fluid, spin gap, and d-wave pairing in $YBa_2Cu_4O_8$: A NMR and NQR study. *Phys. Rev. B* **1994**, *50*, 6416–6425. [CrossRef] [PubMed]

48. Brinkmann, D. Comparing Y–Ba–Cu–O superconductors by Cu, O and Ba NMR/NQR. *Appl. Magn. Reson.* **1992**, *3*, 483–494. [CrossRef]

49. Mangelschots, I.; Mali, M.; Roos, J.; Brinkmann, D.; Rusiecki, S.; Karpinski, J.; Kaldis, E. ^{17}O NMR study in aligned $YBa_2Cu_4O_8$ powder. *Phys. C Supercond.* **1992**, *194*, 277–286. [CrossRef]

50. Tomeno, I.; Machi, T.; Tai, K.; Koshizuka, N.; Kambe, S.; Hayashi, A.; Ueda, Y.; Yasuoka, H. NMR study of spin dynamics at planar oxygen and copper sites in YBa$_2$Cu$_4$O$_8$. *Phys. Rev. B* **1994**, *49*, 15327–15334. [CrossRef] [PubMed]

51. Zheng, G.Q.; Kitaoka, Y.; Asayama, K.; Kodama, Y.; Yamada, Y. ^{17}O NMR study of local hole density and spin dynamics in YBa$_2$Cu$_4$O$_8$. *Phys. C Supercond.* **1992**, *193*, 154–162. [CrossRef]

52. Zheng, G.Q.; Kitaoka, Y.; Asayama, K.; Kodama, Y. Spin susceptibility in YBa$_2$Cu$_4$O$_8$: ^{17}O and ^{63}Cu NMR study. *Phys. B Condens. Matter* **1993**, *186–188*, 1001–1003. [CrossRef]

53. Zheng, G.Q.; Kitaoka, Y.; Asayama, K.; Kodama, Y. Magnetic-field enhancement of ^{63}Cu and ^{17}O relaxation rates in the mixed state of YBa$_2$Cu$_4$O$_8$ observation of fermi-liquid state in the vortex cores. *Phys. C Supercond.* **1994**, *227*, 169–175. [CrossRef]

54. Hammel, P.C.; Takigawa, M.; Heffner, R.H.; Fisk, Z.; Ott, K.C. Spin dynamics at oxygen sites in YBa$_2$Cu$_3$O$_7$. *Phys. Rev. Lett.* **1989**, *63*, 1992–1995. [CrossRef]

55. Horvatić, M.; Berthier, Y.; Butaud, P.; Kitaoka, Y.; Ségransan, P.; Berthier, C.; Katayama-Yoshida, H.; Okabe, Y.; Takahashi, T. ^{17}O NMR study of YBa$_2$Cu$_3$O$_{7-\delta}$ (T_c = 92 K). *Phys. C Supercond.* **1989**, *159*, 689–696. [CrossRef]

56. Kitaoka, Y.; Berthier, Y.; Butaud, P.; Horvatić, M.; Ségransan, P.; Berthier, C.; Katayama-Yoshida, H.; Okabe, Y.; Takahashi, T. NMR study of ^{17}O in high T_c superconducting oxides. *Phys. C Supercond.* **1989**, *162–164 Pt 1*, 195–196. [CrossRef]

57. Martindale, J.A.; Barrett, S.E.; O'Hara, K.E.; Slichter, C.P.; Lee, W.C.; Ginsberg, D.M. Magnetic-field dependence of planar copper and oxygen spin-lattice relaxation rates in the superconducting state of YBa$_2$Cu$_3$O$_7$. *Phys. Rev. B* **1993**, *47*, 9155. [CrossRef] [PubMed]

58. Martindale, J.A.; Barrett, S.E.; Durand, D.J.; O'Hara, K.E.; Slichter, C.P.; Lee, W.C.; Ginsberg, D.M. Nuclear-spin-lattice relaxation-rate measurements in YBa$_2$Cu$_3$O$_7$. *Phys. Rev. B* **1994**, *50*, 13645–13652. [CrossRef]

59. Martindale, J.A.; Hammel, P.C.; Hults, W.L.; Smith, J.L. Temperature dependence of the anisotropy of the planar oxygen nuclear spin-lattice relaxation rate in YBa$_2$Cu$_3$O$_y$. *Phys. Rev. B* **1998**, *57*, 11769–11774. [CrossRef]

60. Reven, L.; Shore, J.; Yang, S.; Duncan, T.; Schwartz, D.; Chung, J.; Oldfield, E. ^{17}O nuclear-magnetic-resonance spin-lattice relaxation and Knight-shift behavior in bismuthate, plumbate, and cuprate superconductors. *Phys. Rev. B* **1991**, *43*, 10466. [CrossRef]

61. Yoshinari, Y.; Yasuoka, H.; Ueda, Y.; Koga, K.I.; Kosuge, K. NMR Studies of ^{17}O in the Normal State of YBa$_2$Cu$_3$O$_{6+x}$. *J. Phys. Soc. Jpn.* **1990**, *59*, 3698–3711. [CrossRef]

62. Yoshinari, Y.; Yasuoka, H.; Ueda, Y. Nuclear Spin Relaxation at Planar Copper and Oxygen Sites in YBa$_2$Cu$_3$O$_{6.96}$. *J. Phys. Soc. Jpn.* **1992**, *61*, 770–773. [CrossRef]

63. Ishida, K.; Kitaoka, Y.; Zheng, G.Q.; Asayama, K. ^{17}O and ^{63}Cu NMR Investigations of High-T_c Superconductor La$_{1.85}$Sr$_{0.15}$Cu0$_4$ with T_c = 38 K. *J. Phys. Soc. Jpn.* **1991**, *60*, 3516–3524. [CrossRef]

64. Singer, P.M.; Imai, T.; Chou, F.C.; Hirota, K.; Takaba, M.; Kakeshita, T.; Eisaki, H.; Uchida, S. ^{17}O NMR study of the inhomogeneous electronic state in La$_{2-x}$Sr$_x$CuO$_4$ crystals. *Phys. Rev. B* **2005**, *72*, 014537. [CrossRef]

65. Thurber, K.R.; Hunt, A.W.; Imai, T.; Chou, F.C.; Lee, Y.S. ^{17}O NMR Study of Undoped and Lightly Hole Doped CuO$_2$ Planes. *Phys. Rev. Lett.* **1997**, *79*, 171–174. [CrossRef]

66. Walstedt, R.E.; Shastry, B.S.; Cheong, S.W. NMR, neutron scattering, and the one-band model of La$_{2-x}$Sr$_x$CuO$_4$. *Phys. Rev. Lett.* **1994**, *72*, 3610–3613. [CrossRef] [PubMed]

67. Williams, G.V.M.; Tallon, J.L.; Michalak, R.; Dupree, R. NMR evidence for common superconducting and pseudogap phase diagrams of YBa$_2$Cu$_3$O$_{7-\delta}$ and La$_{2-x}$Sr$_x$CaCu$_2$O$_6$. *Phys. Rev. B* **1996**, *54*, R6909–R6912. [CrossRef] [PubMed]

68. Bobroff, J.; Alloul, H.; Mendels, P.; Viallet, V.; Marucco, J.F.; Colson, D. ^{17}O NMR Evidence for a Pseudogap in the Monolayer HgBa$_2$CuO$_{4+\delta}$. *Phys. Rev. Lett.* **1997**, *78*, 3757–3760. [CrossRef]

69. Crocker, J.; Dioguardi, A.P.; apRoberts-Warren, N.; Shockley, A.C.; Grafe, H.-J.; Xu, Z.; Wen, J.; Gu, G.; Curro, N.J. NMR studies of pseudogap and electronic inhomogeneity in Bi$_2$Sr$_2$CaCu$_2$O$_{8+\delta}$. *Phys. Rev. B* **2011**, *84*, 224502. [CrossRef]

70. Howes, A.; Dupree, R.; Paul, D.; Male, S. ^{17}O NMR of the Bi$_2$Sr$_2$Ca$_2$Cu$_3$O$_{10}$ high temperature superconductor. *Phys. C Supercond.* **1991**, *185–189 Pt 2*, 1137–1138. [CrossRef]

71. Howes, A.; Durpee, R.; Paul, D.; Male, S. An ^{17}O NMR study of the Cu-O planes of $Bi_2Sr_2Ca_2Cu_3O_{10}$. *Phys. C Supercond.* **1992**, *193*, 189–195. [CrossRef]

72. Trokiner, A.; Le Noc, L.; Schneck, J.; Pougnet, A.; Mellet, R.; Primot, J.; Savary, H.; Gao, Y.; Aubry, S. ^{17}O nuclear-magnetic-resonance evidence for distinct carrier densities in the two types of CuO_2 planes of $(Bi,Pb)_2Sr_2Ca_2Cu_3O_y$. *Phys. Rev. B* **1991**, *44*, 2426–2429. [CrossRef]

73. Bellot, P.V.; Trokiner, A.; Zhdonov, Y.; Yakubovskii, A.; Shustov, L.; Verkhovskii, S.; Zagoulaev, S.; Monod, P. Magnetic properties of $(Tl_{1-x}Pb_x)Sr_2CaCu_2O_7$ High-T_c oxide studied by ^{17}O NMR and SQUID: from overdoped superconductor to strongly overdoped metal. *Phys. C Supercond.* **1997**, *282–287 Pt 3*, 1357–1358. [CrossRef]

74. Gerashenko, A.; Piskunov, Y.; Mikhalev, K.; Ananyev, A.; Okulova, K.; Verkhovskii, S.; Yakubovskii, A.; Shustov, L.; Trokiner, A. The ^{63}Cu and ^{17}O NMR studies of spin susceptibility in differently doped $Tl_2Ba_2CaCu_2O_{8-\delta}$ compounds. *Phys. C Supercond.* **1999**, *328*, 163–176. [CrossRef]

75. Han, Z.; Dupree, R.; Howes, A.; Liu, R.; Edwards, P. Charge distribution in $(Tl,Pb)Sr_2Ca_2Cu_3O_{9-\sigma}$ ($T_c = 124K$) an ^{17}O NMR study. *Phys. C Supercond.* **1994**, *235–240 Pt 3*, 1709–1710. [CrossRef]

76. Kambe, S.; Yoshinari, Y.; Yasuoka, H.; Hayashi, A.; Ueda, Y. ^{17}O, ^{63}Cu and ^{205}Tl NMR study of over-doped $Tl_2Ba_2CuO_y$. *Phys. C Supercond.* **1991**, *185–189*, 1181–1182. [CrossRef]

77. Howes, A.P.; Dupree, R.; Han, Z.P.; Liu, R.S.; Edwards, P.P. Anomalous temperature dependence of the static spin susceptibility of $Tl_2Ba_2Ca_2Cu_3O_{10-\delta}$ ($T_c \cong 125$ K) in the normal state. *Phys. Rev. B* **1993**, *47*, 11529–11532. [CrossRef] [PubMed]

78. Zheng, G.Q.; Kitaoka, Y.; Ishida, K.; Asayama, K. Local Hole Distribution in the CuO_2 Plane of High-T_c Cu-Oxides Studied by Cu and Oxygen NQR/NMR. *J. Phys. Soc. Jpn.* **1995**, *64*, 2524–2532. [CrossRef]

79. Zheng, G.Q.; Kitaoka, Y.; Asayama, K.; Hamada, K.; Yamauchi, H.; Tanaka, S. NMR study of local hole distribution, spin fluctuation and superconductivity in $Tl_2Ba_2Ca_2Cu_3O_{10}$. *Phys. C Supercond.* **1996**, *260*, 197–210. [CrossRef]

Temperature independent pseudogap from ^{17}O and ^{89}Y NMR and the single component picture

Marija Avramovska,[1] Jakob Nachtigal,[1] and Jürgen Haase[1]

[1]*University of Leipzig, Felix Bloch Institute for Solid State Physics, Linnéstr. 5, 04103 Leipzig, Germany*
(Dated: December 20, 2021)

Nuclear Magnetic Resonance (NMR) is a powerful local quantum probe of the electronic structure of materials, but in the absence of reliable theory the interpretation of the NMR data can be challenging. This is true in particular for the cuprate high-temperature superconductors. Over the years, a large base of NMR data became available, which makes a review of the early interpretation possible. Recently, it was shown that all planar ^{17}O NMR shift and relaxation data available in the literature point to a temperature independent but doping dependent pseudogap, very similar to what was proposed from the electronic entropy. Here we analyze the anisotropy of the shift and relaxation of planar O to establish whether a single electronic spin component is applicable, since the planar Cu shift anisotropy clearly fails such a description. We find that the orbital shift terms deduced from the data are in agreement with first principle calculations, and the shift data show a temperature independent anisotropy also in agreement with hyperfine coefficients predicted by first principles, which also account for the relaxation anisotropy. Furthermore, we show that the original ^{89}Y shift and relaxation data are in agreement with the proposed temperature independent pseudogap. This pseudogap depends on doping, but also on the family of materials, and the density of states outside or in the absence of the gap is universal for the cuprates; this suggests that the entropy should be similar for all cuprates, as well. Further consequences will be discussed.

I. INTRODUCTION

Nuclear magnetic resonance (NMR), as a bulk probe of material properties with atomic scale resolution, was an early touchstone of understanding cuprate high-temperature superconductors [1], for reviews see [2, 3]. From the parent antiferromagnets to the overdoped conductors, a number of features were discovered and discussed in terms of classical as well as new theory. For the superconducting materials it was concluded that spin-singlet pairing was behind the loss in spin shift and relaxation below the critical temperature of superconductivity (T_c), as known for classical superconductors [4, 5]. But it was also noticed that the shifts (K) and normalized relaxation ($1/T_1T$), start to decrease at temperatures far above T_c, cf. Fig. 1, which marked the discovery of the pseudogap (with ^{89}Y NMR in YBa$_2$Cu$_3$O$_{6+y}$) [6]. Note that in metals the spin shift (K, Knight shift from the Pauli spin susceptibility above T_c), as well as the normalized relaxation ($1/T_1T$) are temperature independent. This metallic behavior is found only for the strongly doped cuprates. The decrease at temperatures above T_c seen in the lower doped materials was attributed to the opening of a spin gap at that temperature. However, the characteristics of the pseudogap did not become clearer as the experimental basis grew over the years, in particular, the thus derived pseudogap temperature is lower that what was found with other probes [7].

Very recently, a different definition of the NMR pseudogap was proposed [9], which is the same as the one based on the specific heat data of Loram et al.[8, 10]. Based on all available planar O data in the literature (more than 35 independent sets of relaxation, and more
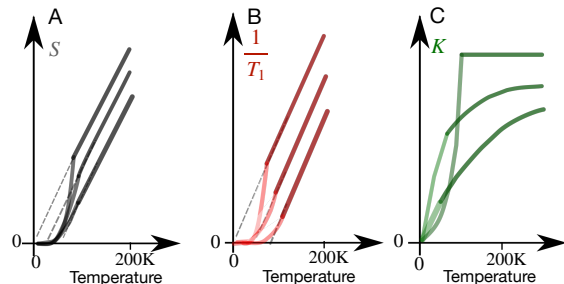

Figure 1. **A** Sketch of entropy (S) vs. temperature (T) as adapted from Loram et al. [8]. **B** Sketch of nuclear relaxation ($1/T_1$) vs. temperature for different doping levels [9]; overdoped systems behave metal-like above the critical temperature for superconductivity T_c; at other doping levels the high-temperature slopes remain unchanged. **C** Sketch of spin shift (K) vs. temperature for different doping levels [9]. Note that the model of the temperature independent pseudogap proposed in [9] does not consider the superconducting gap.

than 45 sets of shifts) it was found that the high-temperature slopes of the nuclear relaxation with respect to temperature ($\Delta(1/T_1)/\Delta(T)$, cf. Fig. 1) are independent on doping, in accordance with a temperature independent pseudogap that opens at the Fermi surface and causes loss of low-energy states. With other words, the states that become available as the Fermi function opens with temperature are metal like and even appear to be ubiquitous to the cuprates [9], as the high-doping slope is the same for all materials and the same as in the absence of the gap. Another simple consequence of such behavior is that the NMR shifts, from excitations across this gap, acquire a temperature dependence due to the

Fermi function, with the hallmark result that even at the highest temperatures, the gapped, low-energy states are missing. Thus, there is a high-temperature shift offset in the spin susceptibility that depends on doping [9]. The consequences of such a temperature independent pseudogap are sketched in Fig. 1. The lower the doping the more states disappear near the Fermi surface as the size of the pseudogap increases.

Whether the average doping (x, as in $La_{2-x}Sr_xCuO_4$), is the best parameter to describe the pseudogap is not clear. NMR can also measure the local charges at planar Cu (n_{Cu}) and planar O (n_O) and determine the sharing of the inherent hole as well as the holes added by doping [11, 12], and a simple relation was found: $1 + \zeta = n_{Cu} + 2n_O$. Here, ζ is the doping measured with NMR and follows from n_{Cu} and n_O. ζ is found to be similar to x for $La_{2-x}Sr_xCuO_4$. This is expected since the equation describes the stoichiometry of the materials. However, there are slight differences between ζ and what was concluded for other materials based on estimates of doping. Interestingly, the sharing of the planar hole content, i.e. n_{Cu}/n_O, varies strongly among the cuprate families and appears to set various material properties [13]. Most notably, the maximum T_c of the hole doped cuprates is proportional to n_O. This dependence of cuprate properties on the hole sharing was very recently proven by theory (cellular DMFT) [14], lending strong support to the NMR findings and the importance of ζ, n_O, n_{Cu}. These parameters may be of importance for the understanding of shift and relaxation, as well. While it is not new that doping plays an important role, there are also family dependences that track those of sharing the charges, such as the planar Cu shift anisotropy. This behavior is at the root of the fact that these shifts cannot be explained with a single temperature dependent spin component [15, 16]. A two component behavior was also proposed for O since the planar O shifts have a very different temperature dependence than that of the shift distributions [17].

It is therefore of great importance to investigate the planar O shift and relaxation anisotropies, which could not be accomplished with the first account of the temperature independent pseudogap [9]. While the number of datasets we could allocate for addressing this question is more limited compared to what was measured with the magnetic field along the crystal c-axis [9], the data are representative for the cuprates. As we will show, the planar O shift and relaxation anisotropies can be understood fully within a single spin component scenario, with the orbital shifts in agreement with what was predicted by first principle calculations [18]. Even the anisotropies follow from an anisotropic hyperfine constant that is in agreement with what was calculated by first principles [19]. Finally, we will show that the original ^{89}Y NMR data [6] are in agreement with a temperature independent pseudogap, and we discuss consequences.

II. DATA COLLECTION

We collected data for planar oxygen with all 3 directions measured in an intensive literature search and found the materials listed in the Appendix. The planar O shift tensor's main principle axis is along the Cu-O-Cu σ-bond (denoted by $K_{\|\sigma}$). The other two axes are assumed to be perpendicular to this bond, and along the crystal c-axis ($^{17}\hat{K}_{\perp c}$) and a-axis ($^{17}\hat{K}_{\perp a}$). The relaxation was also measured with the field along these axes. The temperature dependences of shift and relaxation were manually extracted from the figures, including error bars. For the sets of data that do not share the exact same temperature points for all three directions of the field, the original data were interpolated using a linear fit between the two respective data points. No explicit error bars were reported for $Tl_2Ba_2CuO_y$ [20] and $YBa_{1.92}Sr_{0.08}Cu_3O_7$ [21], and we assume they are similar to those of the other cuprates. A source of systematic uncertainty across all materials is the dependence on sample preparation procedures, in particular the fact that the doping level may not be known with high precision and oxygen isotope exchange may not be homogeneous for single crystals or even affect the actual O doping level. For example, materials from different groups can show somewhat different shifts, as is the case for $La_{1.85}Sr_{0.15}CuO_4$ data from Kitaoka et al. [22], Ishida et al. [23], and Singer et al. [24]. Interestingly, this is also the case even for the stoichiometric compound $YBa_2Cu_4O_8$ (see figures 2 and 3 in [9]). If the shift reference is not stated explicitly we assume it is water (a very convenient choice). As before [9], we show the total, uncorrected shifts with respect to this reference and determine the orbital shifts later to keep data analysis transparent.

III. PLANAR OXYGEN SHIFTS AND RELAXATION

1. Shifts

While we have only a limited number of shifts, the dependences for $^{17}\hat{K}_{\perp c}$ in Fig. 2 are quite representative of the cuprates if one compares to the related much more abundant plots in [9]. In Fig. 2 one finds high-temperature doping-dependent offsets and an onset of the temperature dependence already far above T_c for the underdoped materials, and the shifts nearly vanish at the lowest temperatures without showing special behavior at the superconducting transition temperature. The shifts for the overdoped materials are nearly temperature independent at high temperatures, and drop rapidly near T_c to similar low temperature values. For all 3 directions of the shift tensor we observe this behavior.

We now use the data from Fig. 2 and plot the various shifts against each other, with the results shown in Fig. 3.
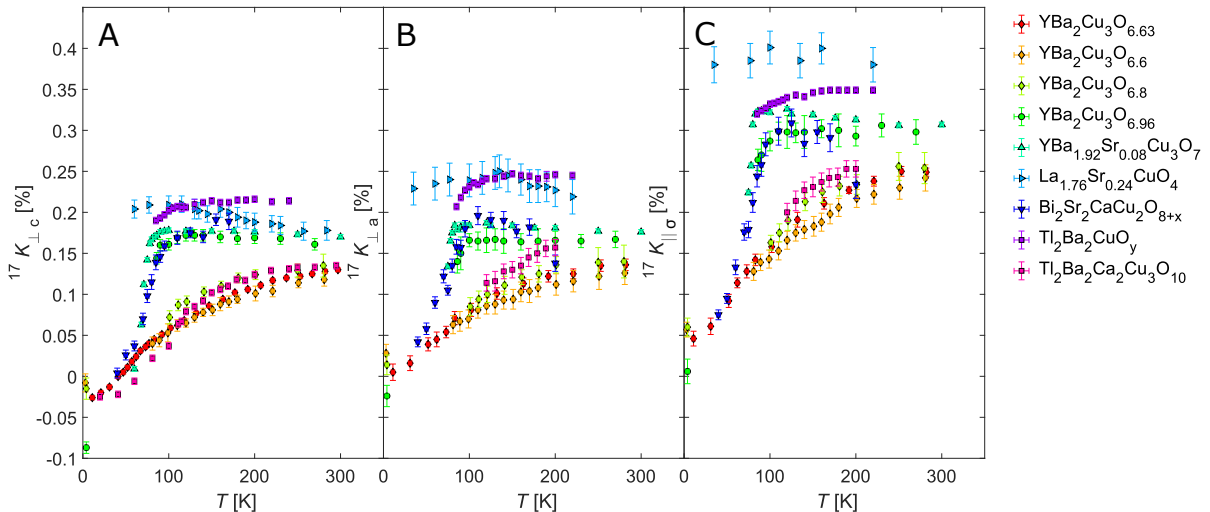
Figure 2. Temperature dependences of the planar oxygen shifts for different cuprate-families for all three directions of the tensor axes. **A** $^{17}\hat{K}_{\perp c}(T)$, **B** $^{17}\hat{K}_{\perp a}(T)$, and **C** $^{17}\hat{K}_{\parallel\sigma}(T)$. Optimally and overdoped systems behave metal-like. Underdoped systems show the expected high-temperature behavior with a doping dependent shift offset. Some materials show a negative spin shift at low temperatures. The highest shift range is observed for $K_{\parallel\sigma}$ with $0.40(5)\,\%$. Error bars are taken from the literature. For $K_{\perp c}(T)$ only subset of the data from [9] is shown as no data for the other directions are available. For the references, see Appendix.
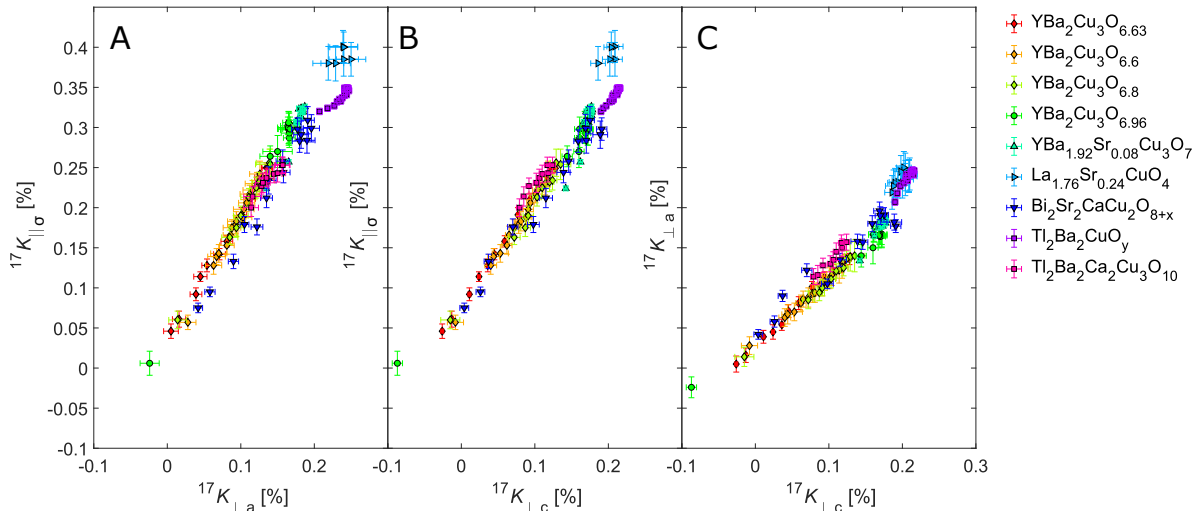

Figure 3. Temperature dependences of the total planar O magnetic shifts from Fig. 2, plotted against each other. **A** $^{17}\hat{K}_{\parallel\sigma}$ vs. $^{17}\hat{K}_{\perp a}$, **B** $^{17}\hat{K}_{\parallel\sigma}$ vs. $^{17}\hat{K}_{\perp c}$ and **C** $^{17}\hat{K}_{\perp a}$ vs. $^{17}\hat{K}_{\perp c}$. If one subtracts the orbital shifts, the shifts are proportional to each other in concordance with a single component picture. Note that one may not conclude with this certainty if considering only a single material.

Given the error bars, one concludes on largely temperature independent slopes, i.e. the shift anisotropy appears to be temperature independent. Furthermore, the slope for the two perpendicular shifts is close to 1, while plots involving the shift along the σ-bond have a larger slope,

about 1.45.

The total magnetic shift can be written as,

$$^{17}\hat{K}_\alpha(T) = {}^{17}K_{\mathrm{L}\alpha} + {}^{17}K_\alpha(T), \qquad (1)$$

where $^{17}K_{\mathrm{L}\alpha}$ is the orbital shift, and $^{17}K_\alpha(T)$ denotes the spin shift. For a single spin component susceptibility,

$\chi(T)$, we have for the spin shift,

$$^{17}K_\alpha(T) = C_\alpha \cdot \chi(T) \equiv (c_{\text{iso}} + c_{\text{dip},\alpha}) \cdot \chi(T), \quad (2)$$

where we assumed the hyperfine coefficient C_α to be the sum of an isotropic term from the O 2s orbital and a (traceless) dipolar term from the 2p orbitals. From the symmetry of the O 2p orbitals one expects $C_{\text{dip}\|\sigma} \approx 2|C_{\text{dip}\perp c,a}|$. The question arises whether the low temperature offsets in Fig. 3 are due to the orbital shifts. Given the uncertainty from a diamagnetic response below T_c, we verified with the high-temperature shifts for those materials that have nearly temperature independent high-temperature shifts, that the offset between the shifts at high temperatures is the same as that found from the low-temperature offsets. This means, a possible diamagnetic contribution below T_c can be neglected. This is in agreement with the fact the the correction from diamagnetism should be smaller than 0.01% [25]. Then, one would argue with Fig. 3 that the orbital shift is only significant for $c \| B_0$ were it is appears to be negative. Note that in panel **A** the slope is nearly 1 and the offset is nearly 0, and any diamagnetic contribution should be nearly isotropic in the plane.

Indeed, first principle calculations of the orbital shifts for La$_{2-x}$Sr$_x$CuO$_4$ [18] report $^{17}K_{\text{Lc}} = -0.034(20)\,\%$, $^{17}K_{\text{La}} = -0.011(10)\,\%$, and $^{17}K_{\text{Lb}} = -0.004(5)\,\%$. Thus, the straight lines observed in Fig. 3 are expected and we deduce the following slopes: $C_{\perp a}^{\text{exp}}/C_{\perp c}^{\text{exp}} \approx 0.90(15)$, $C_{\|\sigma}^{\text{exp}}/C_{\perp a}^{\text{exp}} \approx 1.45(10)$. These numbers are in very good agreement with what we find for La$_{2-x}$Sr$_x$CuO$_4$ and even the other cuprates. Thus this set of orbital shifts applies to all cuprates to a good approximation.

One should note that the linewidths for planar O (that limit the precision of the shifts) typically increase drastically as the temperature is lowered, even much in excess of what is expected from the field variation in the mixed state, making the low T shift values less reliable. Also the penetration depth decreases while the relaxation slows down drastically at low temperatures, making measurement tedious. These are the likely reasons why we find the most low-temperature points for the shifts $^{17}K_{\perp c}$ of YBa$_2$Cu$_3$O$_{6+y}$ and YBa$_2$Cu$_4$O$_8$, since these are also the materials with smallest linewidths.

The magnetic hyperfine coefficients have been determined by first principle calculations, as well [19]. It was found that $c_{\text{iso}} = 1.3$, $c_{\text{dip}\|\sigma} = 0.37$ (in atomic units), whence there is the factor of 1.5 for $C_{\|\sigma}/C_{\perp c,a}$, which is in agreement with what we find from experiment: $^{17}K_{\|\sigma}/^{17}K_{\perp a} \approx 1.45(10)$ and $^{17}K_{\perp a}/^{17}K_{\perp c} \approx 0.90(15)$. As the plots in panels **A, B** of Fig. 4 show, there is no other significant contribution to the shifts above T_c (below T_c the shifts are small and the error bars for their ratio becomes very large).

To summarize, the planar O shifts are fully accounted for by a single spin component coupled to the nucleus with predicted hyperfine coefficients and orbital shifts. The dependence of the spin susceptibility on doping does not affect the anisotropy of the shifts. This is also true, as expected, for the orbital shifts and the hyperfine coefficients.

2. Relaxation

Accounts of the planar oxygen relaxation anisotropy are sparse. We found mainly data for YBa$_2$Cu$_3$O$_{6+y}$ [26–28] and the data are shown in panels **C, D** of Fig. 4. Above T_c, the relaxation anisotropy measured perpendicular to the σ-bond is about 1, and the ratio of the values measured parallel to the σ-bond and perpendicular to it is about 0.7.

In a simple picture [29] the relaxation rates are given by the field fluctuations perpendicular to the direction of the quantization axis (the external field) and we have, for example,

$$1/T_{1\perp c} = \frac{3}{2}\gamma^2[\langle h_{\|\sigma}(t)^2\rangle + \langle h_{\perp a}(t)^2\rangle]\tau_0 \quad (3)$$

where $h_{\|\sigma}(t)$ and $h_{\perp a}(t)$ denote the fluctuating magnetic fields and τ_0 is their correlation time. One can write $\langle h_\alpha(t)^2\rangle$ in terms of the hyperfine coefficients as $\langle h_\alpha(t)^2\rangle = C_\alpha^2/\gamma_n\hbar \cdot \langle S^2\rangle$, where γ is the gyromagnetic ratio of the nucleus and $\langle S^2\rangle$ is the expectation value from the electronic spin. With $C_{\perp a}^{\text{exp}}/C_{\perp c}^{\text{exp}} \approx 0.9$ and $C_{\|\sigma}^{\text{exp}}/C_{\perp c}^{\text{exp}} \approx 1.45$ and expressions similar to (3) for the other directions of measurements, we expect the relaxation perpendicular to the σ-bond to be isotropic, but $(1/T_{1\|\sigma})/(1/T_{1\perp c}) \approx 0.62$. This is again in good agreement with the observations.

While the error bars below T_c grow, it was shown for YBa$_2$Cu$_4$O$_8$ below about 200 K that quadrupolar relaxation is present, as well [30]. This additional term is still within error bars of Fig. 4 **C** and **D**.

This leads us to conclude that also the relaxation for the planar O nucleus is largely described by simple on-site fluctuating spin (in the long wavelength limit) with hyperfine coefficients very close to what is predicted by first principle calculations. No special assumptions about filter functions for transferred spin are necessary [19].

IV. PSEUDOGAP AND ^{89}Y NMR OF YBa$_2$Cu$_3$O$_{7-\delta}$

The ^{89}Y NMR data that mark the discovery of the pseudogap by Alloul et al. [6] were only taken above T_c so that low-temperature values are not available for this nucleus (except for the near optimal doped material [31]), and mostly only available for powders. We reproduce the data in Fig. 5. Despite the uncertainties, shift and relaxation show the typical features of a tempera-
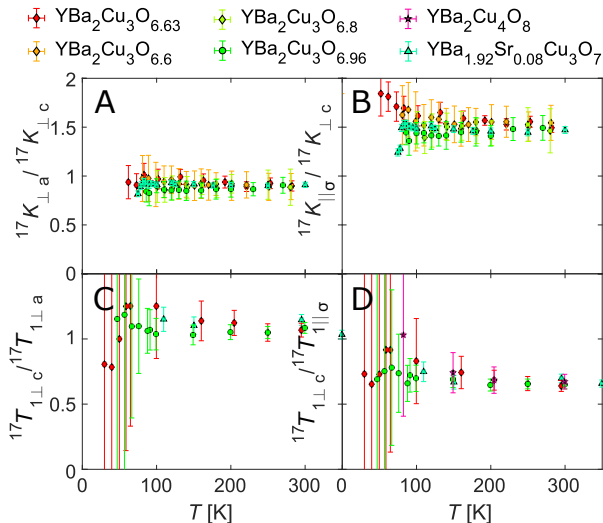
Figure 4. Temperature dependences of the, **A**, **B** shift anisotropies, and **C**, **D** of the corresponding relaxation anisotropies. The experimentally obtained shift and relaxation ratios are in close agreement with the predicted hyperfine coefficients (see main text).
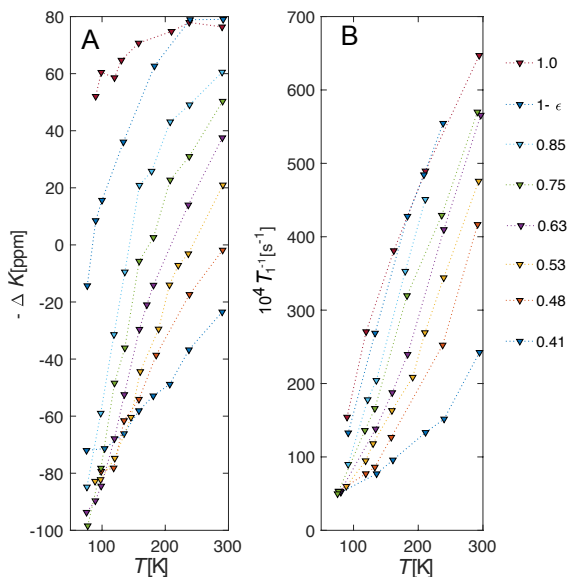

Figure 5. Temperature dependences of the [89]Y shifts, **A**, and relaxation, **B**, from Alloul et al. [6] are also in support of a temperature independent pseudogap (see main text).

ture independent pseudogap, as well. Thus the recent conclusions are in agreement with the [89]Y data.

V. DISCUSSION AND CONCLUSION

We showed previously [9] that the oxygen shift and relaxation data, available in abundance as measurements with the field along the crystal c-axis, can be modeled by a temperature independent gap at the Fermi surface of a simple metal (using a single spin component). The density of states outside the gap is ubiquitous for the cuprates, this includes the density of states when the gap is fully closed. Since this behavior is similar to measurements of the electronic entropy [8, 10] in a few materials, the same doping dependent entropy should govern all cuprates.

We also know from recent Cu NMR analyses that the observations in terms of NMR are more complicated for this nucleus [15, 16], in particular, the Cu shift anisotropy. Therefore, we focused here on the planar O shift anisotropy that was not analyzed previously. We present literature data where the shifts and relaxation were measured for all three directions of the magnetic field with respect to the Cu-O bond and look at the anisotropies. We find that both, shift and relaxation obey the same single spin component scenario, in agreement with what is expected from the hyperfine coefficients calculated in [19], who report: $C_{\perp a}/C_{\perp c} \approx 0.93$ and $C_{\|\sigma}/C_{\perp c,a} \approx 1.5$ while the experimental shifts give $C_{\perp c}^{\exp}/C_{\perp a}^{\exp} \approx 0.9$ and $C_{\|\sigma}^{\exp}/C_{\perp c,a}^{\exp} \approx 1.45$. Furthermore, we find the anisotropic orbital shifts to be rather independent on doping and family, and also in agreement with what was predicted from first principles [18].

For all oxygen relaxation data [9], independent of material, the un-gapped relaxation rate for $c \parallel B_0$ has a slope of 0.35/Ks with temperature (this is also the rate determined from relaxation outside the gap for all doping levels). In case of a simple Fermi liquid the Korringa relation holds [32]: $T_1 T K_s^2 = \kappa(\gamma_e/\gamma_n)^2 \hbar/4\pi k_B$. The prefactor κ is usually introduced to describe electronic correlations. For the [17]O shifts, where we know both, the orbital shifts and the hyperfine coefficients, we obtain that the Korringa law holds for the metallic density of states with $\kappa_O \approx 1.8$, note that we are comparing, e.g., $^{17}K_{\perp c}^2 \propto C_{\perp c}^2$ with $1/^{17}T_{1\|\sigma} \propto [C_{\perp c}^2 + C_{\perp a}^2]$. In [6], it was found that the [89]Y data have $\kappa_Y = 5.3$. Remember that for the [89]Y shifts the orbital contributions are not precisely known.

It was also found that for some highly overdoped cuprates the Korringa law can explain the relation between Cu shift and relaxation [16]. This was taken as an indication that, differently from what was believed earlier, the relaxation is *not* enhanced over what one can expect from the shifts, as the doping and material independent normalized relaxation rate of $1/^{63}T_{1\perp}T \approx 21$/Ks already indicates [33]. Rather, it was shown [16] that the shifts must be suppressed in the underdoped materials. An explanation for the Cu shift suppression could be

that the Cu shifts are affected by the pseudogap, much like the O shifts, however the Cu relaxation rates are not. Moreover, the universal Cu relaxation rate might be connected to the ubiquitous density of states seen with planar O NMR that leads to $1/^{17}T_{1c}T \approx 0.35$ /Ks. This normalized rate is proportional to $\left[C_{\perp a}^2 + C_{\parallel \sigma}^2 \right]$ and if we normalize it to $C_{\perp c}$ we have 0.21 /Ks. With a ratio of $^{63}\gamma/^{17}\gamma \approx 1.96$ we conclude that an effective hyperfine coefficient for Cu should be about $5.1 \cdot C_{\perp c}$, or a spin shift of about 1.2%, which is significantly larger than the high-temperature value of $^{63}K_\perp \sim 0.7\%$. Note that the Cu shifts have a large anisotropy that is family dependent. Only for $c \perp B_0$ the orbital shift appears to be reliable [16]. Furthermore, since $1/^{63}T_{1\perp}T \approx 21$ /Ks (caused by the sum of in-plane and out-of-plane fluctuating field components) is rather material independent in contrast to $1/^{63}T_{1\parallel}$ that varies among the materials, the out-of-plane ($c \parallel B_0$) hyperfine coefficient should dominate the Cu relaxation, which is related to $^{63}K_\parallel$. A two-component model that accounts for the relaxation was proposed recently [34]. Nevertheless, work is underway that addresses Cu shifts and relaxation and comparison with the new results.

The size of the pseudogap was discussed in figure 9 of [9] and it showed a complicated family dependence. Whereas $YBa_2Cu_3O_{6+y}$ has no sizable pseudogap at optimal doping, other cuprates do show a pseudogap. Interestingly, optimally doped $YBa_2Cu_3O_{6+y}$ has the largest ζ [35], meaning that it already on the overdoped side in terms of the NMR doping ζ. Since the precise meaning of this material dependency (n_{Cu}, n_O, ζ) is not fully understood, it is difficult to draw further conclusions on relations with the pseudogap or T_c.

Earlier, a two component picture for the O shift was invoked by comparing the different temperature dependences of the shifts and linewidths [17]. The latter are related to the spatial charge variation in the CuO_2 plane. Now, with the knowledge that a variation of doping must lead to a variation of the pseudogap, an inhomogeneous pseudogap easily explains the differences between shifts and linewidths. It is the susceptibility that depends on two parameters (temperature and doping).

Different temperature dependences of the O axial and isotropic shifts were reported for $YBa_2Cu_4O_8$ by Machi et al. [36]. This finding seems to contradict a single susceptibility scenario, as well. We observe, similarly as in [36] that the oxygen axial shifts, for all the available data, are largely temperature independent, whereas the isotropic shift (or $^{17}K_c$) has a substantial temperature dependence already above T_c. However, we find the overall uncertainty in the axial shift data too large to confirm this scenario.

To conclude, from the study of the anisotropies of planar O relaxation and shift we find that the data can be explained with a single component susceptibility with hyperfine coefficients and orbital shifts very close to what was predicted by first principles. Thus, the data fully support the previously suggested picture of a susceptibility that appears to be that of a simple metal with a density of states universal to the cuprates in the sense that all strongly overdoped materials have the same density of states and as the doping decreases (in a family specific way) a temperature independent gap opens at the Fermi surface while the states outside the gap remain the same. Due to the temperature dependence of the Fermi function, excitations across the gap lead to the deviations of relaxation and shift (and entropy) from simple metal behavior. It remains to be seen how these findings can be reconciled with the planar Cu data that, e.g., show a very unusual shift anisotropy and a relaxation rate not affected by the pseudogap.

AUTHOR CONTRIBUTION

J.H. introduced the main concepts and had the project leadership; M.A. led the writing and preparation of the manuscript; J.N. led the literature data collection, analyses, and presentation in the manuscript; all authors contributed to the writing of the manuscript.

Appendix A: Data Sources

Table I. Reference to literature accounts of data. Compounds shown in figures, with critical temperature T_c, label and reference link.

Compound	T_c	Label	Ref.
$Bi_2Sr_2CaCu_2O_{8+x}$	82 K	Crocker 2011	[37]
$YBa_2Cu_3O_{6.6}$	60 K	Yoshinari 1990	[38]
$YBa_2Cu_3O_{6.63}$	62 K	Takigawa 1991,	[39]
		Martindale 1998	[40]
$YBa_2Cu_3O_{6.8}$	84 K	Yoshinari 1990	[38]
$YBa_2Cu_3O_{6.96}$	92 K	Yoshinari 1990	[38]
		Martindale 1998	[40]
$YBa_{1.92}Sr_{0.08}Cu_3O_7$	89 K	Horvatic 1993	[27]
$YBa_2Cu_4O_8$	81 K	Suter 1997	[28]
$La_{1.76}Sr_{0.24}CuO_4$	25 K	Zheng 1993	[41]
$Tl_2Ba_2CuO_x$	85 K	Kambe 1993	[20]
$Tl_2Ba_2Ca_2Cu_3O_{10}$	125 K	Zheng 1996	[42]

[1] J. G. Bednorz and K. A. Müller, Z. Phys. B Condens. Matter **193**, 189 (1986).

[2] C. P. Slichter, in *Handbook of High-Temperature Superconductivity*, edited by J. R. Schrieffer and J. S. Brooks (Springer, New York, 2007) pp. 215–256.

[3] R. E. Walstedt, *The NMR Probe of High-T_c Materials*, 1st ed. (Springer, 2007).

[4] L. C. Hebel and C. P. Slichter, Phys. Rev. **113**, 1504 (1959).

[5] K. Yosida, Phys. Rev. **110**, 769 (1958).

[6] H. Alloul, T. Ohno, and P. Mendels, Phys. Rev. Lett. **63**, 1700 (1989).

[7] T. Timusk and B. Statt, Rep. Prog. Phys. **62**, 61 (1999).

[8] J. W. Loram, K. A. Mirza, J. R. Cooper, and J. L. Tallon, J. Phys. Chem. Solids **59**, 2091 (1998).

[9] J. Nachtigal, M. Avramovska, A. Erb, D. Pavićević, R. Guehne, and J. Haase, Condens. Matter **5**, 66 (2020).

[10] J. L. Tallon and J. W. Loram, Sci. Rep. **10**, 22288 (2020).

[11] J. Haase, O. P. Sushkov, P. Horsch, and G. V. M. Williams, Phys. Rev. B **69**, 94504 (2004).

[12] M. Jurkutat, D. Rybicki, O. P. Sushkov, G. V. M. Williams, A. Erb, and J. Haase, Phys. Rev. B **90**, 140504 (2014).

[13] M. Jurkutat, A. Erb, and J. Haase, Condens. Matter **4**, 67 (2019).

[14] N. Kowalski, S. S. Dash, P. Sémon, D. Sénéchal, and A.-M. Tremblay, PNAS **118** (2021), 10.1073/pnas.2106476118.

[15] J. Haase, M. Jurkutat, and J. Kohlrautz, Condens. Matter **2**, 16 (2017).

[16] M. Avramovska, D. Pavićević, and J. Haase, J. Supercond. Nov. Magn. **32**, 3761 (2019).

[17] D. Pavićević, M. Avramovska, and J. Haase, Mod. Phys. Lett. B **34**, 2040047 (2020).

[18] S. Renold, T. Heine, J. Weber, and P. F. Meier, Phys. Rev. B **67**, 24501 (2003).

[19] P. Hüsser, H. U. Suter, E. P. Stoll, and P. F. Meier, Phys. Rev. B **61**, 1567 (2000).

[20] S. Kambe, H. Yasuoka, A. Hayashi, and Y. Ueda, Phys. Rev. B **47**, 2825 (1993).

[21] M. Horvatić, Y. Berthier, P. Butaud, Y. Kitaoka, P. Ségransan, C. Berthier, H. Katayama-Yoshida, Y. Okabe, and T. Takahashi, Phys. C Supercond. **159**, 689 (1989).

[22] Y. Kitaoka, S. Hiramatsu, T. Kondo, and K. Asayama, J. Phys. Soc. Jpn. **57**, 30 (1988).

[23] K. Ishida, Y. Kitaoka, G.-q. Zheng, and K. Asayama, J. Phys. Soc. Jpn. **60**, 3516 (1991).

[24] P. M. Singer, A. W. Hunt, and T. Imai, Phys. Rev. Lett. **88**, 047602 (2002).

[25] J. Haase, D. Rybicki, C. P. Slichter, M. Greven, G. Yu, Y. Li, and X. Zhao, Phys. Rev. B **85**, 104517 (2012).

[26] J. A. Martindale, S. E. Barrett, K. E. O'Hara, C. P. Slichter, W. C. Lee, and D. M. Ginsberg, Phys. Rev. B **47**, 9155 (1993).

[27] M. Horvatić, C. Berthier, Y. Berthier, P. Ségransan, P. Butaud, W. G. Clark, J. A. Gillet, and J. Y. Henry, Phys. Rev. B **48**, 13848 (1993).

[28] A. Suter, M. Mali, J. Roos, D. Brinkmann, J. Karpinski, and E. Kaldis, Phys. Rev. B **56**, 5542 (1997).

[29] C. H. Pennington, D. J. Durand, C. P. Slichter, J. P. Rice, E. D. Bukowski, and D. M. Ginsberg, Phys. Rev. B **39**, 2902 (1989).

[30] A. Suter, M. Mali, J. Roos, and D. Brinkmann, Phys. Rev. Lett. **84**, 4938 (2000).

[31] S. E. Barrett, D. J. Durand, C. H. Pennington, C. P. Slichter, T. A. Friedmann, J. P. Rice, and D. M. Ginsberg, Phys. Rev. B **41**, 6283 (1990).

[32] J. Korringa, Physica **16**, 601 (1950).

[33] M. Jurkutat, M. Avramovska, G. V. M. Williams, D. Dernbach, D. Pavićević, and J. Haase, J. Supercond. Nov. Magn. **155**, 629 (2019).

[34] M. Avramovska, D. Pavićević, and J. Haase, J. Supercond. Nov. Magn. **33**, 2621 (2020).

[35] M. Jurkutat, C. Kattinger, S. Tsankov, R. Reznicek, A. Erb, and J. Haase, arXiv:2109.10157 [cond-mat] (2021), arXiv: 2109.10157.

[36] T. Machi, N. Koshizuka, and H. Yasuoka, Phys. B **284-288**, 943 (2000).

[37] J. Crocker, A. P. Dioguardi, N. apRoberts Warren, A. C. Shockley, H. J. Grafe, Z. Xu, J. Wen, G. Gu, and N. J. Curro, Phys. Rev. B **84**, 224502 (2011).

[38] Y. Yoshinari, H. Yasuoka, Y. Ueda, K.-i. Koga, and K. Kosuge, J. Phys. Soc. Japan **59**, 3698 (1990).

[39] M. Takigawa, A. P. Reyes, P. C. Hammel, J. D. Thompson, R. H. Heffner, Z. Fisk, and K. C. Ott, Phys. Rev. B **43**, 247 (1991).

[40] J. A. Martindale, P. C. Hammel, W. L. Hults, and J. L. Smith, Phys. Rev. B **57**, 11769 (1998).

[41] G. Q. Zheng, T. Kuse, Y. Kitaoka, K. Ishida, S. Ohsugi, K. Asayama, and Y. Yamada, Phys. C Supercond. **208**, 339 (1993).

[42] G.-q. Zheng, Y. Kitaoka, K. Asayama, K. Hamada, H. Yamauchi, and S. Tanaka, Phys. C Supercond. **260**, 197 (1996).

4.3 The pseudogap and a unified picture of Cu and O NMR

In light of the newly developed conclusions regarding the O data where a single-spin component and a temperature-independent pseudogap sufficed in explaining the data, the question arose how does the Cu data relate to this simple picture.

It was shown earlier that the Cu shifts appeared to be suppressed, whereas relaxation seemed to be ubiquitous for all materials and doping levels. Unlike the O data, the Cu shift anisotropy warranted a description with two-spin components.

In this final publication, we present a more coherent phenomenology of Cu and O NMR shift and relaxation. We conclude that the Cu shift suppression discussed earlier is a manifestation of the temperature-independent pseudogap; however, Cu relaxation appears unaffected by it. Namely, the Cu shifts for one direction of the magnetic field ($c \perp B_0$) behave similarly to the O shifts, i.e., suppressed due to the temperature-independent pseudogap, whereas the Cu shifts for $c \parallel B_0$ direction point to a more complicated scenario.

While the suppression of the $c \parallel B_0$ shifts is also present (note that the shift range across all families and doping is similar for both directions of the magnetic field), there is a family dependence, where the $YBa_2Cu_3O_{7-\delta}$ and $La_{2-x}Sr_xCuO_4$ shifts show a peculiar behavior—they are temperature and doping independent—meaning that the pseudogap feature can disappear for some $c \parallel B_0$ shifts.

We propose that this is due to the action of a second spin component residing in the Cu $3d(x^2 - y^2)$ orbital. While the pseudogap is present in both Cu and O shifts, there is still a quantitative difference between the Cu and O shift data, pointing out the fact that while some systems may show features of single-spin component behavior (e.g.$YBa_2Cu_3O_{7-\delta}$ and $YBa_2Cu_4O_8$), this is not true for the rest of the cuprate families, where the Cu vs. O plot show no proportionality.

While O relaxation clearly shows the action of a temperature-independent, doping-dependent gap, with a density of states common to all the cuprates and a relaxation anisotropy in agreement with a simple hyperfine scenario, the Cu relaxation is quite different. Cu relaxation rates do not show the pseudogap. Below T_c all Cu relaxation

rates behave similarly and there is a drop at T_c, different from the Cu shifts and O shift and relaxation, which are all dominated by the effects of the pseudogap.

Planar Cu and O NMR and the Pseudogap of Cuprate Superconductors

Marija Avramovska, Jakob Nachtigal, Stefan Tsankov, and Jürgen Haase*

Felix Bloch Institute for Solid State Physics, University of Leipzig, Linnéstr. 5, 04103 Leipzig, Germany
* Correspondence: j.haase@physik.uni-leipzig.de

Abstract: Recently, an analysis of all available planar oxygen shift and relaxation data for the cuprate high-temperature superconductors showed that the data can be understood with a simple spin susceptibility from a metallic density of states common to all cuprates. It carries a doping dependent but temperature independent pseudogap at the Fermi surface, which causes the deviations from normal metallic behavior, also in the specific heat. Here, a more coherent, unbiased assessment of all data, including planar Cu, is presented and consequences are discussed, since the planar Cu data were collected and analyzed prior to the O data. The main finding is that the planar Cu shifts for one direction of the external magnetic field largely follow from the same states and pseudogap. This explains the shift suppression stated more recently, which leads to the failure of the Korringa relation in contrast to an enhancement of the relaxation due to antiferromagnetic spin fluctuations originally proposed. However, there is still the need for a second spin component that appears to be associated with the Cu $3d(x^2 - y^2)$ hole to explain the complex Cu shift anisotropy and family dependence. Furthermore, it is argued that the planar Cu relaxation which was reported recently to be rather ubiquitous for the cuprates, must be related to this universal density of states and the second spin component, while not being affected by the simple pseudogap. Thus, while this universal metallic density of states with a pseudogap is also found in the planar Cu data, there is still need for a more elaborate scenario that eludes planar O.

Keywords: NMR; cuprates; pseudogap

1. Introduction

Nuclear magnetic resonance (NMR) played an important role in high-temperature superconductivity [1], in particular in its early days with the focus on the $La_{2-x}Sr_xCuO_4$ and $YBa_2Cu_3O_{7-\delta}$ families of materials. Important information about chemical and electronic properties could be obtained, but an unchallenged interpretation was not achieved, as of today, due to conflicting experimental evidence (for an early review see [2]). In particular the question of the description of the cuprates in terms of a single spin component electronic susceptibility remained unanswered, as more recent experiments had shown [3–5].

Two very recent publications [6,7] revealed that *all* planar oxygen NMR relaxation and shift data available from the literature for hole-doped cuprates (more than 60 independent data sets in total) are in agreement with a simple metallic spin susceptibility from a density of states that has a temperature independent pseudogap at the Fermi surface. The pseudogap opens as doping decreases from high levels and can be measured with NMR. The density of states outside the gap or in its absence is *universal* to the cuprates, independent of doping and family [6]. This scenario is similar to what was concluded from specific heat data [8,9]. Thus, lowering the doping opens the gap, and the lost, low-energy states cease to contribute to shift, relaxation, or specific heat. As a consequence, one observes the following in NMR: (i) a high-temperature, doping dependent offset in the relaxation rate, $1/T_1$, that remains metal like in the sense that $\Delta(1/T_1)/\Delta T = const.$, irrespective of material and doping, and (ii) a high-temperature, doping dependent offset in the spin shifts, since electronic polarization from the low energy states is still missing even at the highest T in the presence of the

pseudogap. The states lost near the Fermi surface, in connection with thermal excitations across the gap, cause the typical temperature dependence of the spin shift hitherto ascribed to the opening of the gap (spin gap) at a given temperature. While the gap develops with doping as described, there are family differences, as well. For example, for $YBa_2Cu_3O_{7-\delta}$ the gap is almost closed at optimal doping, while for $La_{2-x}Sr_xCuO_4$ the gap is still sizable at optimal doping. In fact, if one uses ζ, the doping measured with NMR from the charges at planar Cu and O, with $\zeta = n_{Cu} + 2n_O - 1$ [10], this is not surprising as optimally doped $YBa_2Cu_3O_{7-\delta}$ is found to have $\zeta \approx 20\%$, significantly larger than what is typically assumed. Again, this family dependence does not concern the density of states.

The question arises, how planar Cu NMR data relate to this picture. In fact, some of us began collecting and reanalyzing the planar Cu data prior to the planar O data, and accounts have been published [11–13]. For example, it was found that above T_c there must be a *suppression* of the shifts rather than an enhancement of the nuclear relaxation [12] since the Cu shifts vary widely while the Cu relaxation does not (in terms of $1/T_1T$) [13]. This is contrary to what was believed to be the reason for the failure of the Korringa relation between shift and relaxation [2]. With the new planar O analysis, we recognize immediately that the shift suppression is due to the pseudogap, but it does not affect the Cu relaxation. Here we set out to develop a more coherent assessment of all new findings. First, we discuss the overall phenomenology of the magnetic shifts of planar Cu and O. Then, we take a closer look at the assumptions about the hyperfine scenarios and orbital shifts, before we discuss consequences. Thereafter, we turn to the relaxation data, and their explanation in the new scenario.

2. Planar Cu and O Magnetic Shifts

2.1. Overview

We begin with an overview of the experimental shift data, and in order to keep the discussion transparent for the reader we present the bare magnetic shifts that still include, in particular, the van Vleck orbital contribution (the shielding from the core is absent due to shift referencing, for more details see [11]). The data are presented in Fig. 1 and one can draw some apparent, fundamental conclusions: (1) All Cu and O shifts show similar temperature dependences. (2) The range of the temperature dependence for the Cu shifts (panels A and B) is similar for both directions of the magnetic field, about 0.75%. (3) For planar O, the two ranges are different, 0.24% and 0.35% perpendicular and parallel to the σ-bond, respectively (panels C and D). (4) The low temperature shifts for planar Cu are large, 0.3% and 1.3% (supposed to be the orbital shifts), while they play a minor role for planar O.

Based on these observations one is inclined to conclude that one uniform spin susceptibility rules the temperature dependent shifts for both nuclei, and that planar Cu is coupled to the related electronic spin by an *isotropic* hyperfine coupling constant while that for planar O has an anisotropy of about 1.45. Given a partially filled Cu $3d(x^2 - y^2)$ orbital that is σ-bonded with four O $2p$, the above findings are expected for O, but not at all for Cu, for two reasons. First, one expects a large anisotropy for the hyperfine coefficient for spin in the $3d(x^2 - y^2)$ orbital (a factor of at least 6 [14], see also below). Second, the orbital shifts, that follow from this in the low temperature limit, and their anisotropy do not fit this bonding scenario. The hybridization with planar O should result in an orbital shift anisotropy significantly less than 4, the single ion value [14] (see also below). Finally, a closer look at Fig. 1**B** reveals that the planar Cu shifts measured with the B_0 field parallel to the crystal's c-axis ($c \parallel B_0$) show a distinct family dependence that violates the overall view. Some materials seem to have a vanishing shift range for $c \parallel B_0$ ($La_{2-x}Sr_xCuO_4$) while others occupy a different part of the panel (this family dependence is similar to what was found based on the charge sharing in the CuO_2 plane [10]).

Before we continue with a more detailed discussion, we remind the reader of the single spin component picture.
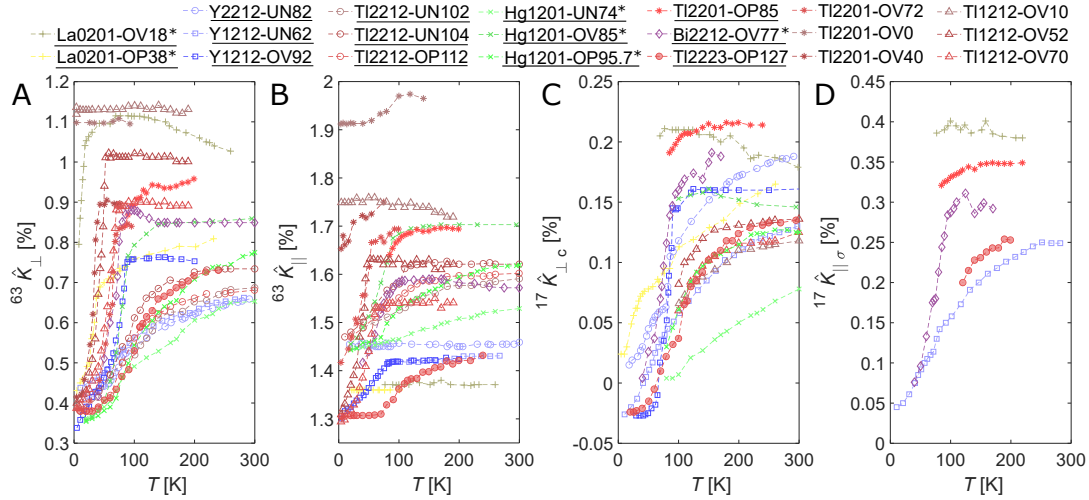
Figure 1. Total magnetic shifts for planar Cu and O as a function of temperature, (A) $^{63}\hat{K}_{\perp}(T)$, (B) $^{63}\hat{K}_{\parallel}(T)$, (C) $^{17}\hat{K}_{\perp c}(T)$, and (D) $^{17}\hat{K}_{\parallel\sigma}(T)$. The vertical axis was adjusted in offset and scale so that the temperature dependences fill about the same space. These are representative data sets of the recently given full accounts [6,11]. The star (*) denotes samples where ^{63}Cu and ^{17}O data had to be taken from different publications and samples (slightly different T_c were reported); an underlined legend entry highlights a material (from [11]) for which oxygen data are available. Note that $^{63}\hat{K}_{\parallel,\perp}$ denotes the planar Cu total magnetic shifts measured with the magnetic field parallel and perpendicular to the crystal c-axis (the in-plane direction is often not known); for planar O the total magnetic shifts are specified for the field direction with respect to the σ-bonding between Cu and O: for $^{17}\hat{K}_{\parallel\sigma}$ the field is along the sigma bond, while for $^{17}\hat{K}_{\perp c}$ the field is perpendicular to the σ-bond and parallel to the crystal c axis; with the field along the σ-axis $^{17}\hat{K}_{\perp a}$ can be measured as a 2nd planar O peak.

2.2. Single Spin Component Picture

In case of a simple electronic spin susceptibility, $\chi(T)$, that leads to a uniform electronic spin component, $\langle S_z \rangle$, in linear response to the applied external magnetic field, B_0, we have,

$$\langle S_z \rangle(T) = \chi(T)\, B_0 / \gamma_e \hbar. \tag{1}$$

And all (non-trivial) spin shifts, $^n K_\theta$, observed at a nucleus, n, for different orientations, θ, of the external magnetic field with respect to the crystal axes must then be proportional to $\langle S_z \rangle$, and thus to each other. The proportionally constants define the hyperfine coefficients, $^n H_\theta$. Note, however, with NMR we measure the total magnetic shift (as given in Fig. 1),

$$^n\hat{K}_\theta(T) = {}^n K_{L\theta} + {}^n H_\theta \cdot \chi(T), \tag{2}$$

where the orbital (chemical) shift term, $^n K_{L\theta}$, follows from the orbital (van Vleck) susceptibility that is expected to be temperature independent (but is very different for different nuclei, reflecting the bonding). The spin shift is given by,

$$^n K_\theta(T) = {}^n H_\theta \cdot \chi(T). \tag{3}$$

Then, if we plot one shift vs. another, for every measured temperature point, T_i, (i.e. $^{n}\hat{K}_{\theta_1}(T_i)$ vs. $^{k}\hat{K}_{\theta_2}(T_i)$), we must observe straight lines with slope $^{k}H_{\theta_1}/^{n}H_{\theta_2}$, with an offset given by the orbital shifts, and with (2) and (3), we get,

$$^{n}\hat{K}_{\theta_1}(T) = \frac{^{n}H_{\theta_1}}{^{k}H_{\theta_2}} \cdot {}^{k}\hat{K}_{\theta_2}(T) + \left[{}^{n}K_{L\theta_1} - \frac{^{n}H_{\theta_1}}{^{k}H_{\theta_2}} \cdot {}^{k}K_{L\theta_2} \right]. \tag{4}$$

2.3. Hyperfine Coefficients and Orbital Shifts

Before we discuss the shifts in more detail, we revisit the assumptions about the hyperfine scenarios and orbital shifts.

First, we address the ^{17}O NMR. Here, one expects from the bonding in the CuO_2 plane a (traceless) dipolar hyperfine tensor, with principle values $c_{dip,\theta}$, and an isotropic term c_{iso}, from the $2p$ and $2s$ orbitals, respectively. The dipolar tensor will have its largest principle value along the σ-bond and it is expected to be symmetric with respect to the other two main axes, and one has for the spin shift,

$$^{17}K_{\theta}(T) = \left[c_{iso} + c_{dip,\theta} \right] \cdot \chi(T) \equiv C_{\theta} \cdot \chi(T). \tag{5}$$

The orbital shifts are expected to be small so that (2) should be well approximated by (5). This is indeed the case [7] and by applying (4) one finds small orbital shifts that coincide with values predicted by first principles [15]. From the slopes one infers hyperfine coefficients that are again in agreement with first principle calculations [7,16].

For planar Cu the situation is more complicated. Early on, one expected a large but negative $^{63}K_{\parallel}$ from spin of the partly filled $3d(x^2 - y^2)$ orbital, as well as a large anisotropy due to the related hyperfine coefficient, $|A_{\perp}| \lesssim |A_{\parallel}|/6$, the sign of $A_{\perp}$ is not known with certainty [14,16]. However, the shifts in Fig. 1 are positive. So it was suggested that a transfer of spin density from the 4 neighboring Cu ions (in a single band picture) could be the reason for a positive hyperfine interaction [17], i.e.,

$$^{63}H_{\parallel,\perp} = A_{\parallel,\perp} + 4B, \tag{6}$$

where B is the related (positive) isotropic constant from transferred spin. With a single spin component one concluded on,

$$^{63}K_{\parallel,\perp}(T) = \left[A_{\parallel,\perp} + 4B \right] \cdot \chi(T). \tag{7}$$

Then, since for $La_{2-x}Sr_xCuO_4$ and $YBa_2Cu_3O_{7-\delta}$ the shifts for $c \parallel B_0$ are temperature independent, the famous accidental cancellation was invoked,

$$A_{\parallel} + 4B \approx 0. \tag{8}$$

In view of Fig. 1**B** this is clearly not applicable for all cuprates, as $^{63}K_{\parallel}(T)$ can be as large as $^{63}K_{\perp}(T)$. The assumption (8) has also consequences for the nuclear relaxation from field fluctuations parallel to the crystal c-axis: only fluctuations near the antiferromagnetic wave vector can contribute. With other words, any relaxation due to fields along the c-axis are interpreted as fluctuations at the antiferromagnetic wave vector even if this is not the case.

If one reflects on this scenario with the data from Fig. 1, one may be inclined to conclude that the hyperfine constant $A_{\parallel}$ must be family dependent, such that $A_{\parallel} \approx -4B$ for $La_{2-x}Sr_xCuO_4$, a slightly more positive value for $YBa_2Cu_3O_{7-\delta}$, and $A_{\parallel} \approx 0$ for other families. These would be very large changes of $A_{\parallel}$ and we dismiss this explanation. Also, one would expect that B should be affected, as well, if $A_{\parallel}$ changes significantly, but Fig. 1 does not support this, neither larger changes of the planar O hyperfine term or Cu nuclear relaxation (see below).

The various expected contributions to the magnetic hyperfine constants were pointed out early on [14,16]. Spin in the unfilled $3d(x^2 - y^2)$ shell will interact with the nucleus through a (anisotropic)

spin-orbit coupling, $a_{so,\theta}$, a (traceless) dipolar term, $a_{dip,\theta}$, and a (isotropic) core polarization of the s-shells, a_{cp}. These various contributions add up to the traditional 'core polarization' term, $A_\theta = a_{so,\theta} + a_{dip,\theta} + a_{cp}$, which is known to be negative for $c \parallel B_0$ and $|A_\parallel|/|A_\perp| \gtrsim 6$ for Cu^{2+} ions [14]. One would also expect that $A_{\parallel,\perp}$ is independent on the materials.

First principle cluster calculations of the hyperfine interaction in $La_{2-x}Sr_xCuO_4$ [16] support the above view. $A_\parallel$ is found to be negative and its magnitude is about 6 times larger than that of $A_\perp$. While $|A_\perp|$ is small, its sign may not be certain (the spin-orbit interaction is not well known and does not follow from the calculations). A large isotropic and positive transferred term B (that depends on the number of Cu atoms in the cluster calculations) is found to have, indeed, a similar size but an opposite sign compared to $A_\parallel$. The following numbers were given (in atomic units) [16]: $a_{so,\parallel} \approx +2.405, a_{so,\perp} \approx +0.427, a_{dip,\parallel} \approx -3.644, a_{dip,\perp} \approx +1.82, a_{cp} \approx -1.78, 4b \approx +2.86$, thus in our nomenclature $A_\parallel \approx -3.02, A_\perp \approx +0.47, 4B = +2.86$ so that $A_\parallel + 4B \approx 0$ ($^{63}H_\parallel \approx -0.16$, $^{63}H_\perp \approx 3.33$).

Another early assumption concerns the orbital shifts for planar Cu. In view of Fig. 1**A** and **B** it was assumed that it is given by the low-temperature shifts (since spin singlet pairing leads to the complete loss of spin shift). As Fig. 1 reveals, however, there is only a common $^{63}K_{L\perp} \approx 0.3\%$ while the low temperature values vary between families for $c \parallel B_0$. While this cannot be excluded, given the family dependent charge sharing between Cu and O [10], the fact that it does not affect $^{63}K_{L\perp}$ is surprising since the orbital shift anisotropy is expected to be given by matrix elements and the overall symmetry, and both orbital shifts should be affected. In fact, first principle calculations for $La_{2-x}Sr_xCuO_4$ do predict the observed orbital shift for $c \perp B_0$, $^{63}K_{L\perp} \approx 0.30\%$. However, for $c \parallel B_0$ the same calculations predict $^{63}K_{L\parallel} \approx 0.72\%$, which is much smaller than what is observed even for $La_{2-x}Sr_xCuO_4$, cf. Fig. 1, where $^{63}K_{L\parallel} \gtrsim 1.3\%$. Also on general grounds, since the single ion orbital shift has an anisotropy of 4, the hybridization with the planar O σ-bond should lead to a much smaller anisotropy (in support of the first-principle calculations [15]).

2.4. Two Spin Components

Before we enter a deeper discussion, we give a few definitions for the uniform response in a two-component picture.

If a single spin susceptibility as in (4) fails to explain the data, it may be useful to introduce another susceptibility. Thus, instead of (1), we have two spin polarizations in the magnetic field, which can have different temperature and doping dependences,

$$\langle S_{1,z}\rangle(T) = \chi_1(T)\, B_0/\gamma_e\hbar \tag{9}$$
$$\langle S_{2,z}\rangle(T) = \chi_2(T)\, B_0/\gamma_e\hbar. \tag{10}$$

For the spin shifts one has instead of (2),

$$^n\hat{K}_\alpha(T) = {}^nK_{L\theta} + {}^nH_{1\theta} \cdot \chi_1(T) + {}^nH_{2\theta} \cdot \chi_2(T), \tag{11}$$

since a nuclear spin couples to the two spin components with different hyperfine constants, $^nH_{j\theta}$, (if the two hyperfine constants were very similar, one would arrive at an effective single component description in (11)). In general, the two spin components in (9) and (10) will have some sort of interaction, so that,

$$\chi_1 = \chi_{11} + \chi_{12} \tag{12}$$
$$\chi_2 = \chi_{22} + \chi_{12}, \tag{13}$$

(note that an antiferromagnetic coupling χ_{12} between the two spins with χ_{11} and χ_{22} could reduce the overall uniform spin response, $\chi_1 + \chi_2 = \chi_{11} + \chi_{22} + 2\chi_{12}$, significantly). We will simplify the
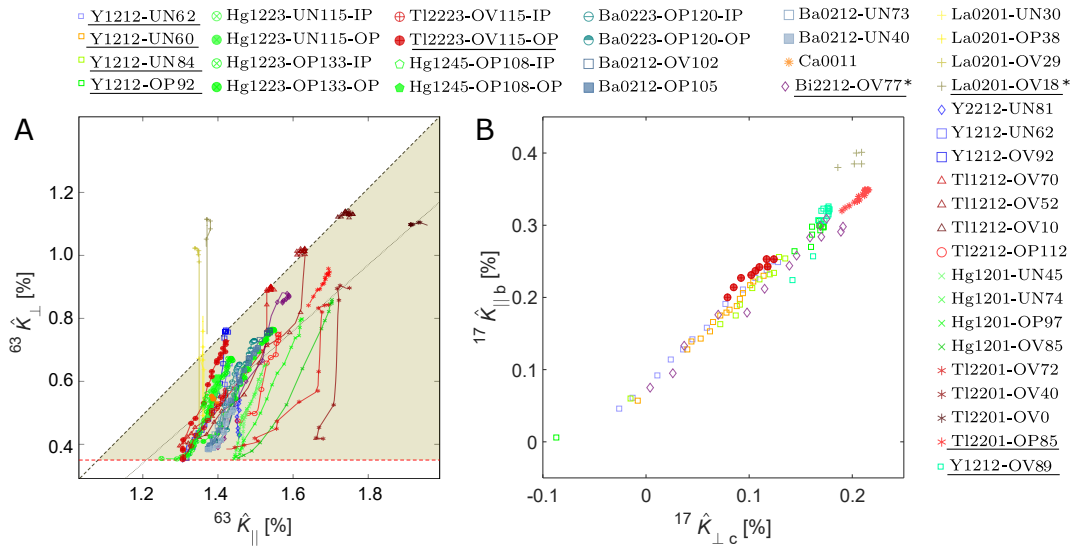
Figure 2. The complex shift anisotropy of planar Cu (A) is contrasted with the simple behavior found for planar O (B). The plot in (A) is adapted from Ref. [11] that also discusses the salient features. For example, 3 different segments of slopes seem to be necessary to explain the data. The steep slope is assumed by, e.g. $La_{2-x}Sr_xCuO_4$ but also other materials in certain ranges of temperature; the "isotropic shift lines" (grey lines) have slope 1, i.e., both shifts change by the same amount as function of doping or temperature; finally, the slope 2.5 is assumed for a number of materials (only as a function of doping, not temperature). All ^{63}Cu shifts for $c \perp B_0$ have similar low T shift values not far from 0.30% calculated by first principles [15], however, the same calculations predict 0.72% for $c \parallel B_0$, very different from what the experiments seem to show in (A). The planar O anisotropy is simple and the deduced small orbital shifts have been calculated, as well [15], and a simple anisotropic hyperfine coefficient explains the data (it is also in very good agreement with first principle calculations [16]).

nomenclature with the definitions: $a \equiv \chi_{11}$, $b \equiv \chi_{22}$, $c \equiv \chi_{12}$ (as used before [12]). Then we have with (11) the following formal expression for the (total) magnetic shift observed at a nucleus (n),

$$^n\hat{K}_\theta(T) = {}^nK_{L\theta} + {}^nH_{1\theta} \cdot [a(T) + c(T)] + {}^nH_{2\theta} \cdot [b(T) + c(T)]. \qquad (14)$$

2.5. Discussion of Cu and O Shifts

The planar O data, at all doping levels, are in agreement with a single spin component from a metallic density of states with a temperature independent pseudogap at the Fermi surface. The experimentally determined orbital shifts and hyperfine coefficients are in accord with first principles calculations [6,7,15,16]. Despite this convincing, simple picture, we should point out that there is scatter between different systems above as well as below T_c, cf. Fig. 2**B** and the discussion in [7]. As pointed out previously [6,18], a spatial distribution of the planar O hole content, n_O, that is often observed as NMR quadrupolar linewidth may cause a spatial variation of the pseudogap. In such a case the temperature dependence of the shift can change significantly as smaller gaps dominate at lower temperature. This fact, and the notorious consequences of the ^{17}O isotope exchange harbor not well understood errors. Nevertheless, there is no obvious family dependence in terms of the temperature dependence of the shift, while the size of the pseudogap determined from fitting the planar O relaxation does depend on the materials to some extent [6].

The situation is very different for the planar Cu shifts. In view of Fig. 1 one is inclined to conclude, as remarked above, that the planar Cu shifts appear to be dominated by an *isotropic* hyperfine coefficient and a spin susceptibility with the temperature independent pseudogap that reigns the planar O data.

The ranges of the shifts for both directions of the field are similar, $\Delta^{63}K_{\parallel,\perp}(T) \sim 0.75\%$, despite spin in the $3d(x^2 - y^2)$, which should lead to a large shift anisotropy that is not found at all. A closer look reveals that there is a peculiar family dependence for $c \parallel B_0$: $La_{2-x}Sr_xCuO_4$ has the smallest and temperature independent shift, $YBa_2Cu_3O_{7-\delta}$ ranges a bit higher and has a slight temperature dependence, while other materials fill in the larger shift range, also with large temperature dependences. This family dependence bears similarities to that of how the inherent hole is shared between Cu (n_{Cu}) and O (n_O), and how doped holes enter the CuO_2 plane ($\Delta n_{Cu}/\Delta n_O$) [10]. We argued above that this cannot be caused by changes in $A_{\parallel}$. Consequently, an interplay between (at least) two spin components has to be considered.

In fact, if we take both Cu shifts in Fig. 1 and plot them against each other, cf. Fig. 2**A**, we do not observe a straight line as expected from (4) and seen in Fig. 2**B** for planar O [7]. Rather, for Cu we find three different slopes as a function of temperature and/or doping, as was pointed out with the original shift collection [11],

$$\kappa_1 \approx \gtrsim 10, \quad \kappa_2 \approx 1, \quad \kappa_3 \approx 2.5, \text{ with}$$
$$\kappa_n = \Delta^{63}_{x,T}K_{\perp}(T)/\Delta^{63}_{x,T}K_{\parallel}(T). \tag{15}$$

Note that this behavior also argues for spin effects as cause for the shift anisotropy since the three different slopes would require 3 different ratios of hyperfine coefficients in certain ranges of temperature or doping.

Finally, there is the orbital shift conundrum which suggests that the old hyperfine scenario fails, and some of us suggested this can be solved by a negative spin polarization of the $3d(x^2 - y^2)$ orbital (due to exchange with a second, positive component likely residing on planar O) [11,12]. In principle, orbital currents [19] could represent or contribute to this shift. Since we see no clear scenario for this, we discuss the missing shift in terms of spin shift for the time being. That is, we set out to analyze the spin shifts in terms of (14),

$$^{63}K_{\theta}(T) = A_{\theta} \cdot [a(T) + c(T)] + 4B \cdot [b(T) + c(T)], \tag{16}$$
$$^{17}K_{\theta}(T) = C_{\theta} \cdot [b(T) + c(T)]. \tag{17}$$

While we can view the above equations as the defining equations for the hyperfine coefficients, information about them can be drawn from Fig. 1. Since $^{63}K_{\perp}(T)$ is similar to $^{17}K_{\theta}(T)$, one concludes that $|A_{\perp}|$ must be small compared to $|A_{\parallel}|$ and $4B$ (the transferred hyperfine coefficient should be isotropic). Note that such $A_{\parallel,\perp}$ is expected from an unfilled $3d(x^2 - y^2)$ orbital. Thus, the choice above is reasonable.

With all planar O shifts and $^{63}K_{\perp}$ disappearing at low temperatures, $(b + c)$ approaches zero at low temperature: $(b_0 + c_0) = 0$. Furthermore, $^{63}K_{\parallel}(T \to 0) = A_{\parallel}(a_0 + c_0) \sim 0.6\%$ for a few systems and perhaps a bit larger for some other systems, cf. Fig. 1, while the high temperature value of this contribution is given by $A_{\parallel}(a + c) \sim 0.3\%$, as one infers from the intersection of the high-temperature slope $\kappa_2 \approx 1$ with the abscissa(cf. 2, **A**), $^{63}\hat{K}_{\perp} \approx 0.3\%$. Thus, $(a + c)$ grows more negative as the temperature is lowered, quite different from $(b + c)$ that vanishes at low temperatures. Some of us argued before [12,20] about plausible assumptions with regard to (16) and (17): $\kappa_2 = 1$ would result from a variation of b only, and a large slope (κ_1) results if $4B/(A_{\parallel} + 4B)$ is large. A variation of a only would result in a very small slope, observed for just one system at very low temperatures, cf. Fig. 2**A**. Finally, the slope of $\kappa_3 = 2.5$ must involve more than one component.

Since first principle calculations support that $|A_{\parallel}| \sim 4B$, we will adopt this to approximate the Cu shifts by (16) and (17),

$$^{63}K_{\parallel}(T) \approx 4B \cdot [b - a] \tag{18}$$
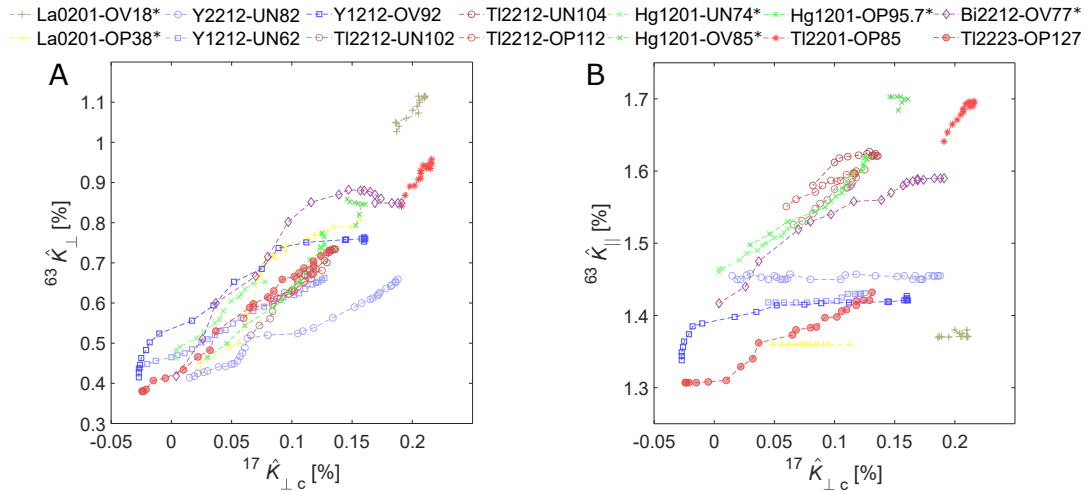$$^{63}K_{\perp}(T) \approx 4B \cdot [b + c], \tag{19}$$

Figure 3. ^{63}Cu and ^{17}O shift plotted against each other. (A), $^{63}\hat{K}_\perp$ vs. $^{17}\hat{K}_{\perp c}$, and (B), $^{63}\hat{K}_\parallel$ vs. $^{17}\hat{K}_{\perp c}$. The differences between the two plots are in agreement with Fig. 2. Note that such plots were invoked for to prove the single fluid picture, early on, as well as its failure more recently (see main text for deeper discussion). The star (*) denotes samples where ^{63}Cu and ^{17}O data had to be taken from different publications and samples (slightly different T_c were reported)

and we note that since c is missing in (18) its variation could be at the root of the interesting behavior of the shift anisotropy in Fig. 2**A**. Unfortunately, one has three variables to explain the shifts in a two-dimensional plot.

Finally, we notice that since $^{63}K_\perp(T)$ and $^{17}K_\theta(T)$ are functions of $[b + c]$ only, a plot of the two shifts with respect to each other should result in a straight line with a slope given by $4B/C \approx 3.0$, if one uses the the calculated hyperfine coefficients [16]. This plot is shown in Fig. 3**A**, and holds a surprise. First of all, there is no well defined slope, rather, the temperature dependences appear somewhat erratic and lie between the two slopes of $4B/C \approx 2.0$ to 3.9. Note that the plot in panel **B** does not hold new information if one considers the plot in Fig. 2**A**, it is only shown for completeness. We must conclude that (16) and (17) only describe the situation on average. We cannot offer a clear explanation, but we would like to point to a few thoughts. In view of the behavior of planar O, cf. Fig. 2**B** (cf. also discussion in [7]), the uncertainty in the planar O shift cannot explain the observation. For planar Cu the linewidths can be very large, but even there we do not find a dependence that points to an uncertainty in the determination of the average shift (or its meaning). Note that $^{63}K_\perp$ follows after the subtraction of the material dependent quadrupole shift (in 2nd order) that may harbor unexpected errors, but the agreement with regard to the orbital shift, as well as the clear behavior in terms of only a few slopes in Fig. 2**A** argue against this. Note that an overall change in spin density between O and Cu as a function of temperature could explain the finding, and we do know that the intra unit cell charger ordering seen with NMR [21] can respond to temperature, but there is no evidence for a large change in the magnetic shift [21]. However, such short range variations can lead to a different shift for Cu than for O (similar to the argument for charge ordering [22]). Obvious differences between Cu and O arise from the two spin components. Apparently, planar O is not significantly affected by the Cu $3d(x^2 - y^2)$ spin, only in terms of the description in terms of $(b + c)$, i.e. the coupling to it. Perhaps, the close proximity of both component on Cu do not follow such a simple description in detail (e.g. slight changes in the transferred coupling).

It is important to remember, that such plots have been used, many years ago, to prove the so-called single fluid picture for $YBa_2Cu_3O_{6.63}$ [23] and $YBa_2Cu_4O_8$ [24]. For both systems the dependences in Fig. 3 may be taken as such, but in view of the dependences for other families, this conclusion cannot be taken as rigorous proof for all cuprates. Also, we now understand why similar plots for other

systems, $La_{2-x}Sr_xCuO_4$ [3] and $HgBa_2CuO_{4+\delta}$ [4,5], led to the opposite conclusion. We believe the latter still holds in view of the data, but the shift anisotropies in Fig. 2 may be even more convincing.

3. Planar Cu and O Nuclear Relaxation

We pointed to the main facts about the Cu and O relaxation above, details have been published [6,12,13,20]. The planar O relaxation of all cuprates follows from a density of states that is common to all cuprates and a doping dependent gap, the relaxation anisotropy is in agreement with the simple hyperfine scenario (5), as well. With the magnetic field along the σ-bond we have $1/T_{1\|\sigma}T \approx 0.23$ /Ks and this relates to a $^{17}K_{\perp c} \approx 0.2\%$, i.e. the Korringa relation holds as for a simple metal. For planar Cu the situation is quite different, yet also simple. The Cu relaxation rates *do not* show pseudogap behavior at all. But the planar Cu relaxation rate just above T_c is common to all cuprates, in the sense that $1/T_{1\perp}T_c \approx 21$ /Ks (i.e. if measured with the field B_0 in the CuO_2 plane). $La_{2-x}Sr_xCuO_4$ is an outlier as its relaxation rate is about 3 times larger (60 /Ks). However, all cuprates have a temperature independent relaxation anisotropy (above and below T_c) and it varies between about 1.0 for some highly doped materials and about 3.4 for the $YBa_2Cu_3O_{7-\delta}$ family ($La_{2-x}Sr_xCuO_4$ has an anisotropy of about 2.4). Thus, the nuclear Cu spins are coupled by an anisotropic interaction to a metallic bath with a fixed density of states, as well (but no pseudogap). Importantly, below T_c all relaxation rates behave very similar in terms of T/T_c, as in the classical case (yet without a coherence peak) [13]. In fact, the planar Cu relaxation rate shows the sudden condensation at T_c very clearly, different from Cu shifts and planar O shift and relaxation since these are all dominated by the pseudogap.

A model for the planar Cu relaxation was discussed recently [20] assuming two spin components α and β that contribute to the fluctuating field at the Cu nucleus ($A_{\|,\perp} \cdot \alpha$ and $4B \cdot \beta$ with $A_\| = -4B$ and $f = |A_\perp/A_\||$). It was found that if both components are fully correlated, $\langle \alpha \cdot \beta \rangle = +1$ and $\langle \beta \cdot \beta \rangle = +1$, one can fit the planar Cu relaxation data and its anisotropy by varying $4\beta/\alpha$ from about 0.2 to 0.4. This means, a dominating spin component α that is correlated with the neighboring components β can account for the observed relaxation and its anisotropy. Note that a normalized relaxation rate of $1/T_{1\perp}T = 20$ /Ks gives a planar Cu shift of about 0.89% if one invokes the Korringa relation. This is approximately the shift range of planar Cu.

Finally, we note that an antiferromagnetic coupling between two α components on adjacent Cu atoms frustrates the correlated spin β, unless they overcome the effective exchange coupling. This mechanism could be behind the observed pseudogap from the metallic density of states, and may not influence the planar Cu relaxation beyond a change in anisotropy.

4. Conclusions

To conclude, the recent collection of all available planar O shift and relaxation data [6] uncovered compelling arguments in favor of a simple metallic density of states with a temperature independent pseudogap set by doping. Even the anisotropies of O shift and relaxation [7] support this simple view. The density of states outside the gap is common to all cuprates (independent on the size of the gap) and gives a metallic shift from the Korringa relation that is indeed observed. This raised the question of how this spin susceptibility relates to the phenomenology of the planar Cu data that had been published previously [11–13,20]. By comparing both sets of data we conclude that the planar Cu shifts are dominated by the same pseudogap, in particular, the earlier postulated suppression of the planar Cu shifts is a result of this pseudogap [12]. However, there is a significant family dependence for the Cu shifts for one direction of the field ($c \parallel B_0$), so that this pseudogap feature can disappear for this direction of the field. As before, we endorse the conclusion that it is the action of a second spin component, likely from the spin in the $3d(x^2 - y^2)$ Cu orbital, that is behind the complicated and family dependent planar Cu shift anisotropy. While the consequences of the pseudogap are obvious already in the bare Cu shifts, there is a quantitative difference between O and Cu that seems to be outside the expected uncertainties. It also carries a family dependence and explains why one can conclude on a single component picture for some systems, but not for other. Striking is still the observation of a

doping and family independent metallic planar Cu relaxation that does not show a pseudogap at all [12,13]. One would argue that this must be related to the metallic density of states observed for planar O, perhaps as a result of antiferromagnetic coupling of the planar Cu spins, as argued before [20].

Author contribution

JH had the overall project leadership and introduced the main concepts together with MA. JN led the O data collection and the overall presentation of the data in the manuscript. ST contributed to the preparation of the manuscript. All authors were involved in discussions and in preparing the manuscript.

Conflict of interest

The authors declare no conflict of interest.

References

1. Bednorz, J.G.; Müller, K.A. Possible High T_c Superconductivity in the Ba-La-Cu-O System. *Z. Phys. B Condens. Matter* **1986**, *193*, 189–193. doi:10.1007/BF01303701.

2. Slichter, C.P. Magnetic Resonance Studies of High Temperature Superconductors. In *Handbook of High-Temperature Superconductivity*; Schrieffer, J.R.; Brooks, J.S., Eds.; Springer: New York, 2007; pp. 215–256. doi:10.1007/978-0-387-68734-6_5.

3. Haase, J.; Slichter, C.P.; Williams, G.V.M. Evidence for two electronic components in high-temperature superconductivity from NMR. *J. Phys. Condens. Matter* **2009**, *21*, 455702. doi:10.1088/0953-8984/21/45/455702.

4. Haase, J.; Rybicki, D.; Slichter, C.P.; Greven, M.; Yu, G.; Li, Y.; Zhao, X. Two-component uniform spin susceptibility of superconducting $HgBa_2CuO_{4+\delta}$ single crystals measured using ^{63}Cu and ^{199}Hg nuclear magnetic resonance. *Phys. Rev. B* **2012**, *85*, 104517. doi:10.1103/PhysRevB.85.104517.

5. Rybicki, D.; Kohlrautz, J.; Haase, J.; Greven, M.; Zhao, X.; Chan, M.K.; Dorow, C.J.; Veit, M.J. Electronic spin susceptibilities and superconductivity in $HgBa_2CuO_{4+\delta}$ from nuclear magnetic resonance. *Phys. Rev. B* **2015**, *92*, 081115. doi:10.1103/PhysRevB.92.081115.

6. Nachtigal, J.; Avramovska, M.; Erb, A.; Pavićević, D.; Guehne, R.; Haase, J. Temperature-Independent Cuprate Pseudogap from Planar Oxygen NMR. *Condens. Matter* **2020**, *5*, 66–19. doi:10.3390/condmat5040066.

7. Avramovska, M.; Nachtigal, J.; Haase, J. Temperature independent pseudogap from ^{17}O and ^{89}Y NMR and the single component picture. *arXiv* **2021**. doi:arXiv: 2112.10595.

8. Loram, J.W.; Mirza, K.A.; Cooper, J.R.; Tallon, J.L. SPECIFIC HEAT EVIDENCE ON THE NORMAL STATE PSEUDOGAP. *J. Phys. Chem. Solids* **1998**, *59*, 2091–2094. doi:10.1016/s0022-3697(00)00101-3.

9. Tallon, J.L.; Loram, J.W. Field-dependent specific heat of the canonical underdoped cuprate superconductor $YBa_2Cu_4O_8$. *Sci. Rep.* **2020**, *10*, 22288. doi:10.1038/s41598-020-79017-3.

10. Jurkutat, M.; Rybicki, D.; Sushkov, O.P.; Williams, G.V.M.; Erb, A.; Haase, J. Distribution of electrons and holes in cuprate superconductors as determined from ^{17}O and ^{63}Cu nuclear magnetic resonance. *Phys. Rev. B* **2014**, *90*, 140504. doi:10.1103/PhysRevB.90.140504.

11. Haase, J.; Jurkutat, M.; Kohlrautz, J. Contrasting Phenomenology of NMR Shifts in Cuprate Superconductors. *Condens. Matter* **2017**, *2*, 16. doi:10.3390/condmat2020016.

12. Avramovska, M.; Pavićević, D.; Haase, J. Properties of the Electronic Fluid of Superconducting Cuprates from ^{63}Cu NMR Shift and Relaxation. *J. Supercond. Nov. Magn.* **2019**, *32*, 3761–3771. doi:10.1007/s10948-019-05174-w.

13. Jurkutat, M.; Avramovska, M.; Williams, G.V.M.; Dernbach, D.; Pavićević, D.; Haase, J. Phenomenology of ^{63}Cu Nuclear Relaxation in Cuprate Superconductors. *J. Supercond. Nov. Magn.* **2019**, *155*, 629–8. doi:10.3390/condmat4030067.

14. Pennington, C.H.; Durand, D.J.; Slichter, C.P.; Rice, J.P.; Bukowski, E.D.; Ginsberg, D.M. Static and dynamic Cu NMR tensors of YBa$_2$Cu$_3$O$_{7-\delta}$. *Phys. Rev. B* **1989**, *39*, 2902–2905. doi:10.1103/PhysRevB.39.2902.

15. Renold, S.; Heine, T.; Weber, J.; Meier, P.F. Nuclear magnetic resonance chemical shifts and paramagnetic field modifications in *La$_2$CuO$_4$*. *Phys. Rev. B* **2003**, *67*, 24501. doi:10.1103/PhysRevB.67.024501.

16. Hüsser, P.; Suter, H.U.; Stoll, E.P.; Meier, P.F. First-principles calculations of hyperfine interactions in La$_2$CuO$_4$. *Phys. Rev. B* **2000**, *61*, 1567–1579. doi:10.1103/PhysRevB.61.1567.

17. Mila, F.; Rice, T.M. Analysis of magnetic resonance experiments in YBa$_2$Cu$_3$O$_7$. *Phys. C: Supercond.* **1989**, *157*, 561–570. doi:10.1016/0921-4534(89)90286-4.

18. Pavićević, D.; Avramovska, M.; Haase, J. Unconventional ^{17}O and ^{63}Cu NMR shift components in cuprate superconductors. *Mod. Phys. Lett. B* **2020**, *34*, 2040047–17. doi:10.1142/S0217984920400473.

19. Varma, C.M. Theory of the pseudogap state of the cuprates. *Phys. Rev. B* **2006**, *73*, 155113–155117.

20. Avramovska, M.; Pavićević, D.; Haase, J. NMR Shift and Relaxation and the Electronic Spin of Superconducting Cuprates. *J. Supercond. Nov. Magn.* **2020**, *33*, 2621–2628. doi:10.1007/s10948-020-05498-y.

21. Reichardt, S.; Jurkutat, M.; Guehne, R.; Kohlrautz, J.; Erb, A.; Haase, J. Bulk Charge Ordering in the CuO$_2$ Plane of the Cuprate Superconductor YBa$_2$Cu$_3$O$_{6.9}$ by High-Pressure NMR. *Condens. Matter* **2018**, *3*, 23. doi:10.3390/condmat3030023.

22. Haase, J. Charge density variation in YBa$_2$Cu$_3$O$_{6+y}$. *Phys. Rev. Lett.* **2003**, *91*, 189701. doi:10.1103/PhysRevLett.91.189701.

23. Takigawa, M.; Reyes, A.P.; Hammel, P.C.; Thompson, J.D.; Heffner, R.H.; Fisk, Z.; Ott, K.C. Cu and O NMR studies of the magnetic properties of YBa$_2$Cu$_3$O$_{6.63}$ (T_c=62 K). *Phys. Rev. B* **1991**, *43*, 247–257. doi:10.1103/PhysRevB.43.247.

24. Bankay, M.; Mali, M.; Roos, J.; Brinkmann, D. Single-spin fluid, spin gap, and d-wave pairing in YBa$_2$Cu$_4$O$_8$: A NMR and NQR study. *Phys. Rev. B* **1994**, *50*, 6416–6425. doi:10.1103/PhysRevB.50.6416.

Chapter 5

Conclusion

In this cumulative thesis, I presented six publications, which together form the genesis of a complete phenomenology of Cu and O NMR shift and relaxation data of high-temperature superconducting cuprates. From looking at the cuprate NMR data in its entirety, across all families and doping, we reached conclusions that would otherwise remain elusive by focusing on one material only.

The salient features of this phenomenology are as follows: the Cu shift data revealed that most of the cuprate families do not behave according to the old hyperfine scenario, and that there is a need to introduce a second spin component to explain the data. The Cu relaxation data, on the other hand, showed a ubiquitous Fermi-liquid like relaxation common to all the cuprates, irrespective of doping and material, while showing no signature of the pseudogap. Furthermore, we established that since the nuclear relaxation is similar for all the cuprates, a suppression of the Cu shifts is behind the failure of the Korringa relation, and not an enhancement of the relaxation as assumed earlier.

The planar O data in their totality show a simpler scenario. We found that the high-temperature slopes of the nuclear relaxation with respect to temperature are doping-independent and point to a temperature-independent pseudogap that opens at the Fermi surface and causes a loss of low-energy states. The states above the pseudogap are metal-like and ubiquitous to all the cuprates. The magnetic hyperfine coefficients seem to be in agreement with theoretical predictions from first principle

calculations and the shift and relaxation anisotropies point to a simple explanation using a single-spin component scenario.

From this recent inspection of O data, we could conclude that the temperature-independent pseudogap is behind the suppression of the Cu shifts—only for one direction of the magnetic field—and there is a significant family dependence in the Cu shifts for $c \parallel B_0$ direction. This is strongly reminiscent of the family dependent way in which Cu and O share the charges in the CuO_2 plane. It is quite striking that Cu relaxation remains unaffected by the pseudogap and is metallic-like.

Our model is an attempt to form a coherent picture of the cuprates based on all these observations. Nevertheless, reconciling these findings has been like completing a puzzle with some pieces still missing. It took roughly seven years after the discovery that NMR could measure the total charge and the dependence of maximum T_c on the O hole content, [Jurkutat et al., 2014], [Rybicki et al., 2016], for these findings to be substantiated by theoretical predictions, [Kowalski et al., 2021]. It is still not clear what the consequences for NMR shift and relaxation are, and whether the similarities in the family dependence of the Cu $c \parallel B_0$ shifts and the charge sharing between Cu and O are somehow related. A more detailed consideration of this was done in [Haase, 2022]. The behavior of the Cu NMR linewidths also does not support a single component view. However, it is not yet understood how the Cu and O NMR linewidths fit into our new scenario.

The fact that theoretical predictions, ascribing superconductivity to superexchange, [Kowalski et al., 2021], are in agreement with experiments, [Rybicki et al., 2016], [Ruan et al., 2016], [O'Mahony et al., 2022], is an immense step forward towards understanding the cuprates. We can only hope that our newly established phenomenology of the NMR data presents a solid groundwork that theorists can build upon.

Bibliography

[Abragam, 1961] Abragam, A. (1961). *The principles of nuclear magnetism.* Number 32. Oxford university press.

[Alloul et al., 1989] Alloul, H., Ohno, T., and Mendels, P. (1989). ^{89}Y NMR evidence for a Fermi-liquid behavior in $YBa_2Cu_3O_{6+x}$. *Phys. Rev. Lett.*, 63:1700.

[Avramovska et al., 2022a] Avramovska, M., Nachtigal, J., and Haase, J. (2022a). ^{17}O and ^{89} Y NMR Shift and Relaxation and the Temperature-Independent Pseudogap of the Cuprates. *J. Supercond. Nov. Magn.*, pages 1–7.

[Avramovska et al., 2022b] Avramovska, M., Nachtigal, J., Tsankov, S., and Haase, J. (2022b). Planar Cu and O NMR and the Pseudogap of Cuprate Superconductors. *Condens. Matter*, 7(1).

[Avramovska et al., 2019] Avramovska, M., Pavićević, D., and Haase, J. (2019). Properties of the Electronic Fluid of Superconducting Cuprates from ^{63}Cu NMR Shift and Relaxation. *J. Supercond. Nov. Magn.*, 243(3):337.

[Avramovska et al., 2020] Avramovska, M., Pavićević, D., and Haase, J. (2020). NMR Shift and Relaxation and the Electronic Spin of Superconducting Cuprates. *J. Supercond. Nov. Magn.*, 113(2):1504–8.

[Bardeen et al., 1957] Bardeen, J., Cooper, L. N., and Schrieffer, J. R. (1957). Microscopic theory of superconductivity. *Phys. Rev.*, 106:162.

[Bednorz and Müller, 1986] Bednorz, J. G. and Müller, K. A. (1986). Possible high Tc superconductivity in the Ba-La-Cu-O system. *Z. Phys. B Condens. Matter*, 193:189–193.

[Cava, 2000] Cava, R. J. (2000). Oxide superconductors. *J. Am. Ceram. Soc.*, 83(1):5–28.

[de Bruyn Ouboter, 1987] de Bruyn Ouboter, R. (1987). Superconductivity: Discoveries during the early years of low temperature research at Leiden 1908-1914. *IEEE Transactions on magnetics*, 23(2):355–370.

[Englman and Englman, 1972] Englman, R. and Englman, R. (1972). *The Jahn-Teller effect in molecules and crystals*. John Wiley & Sons.

[Gao et al., 1994] Gao, L., Xue, Y. Y., Chen, F., Xiong, Q., Meng, R. L., Ramirez, D., Chu, C. W., Eggert, J. H., and Mao, H. K. (1994). Superconductivity up to 164 K in $HgBa_2Ca_{m-1}Cu_mO_{2m+2+\delta}$ under quasihydrostatic pressures. *Phys. Rev. B*, 50(6):4260.

[Gavaler, 1973] Gavaler, J. (1973). Superconductivity in Nb–Ge films above 22 K. *Appl. Phys. Lett.*, 23(8):480–482.

[Gugenberger et al., 1994] Gugenberger, F., Meingast, C., Roth, G., Grube, K., Breit, V., Weber, T., Wühl, H., Uchida, S., and Nakamura, Y. (1994). Uniaxial pressure dependence of T c from high-resolution dilatometry of untwinned $La_{2-x}Sr_xCuO_4$ single crystals. *Phys. Rev. B*, 49(18):13137.

[Haase, 2022] Haase, J. (2022). A different NMR view of cuprate superconductors. *J. Supercond. Nov. Magn.*, pages 1–8.

[Haase et al., 2017] Haase, J., Jurkutat, M., and Kohlrautz, J. (2017). Contrasting Phenomenology of NMR Shifts in Cuprate Superconductors. *Condens. Matter*, 2(2):16.

[Haase et al., 2009] Haase, J., Slichter, C. P., and Williams, G. V. M. (2009). Evidence for two electronic components in high-temperature superconductivity from NMR. *J. Phys. Condens. Matter*, 21:455702.

[Haase et al., 2004] Haase, J., Sushkov, O. P., Horsch, P., and Williams, G. V. M. (2004). Planar Cu and O hole densities in high-T_c cuprates determined with NMR. *Phys. Rev. B*, 69:94504.

[Harris et al., 2008] Harris, R. K., Becker, E. D., De Menezes, S. M. C., Granger, P., Hoffman, R. E., and Zilm, K. W. (2008). Further conventions for NMR shielding and chemical shifts (IUPAC recommendations 2008) (Reprinted from Pure Appl. Chem., vol 80, pg 59, 2008). *Magn. Reson. Chem.*, 46(6):582–598.

[Hebel and Slichter, 1959] Hebel, L. C. and Slichter, C. P. (1959). Nuclear Spin Relaxation in Normal and Superconducting Aluminum. *Phys. Rev.*, 113:1504–1519.

[Heitler and Teller, 1936] Heitler, W. and Teller, E. (1936). Time Effects in the Magnetic Cooling Method-I. *Proc. R. Soc. A Math. Phys. Eng. Sci.*, 155:629–639.

[Hüsser et al., 2000] Hüsser, P., Suter, H., Stoll, E., and Meier, P. (2000). First-principles calculations of hyperfine interactions in la 2 cuo 4. *Phys. Rev. B*, 61(2):1567.

[Jurkutat et al., 2019] Jurkutat, M., Avramovska, M., Williams, G. V. M., Dernbach, D., Pavićević, D., and Haase, J. (2019). Phenomenology of ^{63}Cu Nuclear Relaxation in Cuprate Superconductors. *J. Supercond. Nov. Magn.*, 155(12):629–8.

[Jurkutat et al., 2021] Jurkutat, M., Kattinger, C., Tsankov, S., Reznicek, R., Erb, A., and Haase, J. (2021). How pressure enhances the critical temperature for high temperature superconductivity in YBa$_2$Cu$_3$ O$_{6+y}$. *arXiv preprint arXiv:2109.10157*.

[Jurkutat et al., 2014] Jurkutat, M., Rybicki, D., Sushkov, O. P., Williams, G. V. M., Erb, A., and Haase, J. (2014). Distribution of electrons and holes in

cuprate superconductors as determined from ^{17}O and ^{63}Cu nuclear magnetic resonance. *Phys. Rev. B*, 90:140504.

[Knight, 1949] Knight, W. (1949). Nuclear Magnetic Resonance Shift in Metals. *Phys. Rev.*, 76(8):1259–1260.

[Kong et al., 2021] Kong, P., Minkov, V. S., Kuzovnikov, M. A., Drozdov, A. P., Besedin, S. P., Mozaffari, S., Balicas, L., Balakirev, F. F., Prakapenka, V. B., Chariton, S., et al. (2021). Superconductivity up to 243 K in the yttrium-hydrogen system under high pressure. *Nature Comm.*, 12(1):1–9.

[Korringa, 1950] Korringa, J. (1950). Nuclear magnetic relaxation and resonnance line shift in metals. *Physica*, 16:601–610.

[Kowalski et al., 2021] Kowalski, N., Dash, S. S., Sémon, P., Sénéchal, D., and Tremblay, A.-M. (2021). Oxygen hole content, charge-transfer gap, covalency, and cuprate superconductivity. *PNAS*, 118(40).

[Levitt, 2013] Levitt, M. H. (2013). *Spin dynamics: basics of nuclear magnetic resonance.* John Wiley & Sons.

[Li et al., 2022] Li, Z., He, X., Zhang, C., Wang, X., Zhang, S., Jia, Y., Feng, S., Lu, K., Zhao, J., Zhang, J., et al. (2022). Superconductivity above 200 K discovered in superhydrides of calcium. *Nat. Commun.*, 13(1):1–5.

[Loram et al., 1998] Loram, J. W., Mirza, K. A., Cooper, J. R., and Tallon, J. L. (1998). SPECIFIC HEAT EVIDENCE ON THE NORMAL STATE PSEUDO-GAP. *J. Phys. Chem. Solids*, 59(10-12):2091–2094.

[Masuda and Redfield, 1962] Masuda, Y. and Redfield, A. G. (1962). Nuclear Spin-Lattice Relaxation in Superconducting Aluminum. *Phys. Rev.*, 125:159–163.

[Mila and Rice, 1989] Mila, F. and Rice, T. M. (1989). Analysis of magnetic resonance experiments in YBa$_2$Cu$_3$O$_7$. *Phys. C: Supercond.*, 157(3):561–570.

[Nachtigal et al., 2020] Nachtigal, J., Avramovska, M., Erb, A., Pavićević, D., Guehne, R., and Haase, J. (2020). Temperature-Independent Cuprate Pseudogap from Planar Oxygen NMR. *Condens. Matter*, 5(4):66–19.

[Onnes, 1911] Onnes, H. (1911). The superconductivity of mercury. *Comm. Phys. Lab. Univ. Leiden*, 122:122–124.

[O'Mahony et al., 2022] O'Mahony, S. M., Ren, W., Chen, W., Chong, Y. X., Liu, X., Eisaki, H., Uchida, S., Hamidian, M. H., and Davis, J. C. S. (2022). On the electron pairing mechanism of copper-oxide high temperature superconductivity. *PNAS*, 119(37):e2207449119.

[Pennington et al., 1989] Pennington, C. H., Durand, D. J., Slichter, C. P., Rice, J. P., Bukowski, E. D., and Ginsberg, D. M. (1989). Static and dynamic Cu NMR tensors of $YBa_2Cu_3O_{7-\delta}$. *Phys. Rev. B*, 39:2902–2905.

[Pickett, 1989] Pickett, W. E. (1989). Electronic structure of the high-temperature oxide superconductors. *Rev. Mod. Phys.*, 61(2):433.

[Renold et al., 2003] Renold, S., Heine, T., Weber, J., and Meier, P. F. (2003). Nuclear magnetic resonance chemical shifts and paramagnetic field modifications in La_2CuO_4. *Phys. Rev. B*, 67(2):24501.

[Ruan et al., 2016] Ruan, W., Hu, C., Zhao, J., Cai, P., Peng, Y., Ye, C., Yu, R., Li, X., Hao, Z., Jin, C., et al. (2016). Relationship between the parent charge transfer gap and maximum transition temperature in cuprates. *Sci. Bull.*, 61(23):1826–1832.

[Rybicki et al., 2016] Rybicki, D., Jurkutat, M., Reichardt, S., Kapusta, C., and Haase, J. (2016). Perspective on the phase diagram of cuprate high-temperature superconductors. *Nat. Commun.*, 7:1–6.

[Rybicki et al., 2015] Rybicki, D., Kohlrautz, J., Haase, J., Greven, M., Zhao, X., Chan, M. K., Dorow, C. J., and Veit, M. J. (2015). Electronic spin susceptibilities

and superconductivity in $HgBa_2CuO_{4+\delta}$ from nuclear magnetic resonance. *Phys. Rev. B*, 92:081115.

[Schilling et al., 1993] Schilling, A., Cantoni, M., Guo, J., and Ott, H. (1993). Superconductivity above 130 k in the Hg-Ba-Ca-Cu-O system. *Nature*, 363(6424):56–58.

[Schilling, 2007] Schilling, J. S. (2007). High-pressure effects. In *Handbook of High-Temperature Superconductivity*, pages 427–462. Springer.

[Schrieffer, 2007] Schrieffer, J. R. (2007). *Handbook of High-Temperature Superconductivity*. Springer.

[Slichter, 1990] Slichter, C. P. (1990). *Principles of Magnetic Resonance*. Springer, Berlin, third enla edition.

[Suter et al., 1998] Suter, A., Mali, M., Roos, J., and Brinkmann, D. (1998). Mixed magnetic and quadrupolar relaxation in the presence of a dominant static zeeman hamiltonian. *Journal of Physics: Condensed Matter*, 10(26):5977.

[Takigawa et al., 1989a] Takigawa, M., Hammel, P. C., Heffner, R. H., and Fisk, Z. (1989a). Spin susceptibility in superconducting $YBa_2Cu_3O_7$ from ^{63}Cu Knight shift. *Phys. Rev. B*, 39(10):7371–7374.

[Takigawa et al., 1989b] Takigawa, M., Hammel, P. C., Heffner, R. H., Fisk, Z., Smith, J. L., and Schwarz, R. B. (1989b). Anisotropic Cu Knight shift and magnetic susceptibility in the normal state of $YBa_2Cu_3O_7$. *Phys. Rev. B*, 39:300.

[Takigawa et al., 1991] Takigawa, M., Reyes, A. P., Hammel, P. C., Thompson, J. D., Heffner, R. H., Fisk, Z., and Ott, K. C. (1991). Cu and O NMR studies of the magnetic properties of $YBa_2Cu_3O_{6.63}$ (T_c=62 K). *Phys. Rev. B*, 43:247–257.

[Walstedt, 2007] Walstedt, R. E. (2007). *The NMR Probe of High-T_c Materials*. Springer, 1 ed. edition.

[Walstedt et al., 1988] Walstedt, R. E., W W Warren, J., Bell, R. F., Brennert, G. F., Espinosa, G. P., Cava, R. J., Schneemeyer, L. F., and Waszczak, J. V.

(1988). Anisotropic nuclear relaxation in YBa$_2$Cu$_3$O$_7$. *Phys. Rev. B*, 38(13):9299–9302.

[Wu et al., 1987] Wu, M. K., Ashburn, J. R., Torng, C. J., Hor, P. H., Meng, R. L., Gao, L., Huang, Z. J., Wang, Y. Q., and Chu, C. W. (1987). Superconductivity at 93 K in a new mixed-phase Y-Ba-Cu-O compound system at ambient pressure. *Phys. Rev. Lett.*, 58(9):908.

[Yosida, 1958] Yosida, K. (1958). Paramagnetic Susceptibility in Superconductors. *Phys. Rev.*, 110:769–770.

[Zhang and Rice, 1988] Zhang, F. and Rice, T. (1988). Effective Hamiltonian for the superconducting Cu oxides. *Phys. Rev. B*, 37(7):3759.

Author contributions

Each author's contribution is specified at the end of all six publications and I repeat them here.

In [Avramovska et al., 2019], I was involved in the data collection, analysis and discussion, together with D.P. and J.H., while J.H. introduced the main concepts and held the overall leadership. In [Jurkutat et al., 2019], I performed independent collection and verification of the data collected by D.D. and M.J. I was involved in discussion of the data together with J.H., D.P., M.J. and G.V.M.W. The preparation of the manuscript was done equally by me, M.J. and J.H., while J.H. led the overall project. In [Avramovska et al., 2020], all authors were involved in data analysis and discussion equally, as well as in preparing the manuscript. J.H. introduced the main concepts and held the overall leadership. In [Nachtigal et al., 2020], I was involved in the earlier stages of the discussion and performed data collection and analysis of part of the data, together with D.P. Afterwards, J.N. and J.H. did the collection and analysis of the entirety of the O data. R.G., J.N., J.H. worked mainly on the preparation of the manuscript. In [Avramovska et al., 2022a], I led the writing and preparation of the manuscript; J.N. led the literature data collection and analysis; all authors contributed to the preparation of the manuscript. J.H. introduced the main concepts and had the project leadership; In [Avramovska et al., 2022b], J.H. had the overall project leadership and introduced the main concepts together with M.A.. J.N. led the O data collection and the overall presentation of the data in the manuscript. S.T. contributed to the preparation of the manuscript. All authors were involved in discussions and in preparing the manuscript.